Toni Itkonen

PARALLEL-OPERATING THREE-PHASE VOLTAGE SOURCE INVERTERS – CIRCULATING CURRENT MODELING, ANALYSIS AND MITIGATION

Thesis for the degree of Doctor of Science (Technology) to be presented with due permission for public examination and criticism in the Auditorium of the Student Union House, Lappeenranta, Finland, on the 21th of June, 2010, at noon.

Acta Universitatis
Lappeenrantaensis
389

Supervisors	Professor Olli Pyrhönen Department of Electrical Engineering Institute of Energy Technology Lappeenranta University of Technology Finland
	Professor Pertti Silventoinen Department of Electrical Engineering Institute of Energy Technology Lappeenranta University of Technology Finland
Reviewers	Professor Lennart Harnefors ABB Power Systems – HVDC Sweden
	Professor Kai Zenger School of Science and Technology Aalto University Finland
Opponent	Professor Lennart Harnefors ABB Power Systems – HVDC Sweden

ISBN 978-952-214-943-5
ISBN 978-952-214-944-2 (PDF)
ISSN 1456-4491

Lappeenrannan teknillinen yliopisto
Digipaino 2010

Abstract

Toni Itkonen

Parallel-Operating Three-Phase Voltage Source Inverters – Circulating Current Modeling, Analysis and Mitigation

Acta Universitatis Lappeenrantaensis 389

Dissertation, Lappeenranta University of Technology
115 p.
Lappeenranta 2010
ISBN 978-952-214-943-5, ISBN 978-952-214-944-2 (PDF)
ISSN 1456-4491

The maximum realizable power throughput of power electronic converters may be limited or constrained by technical or economical considerations. One solution to this problem is to connect several power converter units in parallel. The parallel connection can be used to increase the current carrying capacity of the overall system beyond the ratings of individual power converter units. Thus, it is possible to use several lower-power converter units, produced in large quantities, as building blocks to construct high-power converters in a modular manner. High-power converters realized by using parallel connection are needed for example in multimegawatt wind power generation systems. Parallel connection of power converter units is also required in emerging applications such as photovoltaic and fuel cell power conversion.

The parallel operation of power converter units is not, however, problem free. This is because parallel-operating units are subject to overcurrent stresses, which are caused by unequal load current sharing or currents that flow between the units. Commonly, the term 'circulating current' is used to describe both the unequal load current sharing and the currents flowing between the units. Circulating currents, again, are caused by component tolerances and asynchronous operation of the parallel units. Parallel-operating units are also subject to stresses caused by unequal thermal stress distribution. Both of these problems can, nevertheless, be handled with a proper circulating current control.

To design an effective circulating current control system, we need information about circulating current dynamics. The dynamics of the circulating currents can be investigated by developing appropriate mathematical models. In this dissertation, circulating current models are developed

for two different types of parallel two-level three-phase inverter configurations. The models, which are developed for an arbitrary number of parallel units, provide a framework for analyzing circulating current generation mechanisms and developing circulating current control systems.

In addition to developing circulating current models, modulation of parallel inverters is considered. It is illustrated that depending on the parallel inverter configuration and the modulation method applied, common-mode circulating currents may be excited as a consequence of the differential-mode circulating current control. To prevent the common-mode circulating currents that are caused by the modulation, a dual modulator method is introduced. The dual modulator basically consists of two independently operating modulators, the outputs of which eventually constitute the switching commands of the inverter. The two independently operating modulators are referred to as primary and secondary modulators.

In its intended usage, the same voltage vector is fed to the primary modulators of each parallel unit, and the inputs of the secondary modulators are obtained from the circulating current controllers. To ensure that voltage commands obtained from the circulating current controllers are realizable, it must be guaranteed that the inverter is not driven into saturation by the primary modulator. The inverter saturation can be prevented by limiting the inputs of the primary and secondary modulators. Because of this, also a limitation algorithm is proposed. The operation of both the proposed dual modulator and the limitation algorithm is verified experimentally.

Keywords: voltage source inverter, two-level, three-phase, parallel operation, circulating current
UDC 621.314.2:51.001.57:621.3.014

Acknowledgments

The research documented in this work was carried out at the Department of Electrical Engineering, Institute of Energy Technology, Lappeenranta University of Technology (LUT) in several parts during the years 2005–2009. The research was mainly funded by Vacon Plc and Lappeenranta University of Technology.

First of all, I would like to thank my supervisors, Professor Olli Pyrhönen and Professor Pertti Silventoinen, for giving me the opportunity to work in a vivid group full of enthusiastic researchers and for their valuable comments and encouragement during the project. I am also grateful to the reviewers, Professor Lennart Harnefors and Professor Kai Zenger, for their proposals and valuable comments which helped to improve the manuscript of the thesis.

I express my gratitude to Dr. Julius Luukko and Dr. Riku Pöllänen for the technical discussions which proved to be valuable for me numerous times. I am also grateful to Dr. Hanna Niemelä for her contribution to improve the language of the manuscript.

I would also like to thank my colleague Mr Tommi Laakkonen. Without his contribution many of my ideas would not have been tested experimentally. I would also like to thank all the other personnel I have worked with at the Department of Electrical Engineering.

The financial support for this work by Walter Ahlström Foundation, Jenny and Antti Wihuri Foundation, The Finnish Cultural Foundation Central Fund, and Lauri ja Lahja Hotinen Fund is sincerely appreciated.

Finally, I express my deepest gratitude to my wife Tanja and to our daughter Kiia for their love and support during the preparation of this thesis.

Vaasa, June 9, 2010

Toni Itkonen

Contents

Nomenclature

Subscripts

0	zero axis component
$1, 2, \cdots, n$	index of parallel unit
abc	vector or matrix containing abc coordinate quantities
a, b, c	abc coordinate quantity
α	real axis quantity in the stationary $\alpha\beta$ reference frame
$\alpha\beta$	vector or matrix containing stationary $\alpha\beta$ reference frame quantities
$\alpha\beta 0$	vector or matrix containing $\alpha\beta 0$ coordinate quantities
β	imaginary axis quantity in the stationary $\alpha\beta$ reference frame
dq	vector or matrix containing rotating dq reference frame quantities
$dq0$	vector or matrix containing $dq0$ coordinate quantities
dc	direct voltage link
$\max$	maximum
n	nominal
ref	reference
sw	switching frequency or switching period
d	direct axis quantity in the rotating dq reference frame
q	quadrature axis quantity in the rotating dq reference frame

Superscripts

$+$	positive direct voltage bus
$-$	negative direct voltage bus
cc	circulating current
com	common direct voltage source
l	limited variable
n	negative phase current

p	positive phase current
r	denotes that the space vector is expressed in the rotating reference frame
sep	separate direct voltage sources
s	denotes that the space vector is expressed in the stationary reference frame

Other Symbols

$\mathbf{I}$	identity matrix
$\mathbf{A}$	state-space model state matrix
$\mathbf{B}$	state-space model input matrix
$\mathbf{C}$	state-space model output matrix
$\mathbf{D}$	state-space model feedforward matrix
$\mathbf{u}$	state-space model input vector
$\mathbf{x}$	state-space model state vector
$\mathbf{y}$	state-space model output vector
D	anti-parallel diode
T	switching device
C	capacitance
d	duty cycle
i	instantaneous current
L	inductance
R	resistance
t	time
u	instantaneous voltage

Acronyms

ac	alternating current
dc	direct current
FC	fuel cell
FPGA	field programmable gate array
IGBT	insulated gate bipolar transistor
KCL	Kirchhoff's current law

KVL	Kirchhoff’s voltage law
LTI	linear time-invariant
PC	personal computer
PV	photovoltaic
PWM	pulse width modulation
SPDT	single-pole double-throw
SPST	single-pole single-throw
SVD	singular value decomposition
SVM	space vector modulation
VSC	voltage source converter
VSI	voltage source inverter

Chapter 1

Introduction

Modern power electronic converters are used to convert and control electrical energy in the wide range of milliwatts to gigawatts (Bose, 2009). Typical applications include for example battery chargers, heating and lighting control, active harmonic filters, high-voltage dc (HVDC) systems, photovoltaic (PV) and fuel cell (FC) power conversion, and motor drives. The wide area of motor drives includes applications in transportation, paper and textile mills, wind power generation systems, air-conditioning and heat pumps, rolling and cement mills, ship propulsion, and the like.

Power electronic converters perform the power conversion by means of power semiconductor devices. Although the power ratings of power semiconductor devices have increased considerably since the introduction of the first commercial power semiconductor device in the early 1960s (Wilson, 2000), the maximum realizable power throughput of power electronic converters may be limited or constrained by technical or economical considerations. In other words, even though there are power semiconductor devices available with the desired power ratings, their switching characteristics may not be sufficient, or vice versa. It is also possible that although there are devices available with the desired power ratings and switching characteristics, they are too expensive because they are not manufactured in large quantities (Luniewski and Jansen, 2007; Zorngiebel et al., 2009).

Power ratings can be increased beyond the ratings of individual power semiconductor devices with a series or parallel connection. The series connection can be used to increase the voltage blocking capability, while the parallel connection can be used to increase the current carrying capacity. Both the series and parallel connection methods can be basically divided into three different levels.

At the lowest level, power semiconductor devices are connected in series (Sasagawa et al., 2004) or in parallel (Azar et al., 2008). At the next level, power modules, which may incorporate series- or parallel-connected power semiconductor devices, are connected in series or in parallel (Bortis et al., 2008). At the highest level, complete power converter units which are constructed around the power modules are connected in series (Naumanen et al., 2009) or in parallel (Baumann and Kolar, 2007). Individual power converter units, again, may include several series- or parallel-connected power modules.

1.1 Motivation of the work

As discussed above, parallel connection of power converter units can be used to increase the current carrying capacity of the overall system beyond the ratings of individual power semiconductor devices. Parallel-operating power converters are, however, subject to overcurrent

stresses, which are caused by unequal load current sharing or currents that flow between the units. Commonly, the term 'circulating current' is used to describe both the unequal load current sharing and the currents flowing between the units (Pan and Liao, 2007, 2008). Circulating currents are caused by component tolerances and asynchronous operation of the parallel units (Cai et al., 2008).

Parallel-operating power converters are also subject to unequal thermal stress distribution (Joseph et al., 2004; Chen et al., 2006). Although the unequal thermal stress distribution might be caused by the circulating currents, in general, the equal load current sharing does not guarantee equal thermal stress distribution. However, the thermal stress distribution can be affected by controlling the load current sharing between the parallel units.

Several contributions have dealt with the circulating current modeling, analysis, and the control of parallel-operating multi-phase power converters (Ye et al., 2002; Shi and Venkataramanan, 2004; Mazumder, 2005; Chen, 2006; Fu et al., 2008; Neacsu et al., 2008). The majority of these contributions deal only with the parallel connection of two units, which is a special case. The number of applications that require parallel connection of several power converter units is, however, on the rise. These applications include for example photovoltaic and fuel cell power conversion systems (Chen and Smedley, 2008; Yu et al., 2008).

Although much work has been carried out to investigate circulating current dynamics of parallel multi-phase converters, very few contributions deal with the circulating current modeling and the analysis of an arbitrary number of parallel units. Such work would, however, lead into better understanding of circulating current behavior and provide a framework for designing circulating current controllers for any number of parallel-operating units.

1.2 Objective of the work

In this dissertation, parallel-operating voltage source frequency converters are studied. The voltage source frequency converter refers in this work to a converter comprised of line-side L-filters, a full-wave diode rectifier bridge, a direct voltage link capacitor, and a three-phase inverter bridge as illustrated in Fig. 1.1. In brief, the function of a frequency converter is to first convert the supplied alternating voltage into direct voltage and then convert the direct voltage into alternating voltage of desired frequency and amplitude.

The parallel frequency converter configurations studied in this dissertation are presented in Fig. 1.2. As we can see, we will consider parallel-operating frequency converters with separate and common direct voltage links. To be precise, we will concentrate on the parallel operation of three-phase inverter bridges. Moreover, even though the figures show only parallel connection of two units, we will consider parallel connection of an arbitrary number of units.

The principal objective of this work is to investigate the main differences between the considered parallel inverter configurations from the circulating point of view. The main objective is met by developing mathematical circulating current models for both of the studied configurations and for an arbitrary number of parallel-connected units. Although the developed models are basically used only to study circulating current generation mechanisms and to analyze differences between the studied configurations, they can also be used in designing circulating current controllers. The circulating current control design is, however, outside the scope of this dissertation.

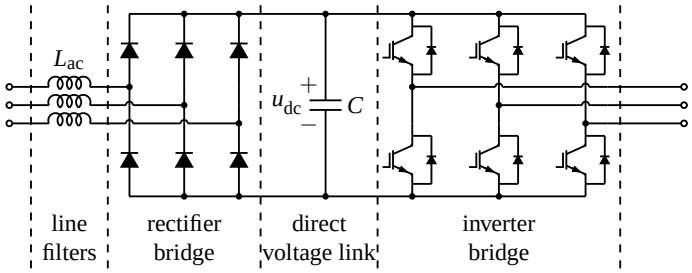

Fig. 1.1: Single voltage source frequency converter consisting of line-side L-filters, a full-wave diode rectifier bridge, a direct voltage link capacitor, and a three-phase inverter bridge.

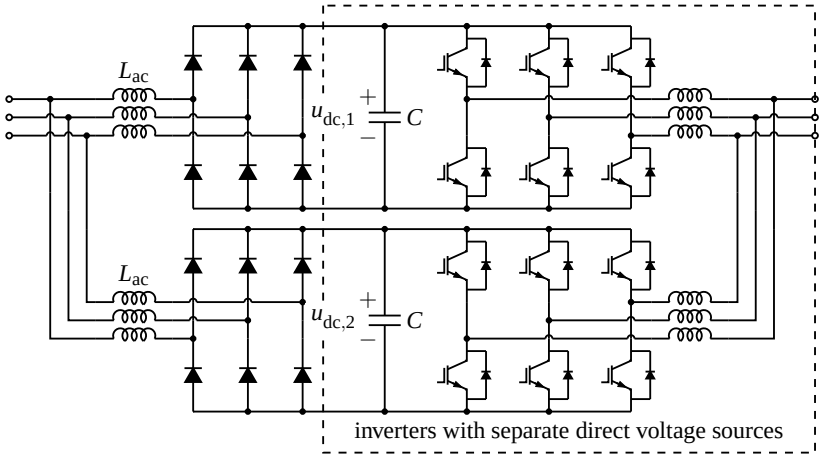

(a) Parallel voltage source frequency converters with separate direct voltage links.

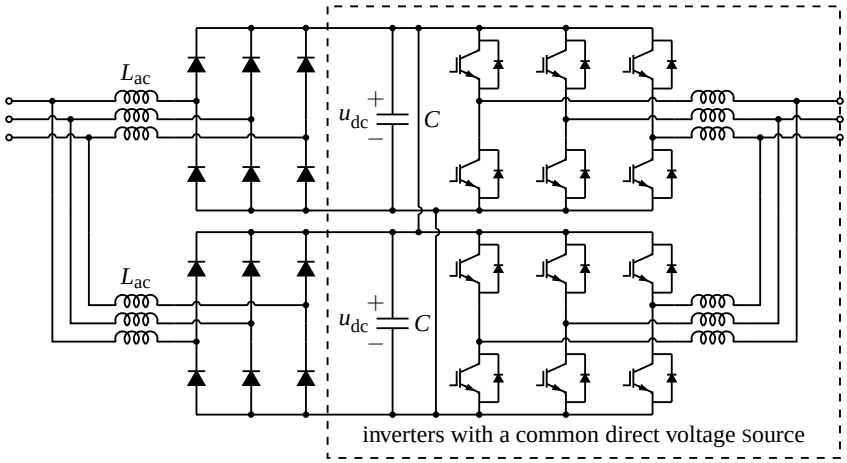

(b) Parallel voltage source frequency converters with a common direct voltage link.

Fig. 1.2: Parallel voltage source frequency converter configurations considered in this dissertation. The study concentrates on the parallel operation of the inverter bridges. The inductors added to the frequency converter outputs are current sharing inductors.

The developed circulating current models show that a common-mode circulating current may flow between the parallel inverters depending on the applied configuration. It is also illustrated that depending on the applied pulse width modulation (PWM) method, common-mode circulating currents may be excited as a consequence of the differential-mode circulating current control. To prevent the common-mode circulating currents that are caused by the modulation, a dual modulator method is introduced. The introduction of the dual modulator method is the secondary objective of this dissertation.

1.3 Outline of the thesis

The main contents of the rest of the chapters are summarized in the following:

Chapter 2 addresses small-signal modeling of two different parallel three-phase two-level voltage source inverter configurations. Small-signal models are developed for both of the studied configurations and for an arbitrary number of parallel units. Furthermore, an effort is made to describe the applied modeling techniques.

Chapter 3 deals with the circulating current modeling and analysis. The analysis is based on the circulating current models that are derived from the parallel inverter models developed in the previous chapter. The circulating current models are derived also for an arbitrary number of parallel units.

Chapter 4 first studies an application of the space-vector-based modulation methods in the control of parallel inverters. It is illustrated that the space-vector-based modulation methods may introduce low-frequency zero-sequence circulating currents depending on the applied parallel inverter configuration. The main contribution of this chapter is the introduction of a dual modulator method that can avoid the above-mentioned problem.

Chapter 5 introduces a limitation algorithm that was developed to be used together with the proposed dual modulator method.

Chapter 6 presents experimental results to verify the operation of the proposed dual modulator method and the limitation algorithm.

Chapter 7 concludes the dissertation. The main results are discussed and summarized, and suggestions for future work are made.

1.4 Scientific contributions and publications

The scientific contributions of this doctoral dissertation are:

- Development of parallel inverter models for two different parallel three-phase two-level voltage source inverter configurations in the case of n parallel units.
- Development of circulating current models for two different parallel three-phase voltage source inverter configurations in the case of n parallel units.
- Development of a model for estimating circulating currents caused by a blanking time required to prevent a short-circuit in the inverter phase leg, finite turn-on and turn-off times

of switching devices, and forward voltage drops of switching devices and anti-parallel diodes.

- Development of a dual modulator method for parallel three-phase power converters to mitigate modulation-based circulating currents.
- Development of a limitation algorithm that can be used to combine the existing space vector limitation methods with the zero-sequence component limitation method.
- Experimental verification of both the proposed dual modulator method and the proposed limitation algorithm.

The author has published research results related to the subjects covered in this doctoral dissertation in the following publications:

P1 Itkonen, T., Luukko, J., Laakkonen, T., Silventoinen, P., and Pyrhönen, O. (2008), "Switching Effects in Directly Paralleled Three-Phase AC/DC/AC Converters with Separate DC Links," in *Power Electronics Specialists Conference, 2008. PESC 2008. IEEE*, pp. 1937–1943.

P2 Itkonen, T., Luukko, J., and Pöllänen, R. (2009a), "Modeling and Analysis of the Dead-Time Effects in Parallel Two-Level Voltage Source Inverters," in *Energy Conversion Congress and Exposition, 2009. ECCE. IEEE*, pp. 3211–3217.

P3 Itkonen, T., Luukko, J., and Pollanen, R. (2009b), "Analysis of Current Characteristics of Parallel Three-Phase Voltage Source Inverters," in *Power Electronics and Applications, 2009. EPE '09. 13th European Conference on*, pp. 1–10.

P4 Itkonen, T., Luukko, J., Sankala, A., Laakkonen, T., and Pöllänen, R. (2009c), "Modeling and Analysis of the Dead-Time Effects in Parallel PWM Two-Level Three-Phase Voltage-Source Inverters," *Power Electronics, IEEE Transactions on*, vol. 24, no. 11, pp. 2446–2455.

T. Itkonen has been the primary author in publications P1–P4. The background research for publications P1–P4 was entirely carried out by T. Itkonen. Also the simulation studies, the results of which are presented in publications P1–P4, were entirely performed by T. Itkonen. The prototype used in publication P4 was built by Mr. A. Sankala and Mr. J. Hannonen. The synchronization method applied in publication P4 was developed by Mr. T. Laakkonen. The control algorithms used in publication P4 were developed by T. Itkonen and the implementations were made by T. Itkonen and Mr. A. Sankala. The measurements for publication P4 were conducted by T. Itkonen.

The author has also published research results related to parallel-operating voltage source inverters but not covered in this dissertation in the following publications:

- Itkonen, T., Rauma, K., Sarén, H., Laakkonen, O., Pyrhönen, O., and Silventoinen, P. (2006), "Parallel Connected Voltage Source Inverters without Intermodule Reactors," in *Power Electronics and Motion Control Conference, 2006. EPE-PEMC 2006. 12th International*, pp. 641–646.

- Itkonen, T. and Luukko, J. (2008), ”Switching-Function-Based Simulation Model for Three-Phase Voltage Source Inverter Taking Dead-Time Effects into Account,” in *Industrial Electronics, 2008. IECON 2008. 34th Annual Conference of IEEE*, pp. 992–997.

Chapter 2

Small-signal modeling of parallel three-phase voltage source inverters

This chapter addresses small-signal modeling of two-level three-phase voltage source inverters. More precisely, the chapter focuses on developing small-signal models for two kinds of parallel inverter configurations in the case of an arbitrary number of parallel units. In the derivation, various modeling methods are applied. The methods include a phase leg averaging technique, coordinate transformations between stationary and rotating reference frames, and a linearization. Because of this, effort is also put into describing the applied modeling methods.

2.1 Small-signal modeling of ac power electronic systems

Power electronic systems are generally nonlinear, which prevents the direct use of classical analysis methods designed for linear time-invariant (LTI) systems. The behavior of nonlinear systems can, however, be approximated by linear equations around a nominal operation point. The process used to obtain a linear approximation of the nonlinear system is referred to as linearization. The result of linearization is a locally linearized model, which is usually called a small-signal model of the system. The small-signal model is accurate only in the (dc) operation point, but can also predict the behavior of the system in the neighborhood of the operation point (Roubal et al., 2009).

Small-signal modeling of ac power electronic systems is not as straightforward as the above would indicate. This is because there is no dc operation point and because power electronic converters are time-variant by nature because of the switching. The switching-based time variance can be removed by applying averaging techniques such as phase leg averaging (Ye et al., 2000) or arm rail averaging (Ye and Boroyevich, 2001). One solution to the problem of the lacking dc operation point, which is applicable to three-phase systems, is to transform a stationary reference frame model into a rotating reference frame model. An overview of other possible solutions, including also the above-mentioned one, has been presented in Sun (2009).

The systematic small-signal modeling approach presented in (Hiti et al., 1994) for single three-phase voltage source converters applies the phase leg averaging technique, coordinate transformations, and linearization. The same modeling approach has been previously applied also to parallel three-phase converters and inverters for example in (Ye et al., 2002; Zhang et al., 2009b) and is also adopted in this dissertation.

2.2 Applied modeling procedure

A small-signal modeling procedure applied in this dissertation can basically be divided into four stages. These stages can be described as follows. During the first stage, converter circuits are replaced with phase-leg-averaged circuit representations. In the second stage, an averaged stationary reference frame model of the system under investigation is developed. The developed stationary reference frame model is transformed into a rotating reference frame model in the third stage. Finally, in the fourth stage, a small-signal model is obtained by linearizing the rotating reference frame model at the operating point.

To facilitate the understanding of how the small-signal modeling procedure described above is applied, the principles of the phase leg averaging technique, reference frame transformations, and linearization of nonlinear systems are first described in the following subsections. After the overviews, a small-signal modeling of a single three-phase inverter is considered as an example. The purpose of the example is to illustrate the modeling procedure in detail. The example also introduces some notations that are used with the parallel inverter models presented in the following sections.

2.2.1 Principle of the phase leg averaging technique

To present the principle of the phase leg averaging technique, it is convenient to start with the concept of switching functions. In the switching function approach, power converters are directly studied through their converting functions focusing on the relationships between the input and output electric variables, instead of actual topologies (Boroyevich and Burgos, 2003). From the circuit point of view, this means that the actual converter circuit comprised of power semiconductor devices is replaced with controlled current and voltage sources describing the external behavior of the converter. This simplifies the study of the circuits consisting of power converter units, since the circuits become invariant for all valid switching state combinations (Jin, 1997).

To find a unique electrical description of a certain topology, it is necessary to add some topological restrictions to the circuits connected to power converter ports. These restrictions include that the input and output ports must be connected to the appropriate energy storage elements, that is, capacitors or inductors, which may be a part of the connected sources and loads. Furthermore, when the input side is of the current source type, the output side must be of the voltage source type, and vice versa. Moreover, it must be ensured that the operation of the switching circuit is such that the current sources or inductors are not open circuited and the voltage sources or capacitors are not short circuited at any time (Boroyevich and Burgos, 2003).

Let us apply the switching function concept to a single phase leg of a two-level three-phase VSI shown in Fig. 2.1(a). The phase leg consists of two switching cells, which are comprised of a controlled switching device T_p^x and an anti-parallel diode D_p^x. The variable $p \in \{a, b, c\}$ denotes the phase and $x \in \{+, -\}$ is used to distinguish the upper and lower devices. The switching cells can be presented with a single-pole single-throw (SPST) switches as depicted in Fig. 2.1(b). The state of the SPST switch, that is, whether the switch is open or closed, can be indicated by the following switching function for the switches

$$r_p^x = \begin{cases} 1 & \text{, when the switch } \mathrm{S}_p^x \text{ is closed} \\ 0 & \text{, when the switch } \mathrm{S}_p^x \text{ is open} \end{cases} \tag{2.1}$$

The switch S_p^x is closed whenever the switching device T_p^x is controlled to the on-state or current flows through the anti-parallel diode D_p^x, and otherwise the switch is open.

There are switching constraints for the upper switch S_p^+ and the lower switch S_p^-. These constraints include that the capacitor cannot be short circuited and the inductor cannot be open circuited. This means that one of the switches S_p^+ or S_p^- has to be closed, while the other has to be open at any time. This relationship can be expressed by using switch switching functions as

$$r_p^+ + r_p^- = 1 \tag{2.2}$$

The switching constraint (2.2) indicates that the upper switch S_p^+ and the lower switch S_p^- operate as a single-pole double-throw (SPDT) switch illustrated in Fig. 2.1(c). The state of the SPDT switch, that is, whether the switch is connected to the positive or negative direct voltage bus, can be indicated by using a phase switching function as

$$r_p = \begin{cases} 1 & \text{, when } \mathrm{S}_p \text{ is connected to the positive dc bus} \\ 0 & \text{, when } \mathrm{S}_p \text{ is connected to the negative dc bus} \end{cases} \tag{2.3}$$

Let us consider Fig. 2.1(c) in more detail. A phase leg voltage, that is, the voltage between the points p and o, equals $u_{p\mathrm{o}} = u_{\mathrm{dc}}$ when the phase switching function $r_p = 1$ and when $r_p = 0$, $u_{p\mathrm{o}} = 0$. Thus, the phase leg voltage can be defined by using the phase switching function and the dc link voltage as

$$u_{p\mathrm{o}} = r_p u_{\mathrm{dc}} \tag{2.4}$$

Similarly, for the positive dc bus current we can write

$$i_p^+ = r_p i_p \tag{2.5}$$

Based on (2.4) and (2.5), the external behavior of the phase leg can be described with the controlled current and voltage sources as illustrated in Fig. 2.1(d).

The phase switching function (2.3) is a discontinuous function. To get rid of the discontinuities, switching functions can be averaged over a switching period T_{sw} (Wester and Middlebrook, 1973). In the case of phase switching functions, averaging is performed as

$$d_p = \frac{1}{T_{\mathrm{sw}}} \int_{t-T_{\mathrm{sw}}}^{t} r_p \mathrm{d}t \tag{2.6}$$

where d_p denotes an averaged phase switching function, also known as a phase duty cycle. The effect of averaging is approximately that of a low-pass filter with a cut-off frequency $\omega_s = 2\pi/T_{\mathrm{sw}}$ (Wester and Middlebrook, 1973). Because of this, phase duty cycles are useful when frequencies below the cut-off frequency are studied. Using the phase duty cycle, the inverter phase leg can be presented as shown in Fig. 2.1(e). This is the phase-leg-averaged model of a single phase leg of the two-level three-phase VSI.

2.2.2 Reference frame transformations

To present the reference frame transformations, it is convenient to start with a brief introduction to the theory of space vectors that was, according to (Holtz, 1996), formally introduced by

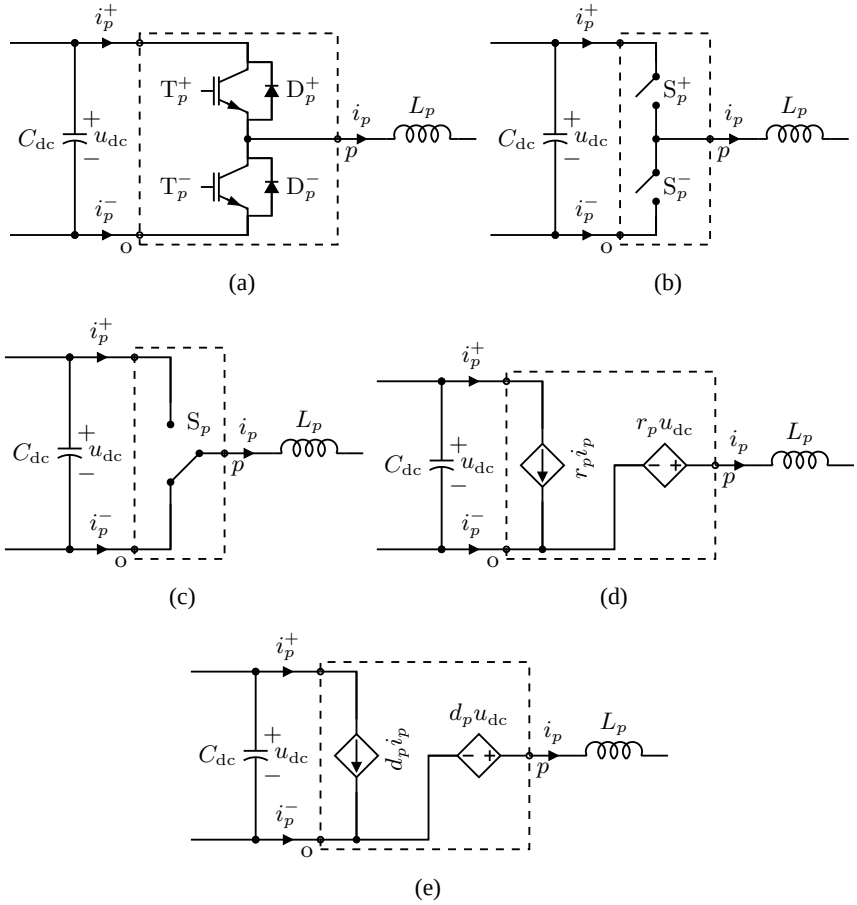

Fig. 2.1: Single phase leg of a two-level voltage source inverter presented using (a) controlled switching devices and anti-parallel diodes, (b) single-pole single-throw switches, (c) a single-pole double-throw switch, and current and voltage sources, which are controlled with (d) instantaneous phase switching functions and (e) averaged phase switching functions also known as phase duty cycles.

Kovács and Rácz (1959). Although the space vector theory was originally intended to be used in the transient analysis of electrical machines, it can be employed as a modeling and analysis tool for any three-phase system of currents, voltages, flux linkages, and so on. The basic idea behind the space vector theory is to represent three-phase quantities with a complex space vector. It must, however, be emphasized that the space vector does not contain information about a real zero-sequence component, which refers to the sum of three-phase quantities.

Consequently, a general three-phase system can be expressed by a complex space vector and a real zero-sequence component, defined as

$$\vec{x}^{\,\mathrm{s}} = c\left(a^0 x_{\mathrm{a}} + a^1 x_{\mathrm{b}} + a^2 x_{\mathrm{c}}\right) = x_\alpha + j x_\beta \tag{2.7}$$

and

$$x_0 = c_0 \left(x_\mathrm{a} + x_\mathrm{b} + x_\mathrm{c} \right) \tag{2.8}$$

respectively. The superscript s is used to denote that the space vector is expressed in a stationary reference frame, c and c_0 are scaling constants and $a = e^{j2\pi/3}$. The unit vectors a^0, a^1, and a^2 are used to indicate the orientation of three-phase axes in a complex plane, and x_a, x_b, and x_c are instantaneous values of the phase quantities. Furthermore, x_α and x_β are the real and imaginary components of the space vector. Although the scaling constants c and c_0 can be chosen freely, they are commonly, and also in this dissertation, chosen as $c = 2/3$ and $c_0 = 1/3$. This is usually referred to as a peak value scaling, since the projections of the space vector on the phase axes directly yield the instantaneous values of the phase quantities. Hereafter, equations relating to space vectors and zero-sequence components are presented assuming peak value scaling.

The transformation of three-phase quantities into the complex space vector (2.7) and the real zero-sequence component (2.8) can be thought of as a transformation from a stationary abc coordinates into a stationary $\alpha\beta 0$ coordinates. This transformation can be expressed by using matrix notations as

$$\underbrace{\begin{bmatrix} x_\alpha \\ x_\beta \\ x_0 \end{bmatrix}}_{\mathbf{x}_{\alpha\beta 0}} = \underbrace{\frac{2}{3} \begin{bmatrix} 1 & -1/2 & -1/2 \\ 0 & \sqrt{3}/2 & -\sqrt{3}/2 \\ 1/2 & 1/2 & 1/2 \end{bmatrix}}_{\mathbf{T}_{\alpha\beta 0}} \underbrace{\begin{bmatrix} x_\mathrm{a} \\ x_\mathrm{b} \\ x_\mathrm{c} \end{bmatrix}}_{\mathbf{x}_{\mathrm{abc}}} \tag{2.9}$$

The transformation back into the abc coordinates can be performed as

$$\underbrace{\begin{bmatrix} x_\mathrm{a} \\ x_\mathrm{b} \\ x_\mathrm{c} \end{bmatrix}}_{\mathbf{x}_{\mathrm{abc}}} = \underbrace{\begin{bmatrix} 1 & 0 & 1 \\ -1/2 & \sqrt{3}/2 & 1 \\ -1/2 & -\sqrt{3}/2 & 1 \end{bmatrix}}_{\mathbf{T}^{-1}_{\alpha\beta 0}} \underbrace{\begin{bmatrix} x_\alpha \\ x_\beta \\ x_0 \end{bmatrix}}_{\mathbf{x}_{\alpha\beta 0}} \tag{2.10}$$

For the analysis and control design purposes, it is convenient to express the space vector in some other coordinate system than in the $\alpha\beta$ coordinates. Usually, the space vector is transformed into a dq coordinate system that rotates at an angular frequency ω. This transformation is particularly useful when the angular speed of the three-phase system equals the angular speed of the rotating dq coordinates. This is because in the steady-state, the space vector quantities become constant. The transformation into dq coordinates is defined as

$$\vec{x}^\mathrm{r} = \vec{x}^\mathrm{s} e^{-j\theta} = 2/3 \left(a^0 x_\mathrm{a} + a^1 x_\mathrm{b} + a^2 x_\mathrm{c} \right) e^{-j\theta} = \left(x_\alpha + j x_\beta \right) e^{-j\theta} \tag{2.11}$$

where the superscript r indicates that the space vector is expressed in the rotating coordinates and θ is the angle between the real axis of the dq coordinates and the real axis of the $\alpha\beta$ coordinates. In the steady-state, the angle can be expressed as $\theta = \omega t + \theta_0$.

Based on (2.11), the transformation into rotating coordinates can be realized using either abc or $\alpha\beta$ coordinate quantities. Let us only consider the former. In this case, the transformation can

be expressed by using matrix notations as

$$\underbrace{\begin{bmatrix} x_\mathrm{d} \\ x_\mathrm{q} \\ x_0 \end{bmatrix}}_{\mathbf{x}_\mathrm{dq0}} = \underbrace{\frac{2}{3}\begin{bmatrix} \cos(\theta) & \cos(\theta+2\pi/3) & \cos(\theta+4\pi/3) \\ \sin(\theta) & \sin(\theta+2\pi/3) & \sin(\theta+4\pi/3) \\ 1/2 & 1/2 & 1/2 \end{bmatrix}}_{\mathbf{T}_\mathrm{dq0}} \underbrace{\begin{bmatrix} x_\mathrm{a} \\ x_\mathrm{b} \\ x_\mathrm{c} \end{bmatrix}}_{\mathbf{x}_\mathrm{abc}} \tag{2.12}$$

It is emphasized that (2.12) contains also a zero-sequence component, which is independent of the reference frame (Sao and Lehn, 2006). Thus, (2.12) can be thought of as a transformation from the stationary abc coordinates into the $dq0$ coordinates, where the dq coordinates are rotating. The transformation back into the stationary abc coordinates can be performed as

$$\underbrace{\begin{bmatrix} x_\mathrm{a} \\ x_\mathrm{b} \\ x_\mathrm{c} \end{bmatrix}}_{\mathbf{x}_\mathrm{abc}} = \underbrace{\begin{bmatrix} \cos(\theta) & \sin(\theta) & 1 \\ \cos(\theta+2\pi/3) & \sin(\theta+2\pi/3) & 1 \\ \cos(\theta+4\pi/3) & \sin(\theta+4\pi/3) & 1 \end{bmatrix}}_{\mathbf{T}_\mathrm{dq0}^{-1}} \underbrace{\begin{bmatrix} x_\mathrm{d} \\ x_\mathrm{q} \\ x_0 \end{bmatrix}}_{\mathbf{x}_\mathrm{dq0}} \tag{2.13}$$

2.2.3 Linearization of nonlinear state-space models

Linearization of a vector of nonlinear functions can be performed by calculating the Jacobian matrix and evaluating the matrix in the steady-state operation point (Antsaklis and Michel, 2006). In brief, a Jacobian matrix is a matrix that contains all first-order partial derivatives of the functions to be linearized with respect to all variables. Let us consider how this is applied to a nonlinear state-space system of the form (Roubal et al., 2009)

$$\dot{\mathbf{x}}(t) = \mathbf{f}(\mathbf{x}(t), \mathbf{u}(t)), \quad \mathbf{x}(0) = \mathbf{x}_0 \tag{2.14a}$$
$$\mathbf{y}(t) = \mathbf{g}(\mathbf{x}(t), \mathbf{u}(t)) \tag{2.14b}$$

where $\mathbf{x}$, $\mathbf{u}$, and $\mathbf{y}$ are vectors containing n_x state, n_u input, and n_y output variables, respectively, $\mathbf{f}$ and $\mathbf{g}$ are vectors of differentiable functions with appropriate dimensions, and t denotes time. For an operation point $\{\mathbf{x}_0, \mathbf{u}_0, \mathbf{y}_0\}$ that satisfies

$$\mathbf{0} = \mathbf{f}(\mathbf{x}_0, \mathbf{u}_0) \tag{2.15a}$$
$$\mathbf{y}_0 = \mathbf{g}(\mathbf{x}_0, \mathbf{u}_0) \tag{2.15b}$$

a linearized model approximating the nonlinear system (2.14) can be expressed as

$$\Delta\dot{\mathbf{x}}(t) = \mathbf{A}\Delta\mathbf{x}(t) + \mathbf{B}\Delta\mathbf{u}(t) \tag{2.16a}$$
$$\Delta\mathbf{y}(t) = \mathbf{C}\Delta\mathbf{x}(t) + \mathbf{D}\Delta\mathbf{u}(t) \tag{2.16b}$$

where the operator Δ denotes the deviation from the operation point

$$\Delta\mathbf{x}(t) = \mathbf{x}(t) - \mathbf{x}_0 \tag{2.17a}$$
$$\Delta\mathbf{u}(t) = \mathbf{u}(t) - \mathbf{u}_0 \tag{2.17b}$$
$$\Delta\mathbf{y}(t) = \mathbf{y}(t) - \mathbf{y}_0 \tag{2.17c}$$

and the state, input, output, and feedforward matrices are given by

$$\mathbf{A} = \left[\begin{array}{cccc} \frac{\partial f_1}{\partial x_1} & \frac{\partial f_1}{\partial x_2} & \cdots & \frac{\partial f_1}{\partial x_{n_\mathrm{x}}} \\ \frac{\partial f_2}{\partial x_1} & \frac{\partial f_2}{\partial x_2} & \cdots & \frac{\partial f_2}{\partial x_{n_\mathrm{x}}} \\ \vdots & \vdots & \ddots & \vdots \\ \frac{\partial f_{n_\mathrm{x}}}{\partial x_1} & \frac{\partial f_{n_\mathrm{x}}}{\partial x_2} & \cdots & \frac{\partial f_{n_\mathrm{x}}}{\partial x_{n_\mathrm{x}}} \end{array}\right]\Bigg|_{(\mathbf{x}_0,\mathbf{u}_0)}, \mathbf{B} = \left[\begin{array}{cccc} \frac{\partial f_1}{\partial u_1} & \frac{\partial f_1}{\partial u_2} & \cdots & \frac{\partial f_1}{\partial u_{n_\mathrm{u}}} \\ \frac{\partial f_2}{\partial u_1} & \frac{\partial f_2}{\partial u_2} & \cdots & \frac{\partial f_2}{\partial u_{n_\mathrm{u}}} \\ \vdots & \vdots & \ddots & \vdots \\ \frac{\partial f_{n_\mathrm{x}}}{\partial u_1} & \frac{\partial f_{n_\mathrm{x}}}{\partial u_2} & \cdots & \frac{\partial f_{n_\mathrm{x}}}{\partial u_{n_\mathrm{u}}} \end{array}\right]\Bigg|_{(\mathbf{x}_0,\mathbf{u}_0)},$$

$$\mathbf{C} = \left[\begin{array}{cccc} \frac{\partial g_1}{\partial x_1} & \frac{\partial g_1}{\partial x_2} & \cdots & \frac{\partial g_1}{\partial x_{n_\mathrm{x}}} \\ \frac{\partial g_2}{\partial x_1} & \frac{\partial g_2}{\partial x_2} & \cdots & \frac{\partial g_2}{\partial x_{n_\mathrm{x}}} \\ \vdots & \vdots & \ddots & \vdots \\ \frac{\partial g_{n_\mathrm{y}}}{\partial x_1} & \frac{\partial g_{n_\mathrm{y}}}{\partial x_2} & \cdots & \frac{\partial g_{n_\mathrm{y}}}{\partial x_{n_\mathrm{x}}} \end{array}\right]\Bigg|_{(\mathbf{x}_0,\mathbf{u}_0)}, \mathbf{D} = \left[\begin{array}{cccc} \frac{\partial g_1}{\partial u_1} & \frac{\partial g_1}{\partial u_2} & \cdots & \frac{\partial g_1}{\partial u_{n_\mathrm{u}}} \\ \frac{\partial g_2}{\partial u_1} & \frac{\partial g_2}{\partial u_2} & \cdots & \frac{\partial g_2}{\partial u_{n_\mathrm{u}}} \\ \vdots & \vdots & \ddots & \vdots \\ \frac{\partial g_{n_\mathrm{y}}}{\partial u_1} & \frac{\partial g_{n_\mathrm{y}}}{\partial u_2} & \cdots & \frac{\partial g_{n_\mathrm{y}}}{\partial u_{n_\mathrm{u}}} \end{array}\right]\Bigg|_{(\mathbf{x}_0,\mathbf{u}_0)}. \tag{2.18}$$

2.2.4 Modeling example - single two-level three-phase inverter

Let us consider, as an example, a single two-level three-phase VSI feeding a resistive-inductive load shown in Fig. 2.2(a). By applying the phase leg averaging technique, we can obtain a phase-leg-averaged circuit model shown in Fig. 2.2(b). Applying Kirchhoff's voltage law (KVL) to loops L_1 and L_2, and the current law (KCL) to node n yields a set of differential and algebraic equations

$$0 = d_\mathrm{a} u_\mathrm{dc} - R_\mathrm{a} i_\mathrm{a} - L_\mathrm{a} \frac{\mathrm{d}}{\mathrm{d}t} i_\mathrm{a} + R_\mathrm{b} i_\mathrm{b} + L_\mathrm{b} \frac{\mathrm{d}}{\mathrm{d}t} i_\mathrm{b} - d_\mathrm{b} u_\mathrm{dc} \tag{2.19}$$

$$0 = d_\mathrm{b} u_\mathrm{dc} - R_\mathrm{b} i_\mathrm{b} - L_\mathrm{b} \frac{\mathrm{d}}{\mathrm{d}t} i_\mathrm{b} + R_\mathrm{c} i_\mathrm{c} + L_\mathrm{c} \frac{\mathrm{d}}{\mathrm{d}t} i_\mathrm{c} - d_\mathrm{c} u_\mathrm{dc} \tag{2.20}$$

$$0 = i_\mathrm{a} + i_\mathrm{b} + i_\mathrm{c} \tag{2.21}$$

Let us now choose the state and input vectors as

$$\mathbf{x}_\mathrm{abc} = \begin{bmatrix} i_\mathrm{a} & i_\mathrm{b} & i_\mathrm{c} \end{bmatrix}^\mathrm{T} \tag{2.22}$$

$$\mathbf{u}_\mathrm{abc} = \begin{bmatrix} d_\mathrm{a} & d_\mathrm{b} & d_\mathrm{c} \end{bmatrix}^\mathrm{T} u_\mathrm{dc} \tag{2.23}$$

The dimensions of the state and input vectors equal in both cases 3×1. Writing (2.19)–(2.21) into the form

$$\mathbf{E}_\mathrm{abc} \frac{\mathrm{d}}{\mathrm{d}t} \mathbf{x}_\mathrm{abc} = \mathbf{F}_\mathrm{abc} \mathbf{x}_\mathrm{abc} + \mathbf{G}_\mathrm{abc} \mathbf{u}_\mathrm{abc} \tag{2.24}$$

where matrices $\mathbf{E}_\mathrm{abc}$, $\mathbf{F}_\mathrm{abc}$, and $\mathbf{G}_\mathrm{abc}$ are used to indicate a leading matrix, a state matrix, and an input matrix, respectively, yields

$$\begin{bmatrix} L_\mathrm{a} & -L_\mathrm{b} & 0 \\ 0 & L_\mathrm{b} & -L_\mathrm{c} \\ 0 & 0 & 0 \end{bmatrix} \begin{bmatrix} \frac{\mathrm{d}}{\mathrm{d}t} i_\mathrm{a} \\ \frac{\mathrm{d}}{\mathrm{d}t} i_\mathrm{b} \\ \frac{\mathrm{d}}{\mathrm{d}t} i_\mathrm{c} \end{bmatrix} = \begin{bmatrix} -R_\mathrm{a} & R_\mathrm{b} & 0 \\ 0 & -R_\mathrm{b} & R_\mathrm{c} \\ 1 & 1 & 1 \end{bmatrix} \begin{bmatrix} i_\mathrm{a} \\ i_\mathrm{b} \\ i_\mathrm{c} \end{bmatrix} + \begin{bmatrix} 1 & -1 & 0 \\ 0 & 1 & -1 \\ 0 & 0 & 0 \end{bmatrix} \begin{bmatrix} d_\mathrm{a} \\ d_\mathrm{b} \\ d_\mathrm{c} \end{bmatrix} u_\mathrm{dc} \tag{2.25}$$

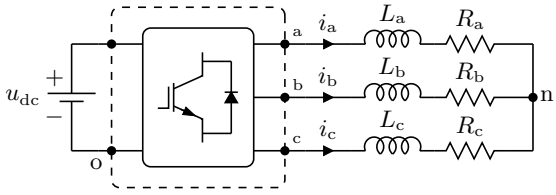

(a) Circuit schematic.

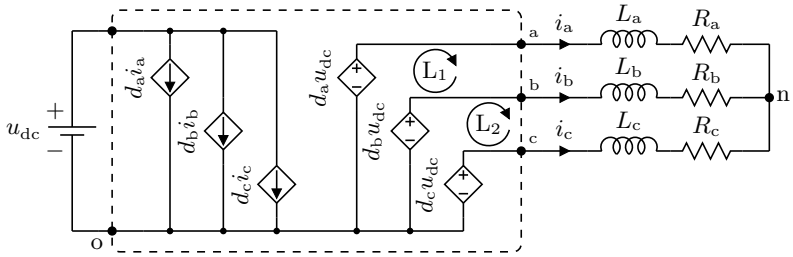

(b) Phase-leg-averaged model.

Fig. 2.2: Circuit schematic and a phase-leg-averaged model of a single two-level three-phase inverter feeding a resistive-inductive load.

In this case, the leading matrix is a singular matrix because of the zero row. In other words, the leading matrix is not invertible. As a consequence, the system of equations (2.25) cannot be directly transformed into a set of first-order differential equations as

$$\frac{\mathrm{d}}{\mathrm{d}t}\mathbf{x}_{\mathrm{abc}} = \mathbf{E}_{\mathrm{abc}}^{-1}\mathbf{F}_{\mathrm{abc}}\mathbf{x}_{\mathrm{abc}} + \mathbf{E}_{\mathrm{abc}}^{-1}\mathbf{G}_{\mathrm{abc}}\mathbf{u}_{\mathrm{abc}} = \mathbf{A}_{\mathrm{abc}}\mathbf{x}_{\mathrm{abc}} + \mathbf{B}_{\mathrm{abc}}\mathbf{u}_{\mathrm{abc}} \tag{2.26}$$

This problem can be solved by differentiating the algebraic equation (2.21). The differentiation results in

$$0 = \frac{\mathrm{d}}{\mathrm{d}t}i_{\mathrm{a}} + \frac{\mathrm{d}}{\mathrm{d}t}i_{\mathrm{b}} + \frac{\mathrm{d}}{\mathrm{d}t}i_{\mathrm{c}} \tag{2.27}$$

Now, the system of equations comprised of (2.19), (2.20), and (2.27), can be expressed in the form of (2.24) as

$$\begin{bmatrix} L_{\mathrm{a}} & -L_{\mathrm{b}} & 0 \\ 0 & L_{\mathrm{b}} & -L_{\mathrm{c}} \\ -1 & -1 & -1 \end{bmatrix} \begin{bmatrix} \frac{\mathrm{d}}{\mathrm{d}t}i_{\mathrm{a}} \\ \frac{\mathrm{d}}{\mathrm{d}t}i_{\mathrm{b}} \\ \frac{\mathrm{d}}{\mathrm{d}t}i_{\mathrm{c}} \end{bmatrix} = \begin{bmatrix} -R_{\mathrm{a}} & R_{\mathrm{b}} & 0 \\ 0 & -R_{\mathrm{b}} & R_{\mathrm{c}} \\ 0 & 0 & 0 \end{bmatrix} \begin{bmatrix} i_{\mathrm{a}} \\ i_{\mathrm{b}} \\ i_{\mathrm{c}} \end{bmatrix} + \begin{bmatrix} 1 & -1 & 0 \\ 0 & 1 & -1 \\ 0 & 0 & 0 \end{bmatrix} \begin{bmatrix} d_{\mathrm{a}} \\ d_{\mathrm{b}} \\ d_{\mathrm{c}} \end{bmatrix} u_{\mathrm{dc}} \tag{2.28}$$

Since the leading matrix is a nonsingular matrix, we can transform (2.28) into a set of first-order differential equations by applying (2.26). The resulting state and input matrices can be given as

$$\mathbf{A}_{\mathrm{abc}} = \begin{bmatrix} -\frac{(L_{\mathrm{b}}+L_{\mathrm{c}})R_{\mathrm{a}}}{(L_{\mathrm{a}}L_{\mathrm{b}}+L_{\mathrm{a}}L_{\mathrm{c}}+L_{\mathrm{b}}L_{\mathrm{c}})} & \frac{L_{\mathrm{c}}R_{\mathrm{b}}}{(L_{\mathrm{a}}L_{\mathrm{b}}+L_{\mathrm{a}}L_{\mathrm{c}}+L_{\mathrm{b}}L_{\mathrm{c}})} & \frac{L_{\mathrm{b}}R_{\mathrm{c}}}{(L_{\mathrm{a}}L_{\mathrm{b}}+L_{\mathrm{a}}L_{\mathrm{c}}+L_{\mathrm{b}}L_{\mathrm{c}})} \\ \frac{L_{\mathrm{c}}R_{\mathrm{a}}}{(L_{\mathrm{a}}L_{\mathrm{b}}+L_{\mathrm{a}}L_{\mathrm{c}}+L_{\mathrm{b}}L_{\mathrm{c}})} & -\frac{(L_{\mathrm{a}}+L_{\mathrm{c}})R_{\mathrm{b}}}{(L_{\mathrm{a}}L_{\mathrm{b}}+L_{\mathrm{a}}L_{\mathrm{c}}+L_{\mathrm{b}}L_{\mathrm{c}})} & \frac{L_{\mathrm{a}}R_{\mathrm{c}}}{(L_{\mathrm{a}}L_{\mathrm{b}}+L_{\mathrm{a}}L_{\mathrm{c}}+L_{\mathrm{b}}L_{\mathrm{c}})} \\ \frac{L_{\mathrm{b}}R_{\mathrm{a}}}{(L_{\mathrm{a}}L_{\mathrm{b}}+L_{\mathrm{a}}L_{\mathrm{c}}+L_{\mathrm{b}}L_{\mathrm{c}})} & \frac{L_{\mathrm{a}}R_{\mathrm{b}}}{(L_{\mathrm{a}}L_{\mathrm{b}}+L_{\mathrm{a}}L_{\mathrm{c}}+L_{\mathrm{b}}L_{\mathrm{c}})} & -\frac{(L_{\mathrm{a}}+L_{\mathrm{b}})R_{\mathrm{c}}}{(L_{\mathrm{a}}L_{\mathrm{b}}+L_{\mathrm{a}}L_{\mathrm{c}}+L_{\mathrm{b}}L_{\mathrm{c}})} \end{bmatrix} \tag{2.29}$$

$$\mathbf{B}_{\mathrm{abc}} = \begin{bmatrix} \frac{(L_\mathrm{b}+L_\mathrm{c})}{(L_\mathrm{a}L_\mathrm{b}+L_\mathrm{a}L_\mathrm{c}+L_\mathrm{b}L_\mathrm{c})} & -\frac{L_\mathrm{c}}{(L_\mathrm{a}L_\mathrm{b}+L_\mathrm{a}L_\mathrm{c}+L_\mathrm{b}L_\mathrm{c})} & -\frac{L_\mathrm{b}}{(L_\mathrm{a}L_\mathrm{b}+L_\mathrm{a}L_\mathrm{c}+L_\mathrm{b}L_\mathrm{c})} \\ -\frac{L_\mathrm{c}}{(L_\mathrm{a}L_\mathrm{b}+L_\mathrm{a}L_\mathrm{c}+L_\mathrm{b}L_\mathrm{c})} & \frac{(L_\mathrm{a}+L_\mathrm{c})}{(L_\mathrm{a}L_\mathrm{b}+L_\mathrm{a}L_\mathrm{c}+L_\mathrm{b}L_\mathrm{c})} & -\frac{L_\mathrm{a}}{(L_\mathrm{a}L_\mathrm{b}+L_\mathrm{a}L_\mathrm{c}+L_\mathrm{b}L_\mathrm{c})} \\ -\frac{L_\mathrm{b}}{(L_\mathrm{a}L_\mathrm{b}+L_\mathrm{a}L_\mathrm{c}+L_\mathrm{b}L_\mathrm{c})} & -\frac{L_\mathrm{a}}{(L_\mathrm{a}L_\mathrm{b}+L_\mathrm{a}L_\mathrm{c}+L_\mathrm{b}L_\mathrm{c})} & \frac{(L_\mathrm{a}+L_\mathrm{b})}{(L_\mathrm{a}L_\mathrm{b}+L_\mathrm{a}L_\mathrm{c}+L_\mathrm{b}L_\mathrm{c})} \end{bmatrix} \tag{2.30}$$

Setting $L = L_\mathrm{a} = L_\mathrm{b} = L_\mathrm{c}$ and $R = R_\mathrm{a} = R_\mathrm{b} = R_\mathrm{c}$, that is, assuming a symmetric three-phase system, results in

$$\mathbf{A}_{\mathrm{abc}} = -\frac{R}{L}\begin{bmatrix} +2/3 & -1/3 & -1/3 \\ -1/3 & +2/3 & -1/3 \\ -1/3 & -1/3 & +2/3 \end{bmatrix} = -\frac{R}{L}\mathbf{T} \tag{2.31}$$

$$\mathbf{B}_{\mathrm{abc}} = \frac{1}{L}\begin{bmatrix} +2/3 & -1/3 & -1/3 \\ -1/3 & +2/3 & -1/3 \\ -1/3 & -1/3 & +2/3 \end{bmatrix} = \frac{1}{L}\mathbf{T} \tag{2.32}$$

The dimensions of the state and input matrices are equal to 3×3. Note also that the matrix $\mathbf{T}$ is defined as

$$\mathbf{T} = \begin{bmatrix} +2/3 & -1/3 & -1/3 \\ -1/3 & +2/3 & -1/3 \\ -1/3 & -1/3 & +2/3 \end{bmatrix} \tag{2.33}$$

Now, a large-signal state-space model of a single two-level three-phase VSI feeding an inductive-resistive load can be given as

$$\frac{\mathrm{d}}{\mathrm{d}t}\mathbf{x}_{\mathrm{abc}} = \mathbf{A}_{\mathrm{abc}}\mathbf{x}_{\mathrm{abc}} + \mathbf{B}_{\mathrm{abc}}\mathbf{u}_{\mathrm{abc}} \tag{2.34a}$$

$$\mathbf{y}_{\mathrm{abc}} = \mathbf{C}_{\mathrm{abc}}\mathbf{x}_{\mathrm{abc}} \tag{2.34b}$$

The dimensions of the output vector $\mathbf{y}_{\mathrm{abc}} = \begin{bmatrix} y_\mathrm{a} & y_\mathrm{b} & y_\mathrm{c} \end{bmatrix}^\mathrm{T}$ equal 3×1, and since all states are measurable, the output matrix $\mathbf{C}_{\mathrm{abc}}$ is equal to an identity matrix

$$\mathbf{I} = \begin{bmatrix} 1 & 0 & 0 \\ 0 & 1 & 0 \\ 0 & 0 & 1 \end{bmatrix} \tag{2.35}$$

Multiplying (2.34a) and (2.34b) by the transformation matrix $\mathbf{T}_{\mathrm{dq0}}$ defined in (2.12) and replacing the state, input and output vectors with $\mathbf{x}_{\mathrm{abc}} = \mathbf{T}_{\mathrm{dq0}}^{-1}\mathbf{x}_{\mathrm{dq0}}$, $\mathbf{u}_{\mathrm{abc}} = \mathbf{T}_{\mathrm{dq0}}^{-1}\mathbf{u}_{\mathrm{dq0}}$ and $\mathbf{y}_{\mathrm{abc}} = \mathbf{T}_{\mathrm{dq0}}^{-1}\mathbf{y}_{\mathrm{dq0}}$, respectively, results in

$$\mathbf{T}_{\mathrm{dq0}}\frac{\mathrm{d}}{\mathrm{d}t}\left(\mathbf{T}_{\mathrm{dq0}}^{-1}\mathbf{x}_{\mathrm{dq0}}\right) = \mathbf{T}_{\mathrm{dq0}}\mathbf{A}_{\mathrm{abc}}\mathbf{T}_{\mathrm{dq0}}^{-1}\mathbf{x}_{\mathrm{dq0}} + \mathbf{T}_{\mathrm{dq0}}\mathbf{B}_{\mathrm{abc}}\mathbf{T}_{\mathrm{dq0}}^{-1}\mathbf{u}_{\mathrm{dq0}} \tag{2.36a}$$

$$\mathbf{T}_{\mathrm{dq0}}\mathbf{T}_{\mathrm{dq0}}^{-1}\mathbf{y}_{\mathrm{dq0}} = \mathbf{T}_{\mathrm{dq0}}\mathbf{C}_{\mathrm{abc}}\mathbf{T}_{\mathrm{dq0}}^{-1}\mathbf{x}_{\mathrm{dq0}} \tag{2.36b}$$

The dimensions of the state, input and output vectors which are denoted by $\mathbf{x}_{\mathrm{dq0}} = \begin{bmatrix} i_\mathrm{d} & i_\mathrm{q} & i_0 \end{bmatrix}^\mathrm{T}$, $\mathbf{u}_{\mathrm{dq0}} = \begin{bmatrix} d_\mathrm{d} & d_\mathrm{q} & d_0 \end{bmatrix}^\mathrm{T} u_{\mathrm{dc}}$, and $\mathbf{y}_{\mathrm{dq0}} = \begin{bmatrix} y_\mathrm{d} & y_\mathrm{q} & y_0 \end{bmatrix}^\mathrm{T}$, respectively, equal in all cases 3×1.

Assuming steady-state operation conditions, that is $\theta = \omega t + \theta_0$, and after some calculations, the model (2.36) can be given as

$$\frac{\mathrm{d}}{\mathrm{d}t}\mathbf{x}_{\mathrm{dq0}} = \mathbf{A}_{\mathrm{dqo}}\mathbf{x}_{\mathrm{dq0}} + \mathbf{B}_{\mathrm{dqo}}\mathbf{v}_{\mathrm{dq0}}u_{\mathrm{dc}} \tag{2.37a}$$

$$\mathbf{y}_{\mathrm{dq0}} = \mathbf{C}_{\mathrm{dqo}}\mathbf{x}_{\mathrm{dq0}} \tag{2.37b}$$

where the output matrix $\mathbf{C}_{\mathrm{dqo}}$ is an identity matrix with the dimensions of 3×3, and the state and input matrices $\mathbf{A}_{\mathrm{dqo}}$ and $\mathbf{B}_{\mathrm{dqo}}$, respectively, are defined as

$$\mathbf{A}_{\mathrm{dqo}} = -\frac{R}{L}\begin{bmatrix}1 & 0 & 0\\ 0 & 1 & 0\\ 0 & 0 & 0\end{bmatrix} + \begin{bmatrix}0 & \omega & 0\\ -\omega & 0 & 0\\ 0 & 0 & 0\end{bmatrix} = -\frac{R}{L}\mathbf{I}' + \boldsymbol{\omega} \tag{2.38}$$

$$\mathbf{B}_{\mathrm{dqo}} = \frac{1}{L}\begin{bmatrix}1 & 0 & 0\\ 0 & 1 & 0\\ 0 & 0 & 0\end{bmatrix} = \frac{1}{L}\mathbf{I}' \tag{2.39}$$

Again, the dimensions of the state and input matrices equal 3×3. Note also that the matrix $\mathbf{I}'$ is defined as

$$\mathbf{I}' = \begin{bmatrix}1 & 0 & 0\\ 0 & 1 & 0\\ 0 & 0 & 0\end{bmatrix} \tag{2.40}$$

and the matrix $\boldsymbol{\omega}$ shows the coupling between the d- and q-axes components

$$\boldsymbol{\omega} = \begin{bmatrix}0 & \omega & 0\\ -\omega & 0 & 0\\ 0 & 0 & 0\end{bmatrix} \tag{2.41}$$

To obtain a small-signal model, the model (2.37) is linearized in the steady-state operation point. The linearization is performed by calculating the Jacobian matrices and evaluating the matrices in the operation point as instructed in Subsection 2.2.3. This procedure eventually yields

$$\frac{\mathrm{d}}{\mathrm{d}t}\Delta\mathbf{x}_{\mathrm{dq0}} = \mathbf{A}_{\mathrm{dqo}}\Delta\mathbf{x}_{\mathrm{dq0}} + \mathbf{B}_{\mathrm{dqo}}\Delta\mathbf{v}_{\mathrm{dq0}} + \mathbf{B}_{\mathrm{dqo}}\Delta\mathbf{w}_{\mathrm{dq0}} \tag{2.42a}$$

$$\Delta\mathbf{y}_{\mathrm{dq0}} = \mathbf{C}_{\mathrm{dqo}}\Delta\mathbf{x}_{\mathrm{dq0}} \tag{2.42b}$$

where the state and input matrices, $\mathbf{A}_{\mathrm{dqo}}$ and $\mathbf{B}_{\mathrm{dqo}}$, are as defined in (2.38) and (2.39), respectively, and the output matrix $\mathbf{C}_{\mathrm{dqo}}$ is an identity matrix with the dimensions of 3×3. Furthermore, the vectors containing deviating variables are defined as $\Delta\mathbf{y}_{\mathrm{dq0}} = \begin{bmatrix}\Delta y_{\mathrm{d}} & \Delta y_{\mathrm{q}} & \Delta y_0\end{bmatrix}^{\mathrm{T}}$, $\Delta\mathbf{x}_{\mathrm{dq0}} = \begin{bmatrix}\Delta i_{\mathrm{d}} & \Delta i_{\mathrm{q}} & \Delta i_0\end{bmatrix}^{\mathrm{T}}$, $\Delta\mathbf{v}_{\mathrm{dq0}} = \begin{bmatrix}\Delta d_{\mathrm{d}} & \Delta d_{\mathrm{q}} & \Delta d_0\end{bmatrix}^{\mathrm{T}} U_{\mathrm{dc}}$, and $\Delta\mathbf{w}_{\mathrm{dq0}} = \begin{bmatrix}D_{\mathrm{d}} & D_{\mathrm{q}} & D_0\end{bmatrix}^{\mathrm{T}} \Delta u_{\mathrm{dc}}$. The constant duty cycles are denoted by D_{d}, D_{q} and D_0 and the constant direct voltage by U_{dc}.

2.3 Small-signal models for parallel three-phase voltage source inverters

Small-signal models for parallel two-level three-phase voltage source inverters with separate direct voltage sources and with a common direct voltage source are presented in this section. Let us, however, first consider the parallel inverter configurations in more detail and define the state and input vectors.

As can be seen in Figs. 2.3 and 2.4, common for both configurations is that the outputs of the inverters are connected in parallel through current-sharing inductors denoted by L_i. The subscript $i \in \{1, 2, ..., n\}$ denotes the index of the parallel unit and n is the number of parallel units. The resistors denoted by R_i are used to represent losses between the sources and the point of common connections. Furthermore, the inverters are used to feed a common three-phase resistive-inductive load denoted by R_{L} and L_{L}. In the following, equal output impedances of the inverters, that is, $R = R_1 = R_2 = \cdots = R_n$ and $L = L_1 = L_2 = \cdots = L_n$, are assumed just for the sake of simplicity.

Let us now define the state vectors. Since the output sides of the inverters contain $3\,(n+1)$ energy storage elements (inductors), a logical choice would be to choose all inductor currents as state variables. Recognizing that the load currents can be expressed as $i_{p,\mathrm{L}} = i_{p,1} + i_{p,2} + \cdots + i_{p,n}$, where the subscript $p \in \{a, b, c\}$ denotes the phase, we can reduce the number of state variables to $3n$. In other words, the output currents of the inverters can be chosen as state variables. Thus, the state vectors in the abc coordinates can be given as

$$\mathbf{x}_{\mathrm{abc}}^{\mathrm{sep}} = \mathbf{x}_{\mathrm{abc}}^{\mathrm{com}} = \begin{bmatrix} \mathbf{i}_{\mathrm{abc},1} \\ \mathbf{i}_{\mathrm{abc},2} \\ \vdots \\ \mathbf{i}_{\mathrm{abc},n} \end{bmatrix} \tag{2.43}$$

where the superscripts sep and com are used to indicate that the state vectors are for the parallel inverters with separate and common direct voltage sources, respectively. Furthermore, the vectors containing output currents of the individual inverters are defined as $\mathbf{i}_{\mathrm{abc},i} = \begin{bmatrix} i_{\mathrm{a},i} & i_{\mathrm{b},i} & i_{\mathrm{c},i} \end{bmatrix}^{\mathrm{T}}$. Since $i \in \{1, 2, ..., n\}$ and n is the number of parallel units, the dimensions of the state vectors equal $3n \times 1$. In the $dq0$ coordinates, the state vectors are defined as

$$\mathbf{x}_{\mathrm{dq0}}^{\mathrm{sep}} = \mathbf{x}_{\mathrm{dq0}}^{\mathrm{com}} = \begin{bmatrix} \mathbf{i}_{\mathrm{dq0},1} \\ \mathbf{i}_{\mathrm{dq0},2} \\ \vdots \\ \mathbf{i}_{\mathrm{dq0},n} \end{bmatrix} \tag{2.44}$$

The vectors containing $dq0$ coordinate currents are defined as $\mathbf{i}_{\mathrm{dq0},i} = \begin{bmatrix} i_{\mathrm{d},i} & i_{\mathrm{q},i} & i_{0,i} \end{bmatrix}^{\mathrm{T}}$. Also in this case, the dimensions of the state vectors are equal to $3n \times 1$.

Let us now define the input vectors. Similarly as in the case of a single inverter unit, the phase leg voltages of the inverters are chosen as the input variables. The input vectors can be defined in the abc coordinates as

$$\mathbf{u}_{\mathrm{abc}}^{\mathrm{sep}} = \mathbf{u}_{\mathrm{abc}}^{\mathrm{com}} = \begin{bmatrix} \mathbf{u}_{\mathrm{abc},1} \\ \mathbf{u}_{\mathrm{abc},2} \\ \vdots \\ \mathbf{u}_{\mathrm{abc},n} \end{bmatrix} \tag{2.45}$$

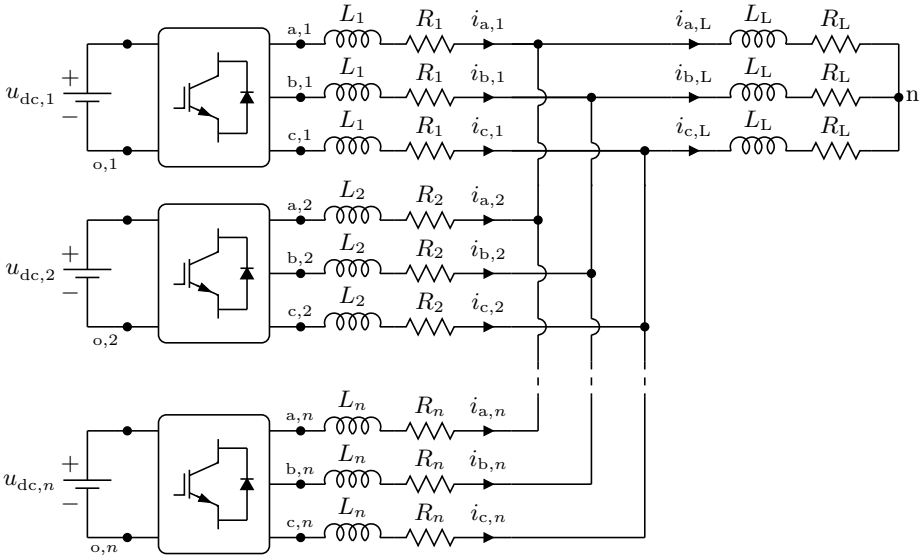

Fig. 2.3: Parallel three-phase voltage source inverters with separate direct voltage sources feeding a resistive-inductive load.

The vectors containing the phase leg voltages of the individual inverters are defined in the case of parallel inverters with separate direct voltage links as $\mathbf{u}_{\mathrm{abc},i} = \begin{bmatrix} d_{\mathrm{a},i} & d_{\mathrm{b},i} & d_{\mathrm{c},i} \end{bmatrix}^{\mathrm{T}} u_{\mathrm{dc},i}$ and in the case of a common direct voltage link as $\mathbf{u}_{\mathrm{abc},i} = \begin{bmatrix} d_{\mathrm{a},i} & d_{\mathrm{b},i} & d_{\mathrm{c},i} \end{bmatrix}^{\mathrm{T}} u_{\mathrm{dc}}$. Again, since $i \in \{1, 2, ..., n\}$ and n is the number of parallel units, the dimensions of the input vectors equal $3n \times 1$. In the $dq0$ coordinates, the input vectors are defined as

$$\mathbf{u}_{\mathrm{dq0}}^{\mathrm{sep}} = \mathbf{u}_{\mathrm{dq0}}^{\mathrm{com}} = \begin{bmatrix} \mathbf{u}_{\mathrm{dq0},1} \\ \mathbf{u}_{\mathrm{dq0},2} \\ \vdots \\ \mathbf{u}_{\mathrm{dq0},n} \end{bmatrix} \tag{2.46}$$

The vectors containing $dq0$ coordinate voltages are defined in the case of parallel inverters with separate direct voltage links as $\mathbf{u}_{\mathrm{dq0},i} = \begin{bmatrix} d_{\mathrm{d},i} & d_{\mathrm{q},i} & d_{0,i} \end{bmatrix}^{\mathrm{T}} u_{\mathrm{dc},i}$ and in the case of a common direct voltage link as $\mathbf{u}_{\mathrm{dq0},i} = \begin{bmatrix} d_{\mathrm{d},i} & d_{\mathrm{q},i} & d_{0,i} \end{bmatrix}^{\mathrm{T}} u_{\mathrm{dc}}$. Also in this case, the dimensions of the input vectors are equal to $3n \times 1$.

2.3.1 Parallel inverters with separate direct voltage sources

For the parallel inverters with separate direct voltage sources, we can write $2n$ differential equations and n algebraic equations by applying Kirchhoff's voltage and current laws. The algebraic equations are obtained by applying KCL to nodes o,i, $i \in \{1, 2, ..., n\}$. The differential equations, again, are obtained by applying KVL to loops that are formed between the inverters and between the inverters and the load. Differentiating the algebraic equations, writing the set of differential equations in the form (2.24), and applying (2.26) results in a large-signal state-space

model expressed in the stationary abc coordinates

$$\frac{\mathrm{d}}{\mathrm{d}t}\mathbf{x}_{\mathrm{abc}}^{\mathrm{sep}} = \mathbf{A}_{\mathrm{abc}}^{\mathrm{sep}}\mathbf{x}_{\mathrm{abc}}^{\mathrm{sep}} + \mathbf{B}_{\mathrm{abc}}^{\mathrm{sep}}\mathbf{u}_{\mathrm{abc}}^{\mathrm{sep}} \tag{2.47a}$$

$$\mathbf{y}_{\mathrm{abc}}^{\mathrm{sep}} = \mathbf{C}_{\mathrm{abc}}^{\mathrm{sep}}\mathbf{x}_{\mathrm{abc}}^{\mathrm{sep}} \tag{2.47b}$$

where the state matrix is defined as

$$\mathbf{A}_{\mathrm{abc}}^{\mathrm{sep}} = \underbrace{-\frac{R}{L}\begin{bmatrix} \frac{n-1}{n}\mathbf{T} & -\frac{1}{n}\mathbf{T} & \cdots & -\frac{1}{n}\mathbf{T} \\ -\frac{1}{n}\mathbf{T} & \frac{n-1}{n}\mathbf{T} & \ddots & \vdots \\ \vdots & \ddots & \ddots & -\frac{1}{n}\mathbf{T} \\ -\frac{1}{n}\mathbf{T} & \cdots & -\frac{1}{n}\mathbf{T} & \frac{n-1}{n}\mathbf{T} \end{bmatrix}}_{\text{"circulating current part"}} \underbrace{-\frac{1}{n}\frac{(R+nR_{\mathrm{L}})}{(L+nL_{\mathrm{L}})}\begin{bmatrix} \mathbf{T} & \mathbf{T} & \cdots & \mathbf{T} \\ \mathbf{T} & \mathbf{T} & \ddots & \vdots \\ \vdots & \ddots & \ddots & \mathbf{T} \\ \mathbf{T} & \cdots & \mathbf{T} & \mathbf{T} \end{bmatrix}}_{\text{"load current part"}} \tag{2.48}$$

and the input matrix as

$$\mathbf{B}_{\mathrm{abc}}^{\mathrm{sep}} = \underbrace{\frac{1}{L}\begin{bmatrix} \frac{n-1}{n}\mathbf{T} & -\frac{1}{n}\mathbf{T} & \cdots & -\frac{1}{n}\mathbf{T} \\ -\frac{1}{n}\mathbf{T} & \frac{n-1}{n}\mathbf{T} & \ddots & \vdots \\ \vdots & \ddots & \ddots & -\frac{1}{n}\mathbf{T} \\ -\frac{1}{n}\mathbf{T} & \cdots & -\frac{1}{n}\mathbf{T} & \frac{n-1}{n}\mathbf{T} \end{bmatrix}}_{\text{"circulating current part"}} + \underbrace{\frac{1}{n}\frac{1}{(L+nL_{\mathrm{L}})}\begin{bmatrix} \mathbf{T} & \mathbf{T} & \cdots & \mathbf{T} \\ \mathbf{T} & \mathbf{T} & \ddots & \vdots \\ \vdots & \ddots & \ddots & \mathbf{T} \\ \mathbf{T} & \cdots & \mathbf{T} & \mathbf{T} \end{bmatrix}}_{\text{"load current part"}} \tag{2.49}$$

The dimensions of the state and input matrices are equal to $3n \times 3n$ and the matrix $\mathbf{T}$ is as defined in (2.33). The output matrix $\mathbf{C}_{\mathrm{abc}}^{\mathrm{sep}}$ is an identity matrix with the dimensions of $3n \times 3n$. Interestingly, the state and input matrices can be divided into two parts, which are termed as "a circulating current part" and "a load current part". The circulating current part shows the dynamics of the currents, which can be excited by the phase leg voltage differences, while the load current part shows the dynamics of the currents, which are dependent on the average phase leg voltages.

Applying the transformation matrix $\mathbf{T}_{\mathrm{dq0}}$ defined in (2.12) and the relationship between the abc and $dq0$ variables (2.13), the model (2.47) can be transformed into a model expressed in the $dq0$ coordinates

$$\frac{\mathrm{d}}{\mathrm{d}t}\mathbf{x}_{\mathrm{dq0}}^{\mathrm{sep}} = \mathbf{A}_{\mathrm{dqo}}^{\mathrm{sep}}\mathbf{x}_{\mathrm{dq0}}^{\mathrm{sep}} + \mathbf{B}_{\mathrm{dqo}}^{\mathrm{sep}}\mathbf{u}_{\mathrm{dq0}}^{\mathrm{sep}} \tag{2.50a}$$

$$\mathbf{y}_{\mathrm{dq0}}^{\mathrm{sep}} = \mathbf{C}_{\mathrm{dqo}}^{\mathrm{sep}}\mathbf{x}_{\mathrm{dq0}}^{\mathrm{sep}} \tag{2.50b}$$

where the state matrix is defined as

$$\mathbf{A}_{\mathrm{dqo}}^{\mathrm{sep}} = \overbrace{-\begin{bmatrix} \boldsymbol{\omega} & \mathbf{0} & \mathbf{0} & \mathbf{0} \\ \mathbf{0} & \boldsymbol{\omega} & \ddots & \mathbf{0} \\ \mathbf{0} & \ddots & \ddots & \mathbf{0} \\ \mathbf{0} & \mathbf{0} & \mathbf{0} & \boldsymbol{\omega} \end{bmatrix}}^{\text{"coupling terms"}} \overbrace{-\frac{R}{L}\begin{bmatrix} \frac{n-1}{n}\mathbf{I}' & -\frac{1}{n}\mathbf{I}' & \cdots & -\frac{1}{n}\mathbf{I}' \\ -\frac{1}{n}\mathbf{I}' & \frac{n-1}{n}\mathbf{I}' & \cdots & \vdots \\ \vdots & \ddots & \ddots & -\frac{1}{n}\mathbf{I}' \\ -\frac{1}{n}\mathbf{I}' & \cdots & -\frac{1}{n}\mathbf{I}' & \frac{n-1}{n}\mathbf{T} \end{bmatrix}}^{\text{"circulating current part"}} \underbrace{-\frac{1}{n}\frac{(R+nR_{\mathrm{L}})}{(L+nL_{\mathrm{L}})}\begin{bmatrix} \mathbf{I}' & \mathbf{I}' & \cdots & \mathbf{I}' \\ \mathbf{I}' & \mathbf{I}' & \ddots & \vdots \\ \vdots & \ddots & \ddots & \mathbf{I}' \\ \mathbf{I}' & \cdots & \mathbf{I}' & \mathbf{T} \end{bmatrix}}_{\text{"load current part"}} \tag{2.51}$$

and the input matrix as

$$\mathbf{B}_{\mathrm{dqo}}^{\mathrm{sep}} = \underbrace{\frac{1}{L}\begin{bmatrix} \frac{n-1}{n}\mathbf{I}' & -\frac{1}{n}\mathbf{I}' & \cdots & -\frac{1}{n}\mathbf{I}' \\ -\frac{1}{n}\mathbf{I}' & \frac{n-1}{n}\mathbf{I}' & \ddots & \vdots \\ \vdots & \ddots & \ddots & -\frac{1}{n}\mathbf{I}' \\ -\frac{1}{n}\mathbf{I}' & \cdots & -\frac{1}{n}\mathbf{I}' & \frac{n-1}{n}\mathbf{I}' \end{bmatrix}}_{\text{"circulating current part"}} + \underbrace{\frac{1}{n}\frac{1}{(L+nL_{\mathrm{L}})}\begin{bmatrix} \mathbf{I}' & \mathbf{I}' & \cdots & \mathbf{I}' \\ \mathbf{I}' & \mathbf{I}' & \ddots & \vdots \\ \vdots & \ddots & \ddots & \mathbf{I}' \\ \mathbf{I}' & \cdots & \mathbf{I}' & \mathbf{I}' \end{bmatrix}}_{\text{"load current part"}} \tag{2.52}$$

The dimensions of the state and input matrices equal $3n \times 3n$. Furthermore, the matrices $\mathbf{I}'$ and $\boldsymbol{\omega}$ are as defined in (2.40) and (2.41), respectively. The output matrix $\mathbf{C}_{\mathrm{dqo}}^{\mathrm{sep}}$, again, is an identity matrix with the dimensions of $3n \times 3n$.

Linearization of the model (2.50) results in

$$\frac{\mathrm{d}}{\mathrm{d}t}\Delta\mathbf{x}_{\mathrm{dq0}}^{\mathrm{sep}} = \mathbf{A}_{\mathrm{dqo}}^{\mathrm{sep}}\Delta\mathbf{x}_{\mathrm{abc}}^{\mathrm{sep}} + \mathbf{B}_{\mathrm{dqo}}^{\mathrm{sep}}\Delta\mathbf{v}_{\mathrm{dq0}}^{\mathrm{sep}} + \mathbf{B}_{\mathrm{dqo}}^{\mathrm{sep}}\Delta\mathbf{w}_{\mathrm{dq0}}^{\mathrm{sep}} \tag{2.53a}$$

$$\Delta\mathbf{y}_{\mathrm{dq0}}^{\mathrm{sep}} = \mathbf{C}_{\mathrm{dqo}}^{\mathrm{sep}}\Delta\mathbf{x}_{\mathrm{dq0}}^{\mathrm{sep}} \tag{2.53b}$$

where the state and input matrices, $\mathbf{A}_{\mathrm{dqo}}^{\mathrm{sep}}$ and $\mathbf{B}_{\mathrm{dqo}}^{\mathrm{sep}}$, are as defined in (2.51) and (2.52), respectively, and the output matrix $\mathbf{C}_{\mathrm{dqo}}^{\mathrm{sep}}$ is an identity matrix with the dimensions of $3n \times 3n$. The vectors containing deviating variables are defined as

$$\Delta\mathbf{y}_{\mathrm{dq0}}^{\mathrm{sep}} = \begin{bmatrix} \Delta\mathbf{y}_{\mathrm{dq0},1} \\ \Delta\mathbf{y}_{\mathrm{dq0},2} \\ \vdots \\ \Delta\mathbf{y}_{\mathrm{dq0},n} \end{bmatrix} \tag{2.54}$$

$$\Delta\mathbf{x}_{\mathrm{dq0}}^{\mathrm{sep}} = \begin{bmatrix} \Delta\mathbf{x}_{\mathrm{dq0},1} \\ \Delta\mathbf{x}_{\mathrm{dq0},2} \\ \vdots \\ \Delta\mathbf{x}_{\mathrm{dq0},n} \end{bmatrix} \tag{2.55}$$

$$\Delta\mathbf{v}_{\mathrm{dq0}}^{\mathrm{sep}} = \begin{bmatrix} \Delta\mathbf{v}_{\mathrm{dq0},1} \\ \Delta\mathbf{v}_{\mathrm{dq0},2} \\ \vdots \\ \Delta\mathbf{v}_{\mathrm{dq0},n} \end{bmatrix} \tag{2.56}$$

$$\Delta\mathbf{w}_{\mathrm{dq0}}^{\mathrm{sep}} = \begin{bmatrix} \Delta\mathbf{w}_{\mathrm{dq0},1} \\ \Delta\mathbf{w}_{\mathrm{dq0},2} \\ \vdots \\ \Delta\mathbf{w}_{\mathrm{dq0},n} \end{bmatrix} \tag{2.57}$$

Furthermore, the vectors containing deviating variables of individual inverters are defined as $\Delta\mathbf{y}_{\mathrm{dq0},i} = \begin{bmatrix}\Delta y_{\mathrm{d},i} & \Delta y_{\mathrm{q},i} & \Delta y_{0,i}\end{bmatrix}^{\mathrm{T}}$, $\Delta\mathbf{x}_{\mathrm{dq0},i} = \begin{bmatrix}\Delta i_{\mathrm{d},i} & \Delta i_{\mathrm{q},i} & \Delta i_{0,i}\end{bmatrix}^{\mathrm{T}}$, $\Delta\mathbf{v}_{\mathrm{dq0},i} = \begin{bmatrix}\Delta d_{\mathrm{d},i} & \Delta d_{\mathrm{q},i} & \Delta d_{0,i}\end{bmatrix}^{\mathrm{T}} U_{\mathrm{dc},i}$, and $\Delta\mathbf{w}_{\mathrm{dq0},i} = \begin{bmatrix}D_{\mathrm{d},i} & D_{\mathrm{q},i} & D_{0,i}\end{bmatrix}^{\mathrm{T}} \Delta u_{\mathrm{dc},i}$, $i \in \{1, 2, ..., n\}$. Therefore, the dimensions of the vectors defined by (2.54), (2.55), (2.56), and (2.57) equal $3n \times 1$. The constant duty cycles are denoted by $D_{\mathrm{d},i}$, $D_{\mathrm{q},i}$ and $D_{0,i}$ and the constant direct voltages by $U_{\mathrm{dc},i}$.

2.3.2 Parallel inverters with a common direct voltage source

For the parallel inverters with a common dc voltage source, we can write $3n - 1$ differential equations and one algebraic equation by applying Kirchhoff's voltage and current laws. The algebraic equation is obtained by applying KCL to node o or n. The differential equations, again, are obtained by applying KVL to loops that are formed between the inverters and between the inverters and the load. Differentiating the algebraic equation, writing the set of differential equations in the form (2.24) and applying (2.26) results in a large-signal state-space model expressed in the stationary abc coordinates

$$\frac{\mathrm{d}}{\mathrm{d}t}\mathbf{x}_{\mathrm{abc}}^{\mathrm{com}} = \mathbf{A}_{\mathrm{abc}}^{\mathrm{com}}\mathbf{x}_{\mathrm{abc}}^{\mathrm{com}} + \mathbf{B}_{\mathrm{abc}}^{\mathrm{com}}\mathbf{u}_{\mathrm{abc}}^{\mathrm{com}} \tag{2.58a}$$

$$\mathbf{y}_{\mathrm{abc}}^{\mathrm{com}} = \mathbf{C}_{\mathrm{abc}}^{\mathrm{com}}\mathbf{x}_{\mathrm{abc}}^{\mathrm{com}} \tag{2.58b}$$

where the state matrix is defined as

$$\mathbf{A}_{\mathrm{abc}}^{\mathrm{com}} = \underbrace{-\frac{R}{L}\begin{bmatrix} \frac{n-1}{n}\mathbf{I} & -\frac{1}{n}\mathbf{I} & \cdots & -\frac{1}{n}\mathbf{I} \\ -\frac{1}{n}\mathbf{I} & \frac{n-1}{n}\mathbf{I} & \ddots & \vdots \\ \vdots & \ddots & \ddots & -\frac{1}{n}\mathbf{I} \\ -\frac{1}{n}\mathbf{I} & \cdots & -\frac{1}{n}\mathbf{I} & \frac{n-1}{n}\mathbf{I} \end{bmatrix}}_{\text{"circulating current part"}} \underbrace{-\frac{1}{n}\frac{(R+nR_{\mathrm{L}})}{(L+nL_{\mathrm{L}})}\begin{bmatrix} \mathbf{T} & \mathbf{T} & \cdots & \mathbf{T} \\ \mathbf{T} & \mathbf{T} & \ddots & \vdots \\ \vdots & \ddots & \ddots & \mathbf{T} \\ \mathbf{T} & \cdots & \mathbf{T} & \mathbf{T} \end{bmatrix}}_{\text{"load current part"}} \tag{2.59}$$

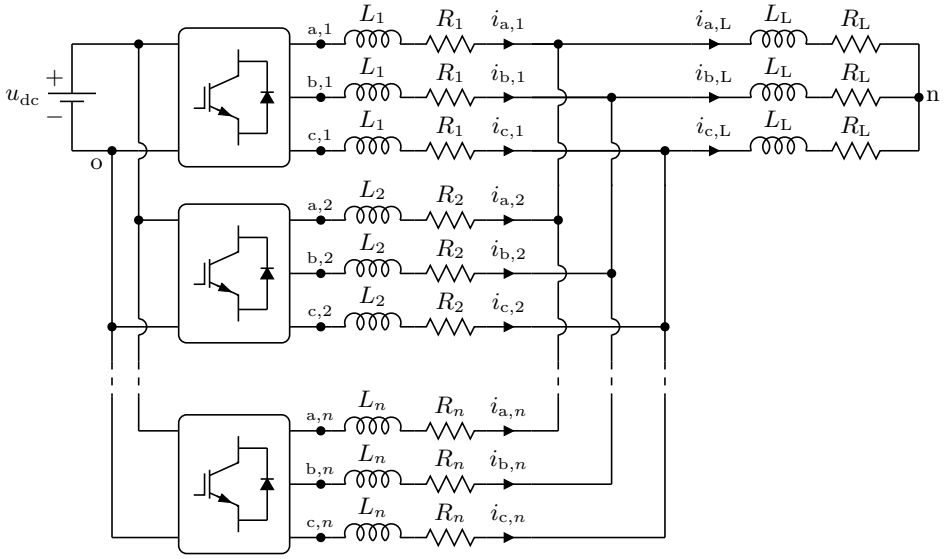

Fig. 2.4: Parallel three-phase voltage source inverters with a common direct voltage source feeding a resistive-inductive load.

and the input matrix as

$$\mathbf{B}_{\mathrm{abc}}^{\mathrm{com}} = \underbrace{\frac{1}{L}\begin{bmatrix} \frac{n-1}{n}\mathbf{I} & -\frac{1}{n}\mathbf{I} & \cdots & -\frac{1}{n}\mathbf{I} \\ -\frac{1}{n}\mathbf{I} & \frac{n-1}{n}\mathbf{I} & \ddots & \vdots \\ \vdots & \ddots & \ddots & -\frac{1}{n}\mathbf{I} \\ -\frac{1}{n}\mathbf{I} & \cdots & -\frac{1}{n}\mathbf{I} & \frac{n-1}{n}\mathbf{I} \end{bmatrix}}_{\text{"circulating current part"}} + \underbrace{\frac{1}{n}\frac{1}{(L+nL_{\mathrm{L}})}\begin{bmatrix} \mathbf{T} & \mathbf{T} & \cdots & \mathbf{T} \\ \mathbf{T} & \mathbf{T} & \ddots & \vdots \\ \vdots & \ddots & \ddots & \mathbf{T} \\ \mathbf{T} & \cdots & \mathbf{T} & \mathbf{T} \end{bmatrix}}_{\text{"load current part"}} \tag{2.60}$$

The dimensions of the state and input matrices are equal to $3n \times 3n$ and the matrices $\mathbf{T}$ and $\mathbf{I}$ are as defined in (2.33) and (2.35), respectively. The output matrix $\mathbf{C}_{\mathrm{abc}}^{\mathrm{com}}$ is an identity matrix with the dimensions of $3n \times 3n$. Interestingly, the only difference between the state matrices (2.48) and (2.59) and the input matrices (2.49) and (2.60) is in the circulating current parts. In the case of separate direct voltage sources, the circulating current part contains the matrix $\mathbf{T}$ defined in (2.33), while in the case of a common direct voltage source, the circulating current part contains the matrix $\mathbf{I}$ defined in (2.35). Although this difference may seem to be insignificant, it has an influence on how the current sharing between the parallel inverters can be affected, as will be analyzed and illustrated in the subsequent sections. Applying the transformation matrix $\mathbf{T}_{\mathrm{dq0}}$ and the relationship between the abc and $dq0$ variables (2.13), the stationary reference frame model (2.58) can be transformed into a model expressed in the $dq0$ coordinates

$$\frac{\mathrm{d}}{\mathrm{d}t}\mathbf{x}_{\mathrm{dq0}}^{\mathrm{com}} = \mathbf{A}_{\mathrm{dqo}}^{\mathrm{com}}\mathbf{x}_{\mathrm{dq0}}^{\mathrm{com}} + \mathbf{B}_{\mathrm{dqo}}^{\mathrm{com}}\mathbf{u}_{\mathrm{dq0}}^{\mathrm{com}} \tag{2.61a}$$

$$\mathbf{y}_{\mathrm{dq0}}^{\mathrm{com}} = \mathbf{C}_{\mathrm{dqo}}^{\mathrm{com}}\mathbf{x}_{\mathrm{dq0}}^{\mathrm{com}} \tag{2.61b}$$

where the state matrix is defined as

$$\mathbf{A}_{\mathrm{dqo}}^{\mathrm{com}} = -\overbrace{\begin{bmatrix} \boldsymbol{\omega} & \mathbf{0} & \mathbf{0} & \mathbf{0} \\ \mathbf{0} & \boldsymbol{\omega} & \ddots & \mathbf{0} \\ \mathbf{0} & \ddots & \ddots & \mathbf{0} \\ \mathbf{0} & \mathbf{0} & \mathbf{0} & \boldsymbol{\omega} \end{bmatrix}}^{\text{"coupling terms"}} - \frac{R}{L}\overbrace{\begin{bmatrix} \frac{n-1}{n}\mathbf{I} & -\frac{1}{n}\mathbf{I} & \cdots & -\frac{1}{n}\mathbf{I} \\ -\frac{1}{n}\mathbf{I} & \frac{n-1}{n}\mathbf{I} & \ddots & \vdots \\ \vdots & \ddots & \ddots & -\frac{1}{n}\mathbf{I} \\ -\frac{1}{n}\mathbf{I} & \cdots & -\frac{1}{n}\mathbf{I} & \frac{n-1}{n}\mathbf{T} \end{bmatrix}}^{\text{"circulating current part"}} \underbrace{- \frac{1}{n}\frac{(R+nR_{\mathrm{L}})}{(L+nL_{\mathrm{L}})}\begin{bmatrix} \mathbf{I}' & \mathbf{I}' & \cdots & \mathbf{I}' \\ \mathbf{I}' & \mathbf{I}' & \ddots & \vdots \\ \vdots & \ddots & \ddots & \mathbf{I}' \\ \mathbf{I}' & \cdots & \mathbf{I}' & \mathbf{T} \end{bmatrix}}_{\text{"load current part"}} \tag{2.62}$$

and the input matrix as

$$\mathbf{B}_{\mathrm{dqo}}^{\mathrm{com}} = \underbrace{\frac{1}{L}\begin{bmatrix} \frac{n-1}{n}\mathbf{I} & -\frac{1}{n}\mathbf{I} & \cdots & -\frac{1}{n}\mathbf{I} \\ -\frac{1}{n}\mathbf{I} & \frac{n-1}{n}\mathbf{I} & \ddots & \vdots \\ \vdots & \ddots & \ddots & -\frac{1}{n}\mathbf{I} \\ -\frac{1}{n}\mathbf{I} & \cdots & -\frac{1}{n}\mathbf{I} & \frac{n-1}{n}\mathbf{I} \end{bmatrix}}_{\text{"circulating current part"}} + \underbrace{\frac{1}{n}\frac{1}{(L+nL_{\mathrm{L}})}\begin{bmatrix} \mathbf{I}' & \mathbf{I}' & \cdots & \mathbf{I}' \\ \mathbf{I}' & \mathbf{I}' & \ddots & \vdots \\ \vdots & \ddots & \ddots & \mathbf{I}' \\ \mathbf{I}' & \cdots & \mathbf{I}' & \mathbf{I}' \end{bmatrix}}_{\text{"load current part"}} \tag{2.63}$$

The dimensions of the state and input matrices equal $3n \times 3n$ and the matrices $\mathbf{I}$, $\mathbf{I}'$ and $\boldsymbol{\omega}$ are as defined in (2.35), (2.40), and (2.41), respectively. The output matrix $\mathbf{C}_{\mathrm{dqo}}^{\mathrm{com}}$, again, is an identity matrix with the dimensions of $3n \times 3n$.

Linearization of the model (2.61) results in

$$\frac{\mathrm{d}}{\mathrm{d}t}\Delta\mathbf{x}_{\mathrm{dq0}}^{\mathrm{com}} = \mathbf{A}_{\mathrm{dqo}}^{\mathrm{com}}\Delta\mathbf{x}_{\mathrm{abc}}^{\mathrm{com}} + \mathbf{B}_{\mathrm{dqo}}^{\mathrm{com}}\Delta\mathbf{v}_{\mathrm{dq0}}^{\mathrm{com}} + \mathbf{B}_{\mathrm{dqo}}^{\mathrm{com}}\Delta\mathbf{w}_{\mathrm{dq0}}^{\mathrm{com}} \tag{2.64a}$$

$$\Delta\mathbf{y}_{\mathrm{dq0}}^{\mathrm{com}} = \mathbf{C}_{\mathrm{dqo}}^{\mathrm{com}}\Delta\mathbf{x}_{\mathrm{dq0}}^{\mathrm{com}} \tag{2.64b}$$

where the state and input matrices, $\mathbf{A}_{\mathrm{dqo}}^{\mathrm{com}}$ and $\mathbf{B}_{\mathrm{dqo}}^{\mathrm{com}}$, are as defined in (2.62) and (2.63), respectively, and the output matrix $\mathbf{C}_{\mathrm{dqo}}^{\mathrm{com}}$ is an identity matrix with the dimensions of $3n \times 3n$. The vectors containing deviating variables are defined as

$$\Delta\mathbf{y}_{\mathrm{dq0}}^{\mathrm{com}} = \begin{bmatrix} \Delta\mathbf{y}_{\mathrm{dq0},1} \\ \Delta\mathbf{y}_{\mathrm{dq0},2} \\ \vdots \\ \Delta\mathbf{y}_{\mathrm{dq0},n} \end{bmatrix} \tag{2.65}$$

$$\Delta\mathbf{x}_{\mathrm{dq0}}^{\mathrm{com}} = \begin{bmatrix} \Delta\mathbf{x}_{\mathrm{dq0},1} \\ \Delta\mathbf{x}_{\mathrm{dq0},2} \\ \vdots \\ \Delta\mathbf{x}_{\mathrm{dq0},n} \end{bmatrix} \tag{2.66}$$

$$\Delta\mathbf{v}_{\mathrm{dq0}}^{\mathrm{com}} = \begin{bmatrix} \Delta\mathbf{v}_{\mathrm{dq0},1} \\ \Delta\mathbf{v}_{\mathrm{dq0},2} \\ \vdots \\ \Delta\mathbf{v}_{\mathrm{dq0},n} \end{bmatrix} \tag{2.67}$$

$$\Delta\mathbf{w}_{\mathrm{dq0}}^{\mathrm{com}} = \begin{bmatrix} \Delta\mathbf{w}_{\mathrm{dq0},1} \\ \Delta\mathbf{w}_{\mathrm{dq0},2} \\ \vdots \\ \Delta\mathbf{w}_{\mathrm{dq0},n} \end{bmatrix} \tag{2.68}$$

Furthermore, the vectors containing deviating variables of individual inverters are defined as $\Delta\mathbf{y}_{\mathrm{dq0},i} = \begin{bmatrix}\Delta y_{\mathrm{d},i} & \Delta y_{\mathrm{q},i} & \Delta y_{0,i}\end{bmatrix}^{\mathrm{T}}$, $\Delta\mathbf{x}_{\mathrm{dq0},i} = \begin{bmatrix}\Delta i_{\mathrm{d},i} & \Delta i_{\mathrm{q},i} & \Delta i_{0,i}\end{bmatrix}^{\mathrm{T}}$, $\Delta\mathbf{v}_{\mathrm{dq0},i} = \begin{bmatrix}\Delta d_{\mathrm{d},i} & \Delta d_{\mathrm{q},i} & \Delta d_{0,i}\end{bmatrix}^{\mathrm{T}} U_{\mathrm{dc}}$, and $\Delta\mathbf{w}_{\mathrm{dq0},i} = \begin{bmatrix}D_{\mathrm{d},i} & D_{\mathrm{q},i} & D_{0,i}\end{bmatrix}^{\mathrm{T}} \Delta u_{\mathrm{dc}}$, $i \in \{1, 2, ..., n\}$. Thus, the dimensions of the vectors defined by (2.65), (2.66), (2.67), and (2.68) equal $3n \times 1$. The constant duty cycles, again, are denoted by $D_{\mathrm{d},i}$, $D_{\mathrm{q},i}$ and $D_{0,i}$ and the constant direct voltage by U_{dc}.

2.4 Discussion

In this chapter, small-signal models for two different parallel two-level three-phase VSI configurations were developed. In both cases, the models were developed for n parallel units. Besides the development of models, the applied modeling procedure was explained in detail for the sake of reproducibility.

The developed models (2.50) and (2.61) show that in the case of parallel inverters with a common direct voltage source, zero-sequence current paths appear between the inverters, while in the case of separate direct voltage sources such paths do not exist. The zero-sequence current paths may, however, also appear in the case of parallel inverters with separate direct voltage sources. To be precise, such paths appear if the direct voltage sources are not isolated (Itkonen et al., 2008). Let us consider this briefly with the help of two parallel voltage source frequency converters depicted in Fig. 2.5.

The direct voltage links of the frequency converters are fed by full-bridge diode rectifier bridges that are used to convert the supplied alternating voltage into direct voltage. Since the inputs of the rectifier bridges are not galvanically isolated, the direct voltage sources of the inverters are separate but non-isolated. Because of this, the output inductors of the inverters may connect as an inductive load to a "rectifier" that comprises the top diodes of one rectifier bridge and the bottom switches of the other rectifier bridge. Furthermore, since this "rectifier" does not contain a filtering capacitor, a zero-sequence current may flow from the alternating voltage source, through the frequency converters, and back into the alternating voltage source whenever the inverters apply different switching states.

In the worst case, all upper switches of one inverter bridge and all lower switches of the other inverter bridge are closed at the same time. In such cases, a pure zero-sequence current path appears through the frequency converters. The term 'pure zero-sequence current' refers to the current that shows up only in the 0-axis (Xing et al., 1999). This example shows that although it was claimed that in the case of parallel inverters with separate direct voltage sources,

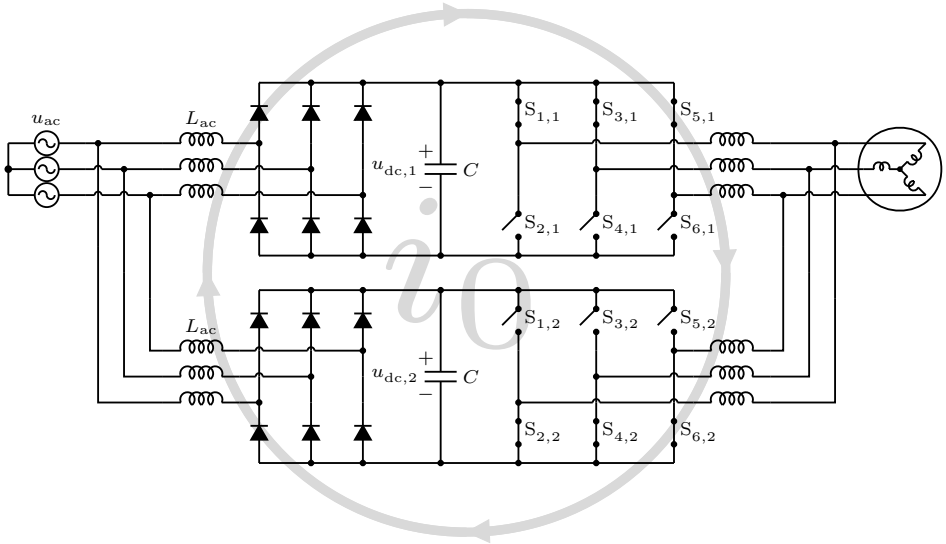

Fig. 2.5: Parallel voltage source frequency converters with separate but non-isolated dc links. When inverters apply different switching states, zero-sequence current paths may appear through the frequency converters. The resulting zero-sequence currents are excited by the supplied ac voltages.

zero-sequence current paths do not exist, a zero-sequence current may nevertheless flow through the inverters. These zero-sequence currents are not, however, excited by the direct voltage link voltages as in the case of parallel inverters with a common direct voltage source as the developed parallel inverter models suggest.

Chapter 3

Circulating current modeling and analysis of parallel voltage source inverters

The previous chapter addressed small-signal modeling of two kinds of parallel two-level three-phase voltage source inverter configurations. In this chapter, circulating current models are developed for both configurations to explain the circulating current dynamics. The circulating current models are developed for an arbitrary number of parallel units. Although the developed models are basically used only to analyze the circulating current generation mechanisms, they can also be used in the design of circulating current controllers. Despite the fact that the circulating current control design is outside the scope of this dissertation, also some subjects related to the circulating current control are considered in this chapter.

3.1 Definition of circulating current

The term circulating current has been widely adopted to describe currents that flow between parallel-operating converter units (Pöllänen et al., 2005; Zhang et al., 2009a; Chen, 2009a). Therefore, this term is used in this dissertation also. Generally speaking, a circulating current can be considered to be a current that deviates from the desired current level. Usually, the desired current level equals the load current divided by the number of parallel units (Pan and Liao, 2007). In other words, a circulating current equals zero when the load current is shared equally between the units. Sometimes the target may be to share the load current unequally between the parallel units. In these cases, the desired current level can be expressed as a certain proportion of the load current (Pan and Liao, 2008).

A mathematical circulating current definition presented by Pan and Liao (2007) defines circulating currents as

$$c_{k,j} = \sum_{m=1}^{n} \frac{i_{k,j} - i_{k,m}}{n} \quad , \quad \begin{array}{l} k \in \{\mathrm{a}, \mathrm{b}, \mathrm{c}\} \\ j, m \in \{1, 2, \ldots, n\} \end{array} \tag{3.1}$$

where j and m are used to indicate the index of the parallel unit and k denotes the phase. An alternative and more general mathematical definition of circulating current was presented by Pan and Liao (2008); they define circulating currents as

$$c_{k,j} = \sum_{m=1}^{n} (h_m i_{k,j} - h_j i_{k,m}) \quad , \quad \begin{array}{l} k \in \{\mathrm{a}, \mathrm{b}, \mathrm{c}\} \\ j, m \in \{1, 2, \ldots, n\} \end{array} \tag{3.2}$$

where j and m, again, are used to indicate the index of the parallel units and k denotes the phase. Furthermore, h_j and h_m are distribution factors of the j^{th} and m^{th} converter, respectively. The

sum of distribution factors equals $\sum_{j=1}^{n} h_j = 1$. By setting the distribution factors $h_j = 1/n$, the definition (3.2) simplifies into (3.1). Thus, the definition (3.1) is included in (3.2) as a special case. Although both of the above definitions were originally derived for each phase of each parallel unit, they can be applied also when currents are expressed in some other coordinate system than in the abc coordinates.

3.2 Circulating current modeling

In this section, circulating current models are presented for both of the parallel inverter configurations considered in the previous chapter. The models are derived and presented in the Laplace domain. For simplicity, it is assumed that the direct voltage link voltages are constant. In other words, the terms denoted by $\mathbf{w}_{\mathrm{dq0}}^{\mathrm{sep}}$ and $\mathbf{w}_{\mathrm{dq0}}^{\mathrm{com}}$ in the small-signal models (2.53) and (2.64) are set to zero. As a consequence of this assumption, also the state-space models expressed in the abc coordinates (2.47) and (2.58) can be considered as linear models. Thus, we can apply the derivation procedure described in the following to the abc coordinate models also.

The derivation of the circulating current models is performed in two stages. In the first stage, transfer function matrices are obtained from the state-space models applying

$$\mathbf{G}\left(s\right) = \frac{\mathbf{Y}\left(s\right)}{\mathbf{U}\left(s\right)} = \mathbf{C}\left(s\mathbf{I} - \mathbf{A}\right)^{-1}\mathbf{B} + \mathbf{D} \tag{3.3}$$

where $\mathbf{G}\left(s\right)$ indicates a transfer function matrix, the input and output vectors are denoted by $\mathbf{Y}\left(s\right)$ and $\mathbf{U}\left(s\right)$, respectively, and $\mathbf{A}$, $\mathbf{B}$, $\mathbf{C}$, and $\mathbf{D}$ are the state, input, output, and feedforward matrices, respectively. Furthermore, the matrix $\mathbf{I}$ is an identity matrix with the appropriate dimensions. Then, in the second stage, circulating current models are obtained by applying the definition (3.1) to the input-output models defined as

$$\mathbf{Y}\left(s\right) = \mathbf{G}\left(s\right)\mathbf{U}\left(s\right) \tag{3.4}$$

The input and output vectors and transfer function matrices of the resulting circulating current models are denoted by $\mathbf{U}^{\mathrm{sep,cc}}\left(s\right)$, $\mathbf{Y}^{\mathrm{sep,cc}}\left(s\right)$ and $\mathbf{G}^{\mathrm{sep,cc}}\left(s\right)$ or $\mathbf{U}^{\mathrm{com,cc}}\left(s\right)$, $\mathbf{Y}^{\mathrm{com,cc}}\left(s\right)$ and $\mathbf{G}^{\mathrm{com,cc}}\left(s\right)$, respectively. The first superscript is used to indicate that the vector or matrix is for parallel inverters with separate or common direct voltage sources, and the second superscript cc denotes circulating current. Furthermore, the subscripts abc and $dq0$ are used to denote that the vector or matrix is expressed in the abc or $dq0$ coordinates.

3.2.1 Parallel inverters with separate direct voltage sources

Let us first consider parallel inverters with separate direct voltage sources. Transforming the state-state space model (2.47) into input-output model by (3.3) and (3.4) and applying the definition (3.1) results in a circulating current model, the transfer function matrix of which is defined as

$$\mathbf{G}_{\mathrm{abc}}^{\mathrm{sep,cc}}\left(s\right) = \frac{1}{Ls + R}\begin{bmatrix} \frac{n-1}{n}\mathbf{T} & -\frac{1}{n}\mathbf{T} & \cdots & -\frac{1}{n}\mathbf{T} \\ -\frac{1}{n}\mathbf{T} & \frac{n-1}{n}\mathbf{T} & \ddots & \vdots \\ \vdots & \ddots & \ddots & -\frac{1}{n}\mathbf{T} \\ -\frac{1}{n}\mathbf{T} & \cdots & -\frac{1}{n}\mathbf{T} & \frac{n-1}{n}\mathbf{T} \end{bmatrix} \tag{3.5}$$

The dimensions of the transfer function matrix equal $3n \times 3n$. Furthermore, the matrix $\mathbf{T}$ is as defined in (2.33). Similarly, we can obtain a circulating current model, which is expressed in the $dq0$ coordinates applying (3.3), (3.4), and (3.1) to the small-signal model (2.53). The transfer function matrix of the resulting circulating current model can be given as

$$\begin{aligned}\mathbf{G}_{\mathrm{dq0}}^{\mathrm{sep,cc}}(s) = &\frac{Ls+R}{(Ls+R)^2+(\omega L)^2}\begin{bmatrix} \frac{n-1}{n}\mathbf{I}' & -\frac{1}{n}\mathbf{I}' & \cdots & -\frac{1}{n}\mathbf{I}' \\ -\frac{1}{n}\mathbf{I}' & \frac{n-1}{n}\mathbf{I}' & \ddots & \vdots \\ \vdots & \ddots & \ddots & -\frac{1}{n}\mathbf{I}' \\ -\frac{1}{n}\mathbf{I}' & \cdots & -\frac{1}{n}\mathbf{I}' & \frac{n-1}{n}\mathbf{I}' \end{bmatrix} \\ &+\frac{L}{(Ls+R)^2+(\omega L)^2}\begin{bmatrix} \frac{n-1}{n}\boldsymbol{\omega} & -\frac{1}{n}\boldsymbol{\omega} & \cdots & -\frac{1}{n}\boldsymbol{\omega} \\ -\frac{1}{n}\boldsymbol{\omega} & \frac{n-1}{n}\boldsymbol{\omega} & \ddots & \vdots \\ \vdots & \ddots & \ddots & -\frac{1}{n}\boldsymbol{\omega} \\ -\frac{1}{n}\boldsymbol{\omega} & \cdots & -\frac{1}{n}\boldsymbol{\omega} & \frac{n-1}{n}\boldsymbol{\omega} \end{bmatrix}\end{aligned} \tag{3.6}$$

where the matrices $\mathbf{I}'$ and $\boldsymbol{\omega}$ are as defined in (2.40) and (2.41), respectively. Again, the dimensions of the transfer function matrix equal $3n \times 3n$. Interestingly, both the abc and $dq0$ coordinate transfer function matrices imply that the circulating currents are not dependent on the load. This is, however, only because the output impedances of the inverters were assumed equal and because the definition (3.1) assumes equal load current sharing between the inverters. In other words, the implication that the circulating currents are not dependent on the load holds true only as a special case.

3.2.2 Parallel inverters with a common direct voltage source

Let us now consider parallel inverters with a common direct voltage source. Transforming the state-state space model (2.58) into an input-output model by (3.3) and (3.4) and applying, again, the definition (3.1) yields a circulating current model, the transfer function matrix of which is defined as

$$\mathbf{G}_{\mathrm{abc}}^{\mathrm{com,cc}}(s) = \frac{1}{Ls+R}\begin{bmatrix} \frac{n-1}{n}\mathbf{I} & -\frac{1}{n}\mathbf{I} & \cdots & -\frac{1}{n}\mathbf{I} \\ -\frac{1}{n}\mathbf{I} & \frac{n-1}{n}\mathbf{I} & \ddots & \vdots \\ \vdots & \ddots & \ddots & -\frac{1}{n}\mathbf{I} \\ -\frac{1}{n}\mathbf{I} & \cdots & -\frac{1}{n}\mathbf{I} & \frac{n-1}{n}\mathbf{I} \end{bmatrix} \tag{3.7}$$

The dimensions of the transfer function matrix equal $3n \times 3n$. Furthermore, the matrix $\mathbf{I}$ is as defined in (2.35). Applying (3.3), (3.4), and (3.1) to the small-signal model (2.64), we obtain a circulating current model that is expressed in the $dq0$ coordinates. The transfer function matrix

of the resulting circulating current model can be given as

$$\begin{aligned}\mathbf{G}_{\mathrm{dq0}}^{\mathrm{com,cc}}(s) = {} & \frac{Ls+R}{(Ls+R)^2+(\omega L)^2}\begin{bmatrix} \frac{n-1}{n}\mathbf{I}' & -\frac{1}{n}\mathbf{I}' & \cdots & -\frac{1}{n}\mathbf{I}' \\ -\frac{1}{n}\mathbf{I}' & \frac{n-1}{n}\mathbf{I}' & \ddots & \vdots \\ \vdots & \ddots & \ddots & -\frac{1}{n}\mathbf{I}' \\ -\frac{1}{n}\mathbf{I}' & \cdots & -\frac{1}{n}\mathbf{I}' & \frac{n-1}{n}\mathbf{I}' \end{bmatrix} \\ & + \frac{L}{(Ls+R)^2+(\omega L)^2}\begin{bmatrix} \frac{n-1}{n}\boldsymbol{\omega} & -\frac{1}{n}\boldsymbol{\omega} & \cdots & -\frac{1}{n}\boldsymbol{\omega} \\ -\frac{1}{n}\boldsymbol{\omega} & \frac{n-1}{n}\boldsymbol{\omega} & \ddots & \vdots \\ \vdots & \ddots & \ddots & -\frac{1}{n}\boldsymbol{\omega} \\ -\frac{1}{n}\boldsymbol{\omega} & \cdots & -\frac{1}{n}\boldsymbol{\omega} & \frac{n-1}{n}\boldsymbol{\omega} \end{bmatrix} \\ & + \frac{1}{Ls+R}\begin{bmatrix} \frac{n-1}{n}\mathbf{I}'' & -\frac{1}{n}\mathbf{I}'' & \cdots & -\frac{1}{n}\mathbf{I}'' \\ -\frac{1}{n}\mathbf{I}'' & \frac{n-1}{n}\mathbf{I}'' & \ddots & \vdots \\ \vdots & \ddots & \ddots & -\frac{1}{n}\mathbf{I}'' \\ -\frac{1}{n}\mathbf{I}'' & \cdots & -\frac{1}{n}\mathbf{I}'' & \frac{n-1}{n}\mathbf{I}'' \end{bmatrix}\end{aligned} \tag{3.8}$$

The dimensions of the transfer function matrix equal $3n \times 3n$ and the matrices $\mathbf{I}'$ and $\boldsymbol{\omega}$ are as defined in (2.40) and (2.41), respectively, and the matrix $\mathbf{I}''$ is defined as

$$\mathbf{I}'' = \begin{bmatrix} 0 & 0 & 0 \\ 0 & 0 & 0 \\ 0 & 0 & 1 \end{bmatrix} \tag{3.9}$$

Again, both the abc and $dq0$ coordinate transfer function matrices imply that the circulating currents are not dependent on the load. However, as explained previously, this holds true only as a special case. Note also that the additional terms in (3.8) compared with (3.6) are related to the zero-sequence dynamics.

3.3 Circulating current control related subjects

Let us consider a few topics related to the circulating current control in the following. First, let us determine how many parallel units should be equipped with the circulating current controllers to ensure that the current flow between the inverters can be controlled. Then, let us consider the number of phase leg voltages required to be controlled to ensure that the commands from the circulating current controllers can be realized in an appropriate way. Finally, let us consider the control effort needed to generate a certain amount of circulating current. The result of this consideration can be used inversely; in other words, we can approximate the control effort needed to mitigate a certain amount of circulating current.

To meet the objectives of this section, we apply a singular value decomposition (SVD) that can be used to factorize any $m \times n$ matrix $\mathbf{A}$ into (Råde and Westergren, 2001)

$$\mathbf{A} = \mathbf{Q}\mathbf{S}\mathbf{P}^{\mathrm{T}} \tag{3.10}$$

In brief, the SVD factorizes the matrix $\mathbf{A}$ into two orthogonal matrices $\mathbf{Q}_{m\times m}$ and $\mathbf{P}^{\mathrm{T}}_{n\times n}$ and a diagonal-type matrix $\mathbf{S}_{m\times n}$, the real and nonzero diagonal elements of which are known as singular values of $\mathbf{A}$. Here, it is pointed out that obtaining of the matrices $\mathbf{Q}$, $\mathbf{P}^{\mathrm{T}}$ and $\mathbf{S}$ is considered in Appendix A.

One of the useful properties of the SVD is that the number of singular values equals the rank of $\mathbf{A}$. The rank, again, defines the maximum number of linearly independent row and column vectors in a matrix (Kreyszig, 1999). If all row (or column) vectors are not linearly independent, there are row (or column) vectors in the matrix that can be expressed as a linear combination of the linearly independent vectors. The vectors that are linear combinations of the linearly independent vectors are unnecessary and can be eliminated. This is because the linear combinations carry the same information as the linearly independent vectors.

3.3.1 Number of required circulating current controllers

Let us now consider the transfer function matrices (3.6) and (3.8), which correspond to the parallel inverters with separate and common direct voltage sources, respectively. Let us also assume a parallel connection of two units ($n = 2$) and that $s = 0$ for the sake of a convenient representation. With these assumptions, the transfer function matrix (3.6) can be given as

$$\mathbf{G}_{\mathrm{dq0}}^{\mathrm{sep,cc}}(0) = \begin{bmatrix} \frac{1}{2}\frac{R}{R^2+\omega^2L^2} & \frac{1}{2}\frac{\omega L}{R^2+\omega^2L^2} & 0 & -\frac{1}{2}\frac{R}{R^2+\omega^2L^2} & -\frac{1}{2}\frac{\omega L}{R^2+\omega^2L^2} & 0 \\ -\frac{1}{2}\frac{\omega L}{R^2+\omega^2L^2} & \frac{1}{2}\frac{R}{R^2+\omega^2L^2} & 0 & \frac{1}{2}\frac{\omega L}{R^2+\omega^2L^2} & -\frac{1}{2}\frac{R}{R^2+\omega^2L^2} & 0 \\ 0 & 0 & 0 & 0 & 0 & 0 \\ -\frac{1}{2}\frac{R}{R^2+\omega^2L^2} & -\frac{1}{2}\frac{\omega L}{R^2+\omega^2L^2} & 0 & \frac{1}{2}\frac{R}{R^2+\omega^2L^2} & \frac{1}{2}\frac{\omega L}{R^2+\omega^2L^2} & 0 \\ \frac{1}{2}\frac{\omega L}{R^2+\omega^2L^2} & -\frac{1}{2}\frac{R}{R^2+\omega^2L^2} & 0 & -\frac{1}{2}\frac{\omega L}{R^2+\omega^2L^2} & \frac{1}{2}\frac{R}{R^2+\omega^2L^2} & 0 \\ 0 & 0 & 0 & 0 & 0 & 0 \end{bmatrix} \tag{3.11}$$

Applying the SVD to (3.11) shows that the matrix has two singular values, see Appendix A.1.1. In other words, there are two linearly independent row vectors at maximum in the matrix. From (3.11) we can see that the fourth row equals to the first row multiplied by -1. Similarly, we can see that the fifth row is equal to the second row multiplied by -1. Thus, the rows $4, 5$ can be written as a linear combination of the rows $1, 2$.

Eliminating the rows $4, 5$ from (3.11) by summing the row 1 into the row 4 and the row 2 into the row 5 results in

$$\mathbf{G}_{\mathrm{dq0}}^{\prime\mathrm{sep,cc}}(0) = \begin{bmatrix} \frac{1}{2}\frac{R}{R^2+\omega^2L^2} & \frac{1}{2}\frac{\omega L}{R^2+\omega^2L^2} & 0 & -\frac{1}{2}\frac{R}{R^2+\omega^2L^2} & -\frac{1}{2}\frac{\omega L}{R^2+\omega^2L^2} & 0 \\ -\frac{1}{2}\frac{\omega L}{R^2+\omega^2L^2} & \frac{1}{2}\frac{R}{R^2+\omega^2L^2} & 0 & \frac{1}{2}\frac{\omega L}{R^2+\omega^2L^2} & -\frac{1}{2}\frac{R}{R^2+\omega^2L^2} & 0 \\ 0 & 0 & 0 & 0 & 0 & 0 \end{bmatrix} \tag{3.12}$$

from which we can see that circulating currents flowing from (or to) the unit number one can be controlled by manipulating the dq-axes voltages of the unit number one or two or both of the units. Since it is unnecessary to use controllers in both of the units, we can write

$$\mathbf{G}_{\mathrm{dq0}}^{\prime\prime\mathrm{sep,cc}}(0) = \begin{bmatrix} \frac{1}{2}\frac{R}{R^2+\omega^2L^2} & \frac{1}{2}\frac{\omega L}{R^2+\omega^2L^2} & 0 \\ -\frac{1}{2}\frac{\omega L}{R^2+\omega^2L^2} & \frac{1}{2}\frac{R}{R^2+\omega^2L^2} & 0 \\ 0 & 0 & 0 \end{bmatrix} \tag{3.13}$$

From (3.13) we can conclude that in the case of two parallel units, the current flow between the parallel units can be controlled by equipping one of the parallel units with the dq-axes circulating current controllers. Further, (3.13) can be expressed more compactly by neglecting the row and column vectors that correspond to the 0 axis, that is, the zero row vector and the zero column vector.

Let us now consider the transfer function matrix

$$\mathbf{G}_{\mathrm{dq0}}^{\mathrm{com,cc}}(0) = \begin{bmatrix} \frac{1}{2}\frac{R}{R^2+\omega^2L^2} & \frac{1}{2}\frac{\omega L}{R^2+\omega^2L^2} & 0 & -\frac{1}{2}\frac{R}{R^2+\omega^2L^2} & -\frac{1}{2}\frac{\omega L}{R^2+\omega^2L^2} & 0 \\ -\frac{1}{2}\frac{\omega L}{R^2+\omega^2L^2} & \frac{1}{2}\frac{R}{R^2+\omega^2L^2} & 0 & \frac{1}{2}\frac{\omega L}{R^2+\omega^2L^2} & -\frac{1}{2}\frac{R}{R^2+\omega^2L^2} & 0 \\ 0 & 0 & \frac{1}{2}\frac{1}{R} & 0 & 0 & -\frac{1}{2}\frac{1}{R} \\ -\frac{1}{2}\frac{R}{R^2+\omega^2L^2} & -\frac{1}{2}\frac{\omega L}{R^2+\omega^2L^2} & 0 & \frac{1}{2}\frac{R}{R^2+\omega^2L^2} & \frac{1}{2}\frac{\omega L}{R^2+\omega^2L^2} & 0 \\ \frac{1}{2}\frac{\omega L}{R^2+\omega^2L^2} & -\frac{1}{2}\frac{R}{R^2+\omega^2L^2} & 0 & -\frac{1}{2}\frac{\omega L}{R^2+\omega^2L^2} & \frac{1}{2}\frac{R}{R^2+\omega^2L^2} & 0 \\ 0 & 0 & -\frac{1}{2}\frac{1}{R} & 0 & 0 & \frac{1}{2}\frac{1}{R} \end{bmatrix} \tag{3.14}$$

which is obtained from (3.8) by setting $n = 2$ and $s = 0$. Applying the SVD to (3.14) shows that the matrix has three singular values, see Appendix A.1.2. Thus, there are three linearly independent row vectors at maximum in the matrix. From (3.14) we can see that the rows $4, 5, 6$ are equal to the rows $1, 2, 3$, respectively, provided that each of the subsequently mentioned row is multiplied by -1. Thus, the rows $4, 5, 6$ can be written as a linear combination of the rows $1, 2, 3$, respectively.

Eliminating the rows $4, 5, 6$ from (3.14) by summing the rows $1, 2, 3$ into the rows $4, 5, 6$, respectively, yields

$$\mathbf{G}_{\mathrm{dq0}}^{\prime\mathrm{com,cc}}(0) = \begin{bmatrix} \frac{1}{2}\frac{R}{R^2+\omega^2L^2} & \frac{1}{2}\frac{\omega L}{R^2+\omega^2L^2} & 0 & -\frac{1}{2}\frac{R}{R^2+\omega^2L^2} & -\frac{1}{2}\frac{\omega L}{R^2+\omega^2L^2} & 0 \\ -\frac{1}{2}\frac{\omega L}{R^2+\omega^2L^2} & \frac{1}{2}\frac{R}{R^2+\omega^2L^2} & 0 & \frac{1}{2}\frac{\omega L}{R^2+\omega^2L^2} & -\frac{1}{2}\frac{R}{R^2+\omega^2L^2} & 0 \\ 0 & 0 & \frac{1}{2}\frac{1}{R} & 0 & 0 & -\frac{1}{2}\frac{1}{R} \end{bmatrix} \tag{3.15}$$

from which we can see that circulating currents flowing from (or to) the unit number one can be controlled by manipulating the $dq0$-axes voltages of the unit number one or two or both of the units. Since it is unnecessary to use controllers in both of the units, we can write

$$\mathbf{G}_{\mathrm{dq0}}^{\prime\prime\mathrm{com,cc}}(0) = \begin{bmatrix} \frac{1}{2}\frac{R}{R^2+\omega^2L^2} & \frac{1}{2}\frac{\omega L}{R^2+\omega^2L^2} & 0 \\ -\frac{1}{2}\frac{\omega L}{R^2+\omega^2L^2} & \frac{1}{2}\frac{R}{R^2+\omega^2L^2} & 0 \\ 0 & 0 & \frac{1}{2}\frac{1}{R} \end{bmatrix} \tag{3.16}$$

From (3.16) we can conclude that also in this case only one of the parallel units must be equipped with the circulating current controllers. The difference compared with the previous case is, however, that in addition to the dq-axes controllers, also 0 axis controller is needed to ensure that the current flow between the parallel units can be controlled. This is a significant difference, since the zero-sequence circulating current control basically requires that all phase leg voltages of the inverter are controlled all the time. This is considered in more detail in the following subsection.

So far, we have demonstrated that in the case of two parallel units, only one of the parallel units must be equipped with the circulating current controllers. In the case of parallel inverters with separate direct voltage sources, one of the inverters must be equipped with the dq-axes controllers, while in the case of a common direct voltage source, $dq0$-axes controllers must be used. Let us generalize these results.

It can be shown that in the case of three parallel units with separate direct voltage sources, the number of singular values of (3.6) equals four, in the case of four parallel units six, and so on. Thus, we can conclude that in the case of n parallel units, the number of singular values equals

$2\,(n-1)$. Performing a similar elimination procedure as in the case of two parallel units, we can eventually conclude that it is necessary to manipulate the dq-axes voltages only in $n-1$ parallel units to ensure that the current flow between the parallel units can be controlled. In other words, the overall number of the required circulating current controllers equals the number of singular values of (3.6), that is, $2\,(n-1)$.

In the case of three parallel units with a common direct voltage source, the number of singular values equals six, in the case of four units nine and so on. Thus, we can conclude that the number of singular values in the case of n parallel units equals $3\,(n-1)$. This, again, implies that it is necessary to manipulate the $dq0$-axes voltages only in $n-1$ parallel units to ensure that the current flow between the parallel units can be controlled. In other words, the overall number of the required circulating current controllers equals the number of singular values of (3.8), that is, $3\,(n-1)$.

3.3.2 Number of phase leg voltages required to be controlled

It was mentioned in the previous subsection that the zero-sequence circulating current control basically requires that all phase leg voltages of the inverter should be controlled all the time to ensure that the current flow between the parallel units can be controlled. This can be understood by recalling that the zero-sequence circulating refers to the averaged sum of the inverter phase currents. A better way to illustrate this is to examine the transfer function matrices expressed in the abc coordinates as has been done in (Itkonen et al., 2009b).

Consider the case of parallel inverters with a common direct voltage source. From (3.7) we can see that the relationships between the phase legs voltages of a certain unit and circulating currents corresponding to the unit in question can be given as

$$\mathbf{G}''^{\mathrm{com,cc}}_{\mathrm{abc}}(s) = \frac{n-1}{n\,(Ls+R)} \begin{bmatrix} 1 & 0 & 0 \\ 0 & 1 & 0 \\ 0 & 0 & 1 \end{bmatrix} \tag{3.17}$$

The rank of this of this matrix equals three. Therefore, there are three linearly independent rows at most in the matrix. Furthermore, since the off-diagonal elements of the matrix equal zero, circulating currents in a certain phase can be controlled only by controlling phase leg voltages of that particular phase.

Let us consider for comparison the case of parallel inverters with separate direct voltage sources. From (3.5) we can see that the relationships between the phase leg voltages of a certain unit and the circulating currents corresponding to the unit in question can be given as

$$\mathbf{G}''^{\mathrm{sep,cc}}_{\mathrm{abc}}(s) = \frac{n-1}{n\,(Ls+R)} \begin{bmatrix} +2/3 & -1/3 & -1/3 \\ -1/3 & +2/3 & -1/3 \\ -1/3 & -1/3 & +2/3 \end{bmatrix} \tag{3.18}$$

The rank of this matrix equals two indicating that there are two linearly independent rows at most in the matrix. This result means that we can control circulating currents in a certain phase either by controlling phase leg voltages of that particular phase or alternatively, phase leg voltages of the other two phases of the inverter.

3.3.3 Control effort considerations

The transfer function matrices (3.6) and (3.8) show the relationships between the inverter output voltages and the circulating currents. With the help of these expressions, we can determine the control effort needed to generate a certain amount of circulating current. The matrices (3.6) and (3.8) are, however, singular indicating that they do not have an inverse. In other words, there is no unique solution that can be obtained from the input-output model as

$$\mathbf{U}(s) = (\mathbf{G}(s))^{-1}\mathbf{Y}(s) \tag{3.19}$$

However, as illustrated in Subsection 3.3.1, we can eliminate and neglect certain rows and columns from the matrices because some of them are linear combinations of the others. The rows and columns that can be eliminated and neglected can be expressed as

$$\mathbf{G}(s) = \begin{bmatrix} \mathbf{G}_{11}(s) & \cdots & \mathbf{G}_{1(n-1)}(s) & \mathbf{G}_{1n}(s) \\ \vdots & \ddots & \vdots & \mathbf{G}_{2n}(s) \\ \mathbf{G}_{1(n-1)}(s) & \cdots & \mathbf{G}_{(n-1)(n-1)}(s) & \vdots \\ \mathbf{G}_{n1}(s) & \mathbf{G}_{n2}(s) & \cdots & \mathbf{G}_{nn}(s) \end{bmatrix} \tag{3.20}$$

In other words, we can eliminate the n^{th} row and neglect the n^{th} column. The remaining subset, the background of which is colored with different shades of gray is invertible. Correct dimensions for $\mathbf{G}_{ij}(s)$, $i,j \in \{1,2,...,n\}$ can be obtained by comparing (3.20) for example with (3.8).

From (3.20) we can conclude that in the case of two parallel units the remaining subset includes only one element, that is, $\mathbf{G}_{11}(s)$. However, in the case of $n > 2$ parallel units the remaining subset contain the elements $\mathbf{G}_{ij}(s)$, $i,j \in \{1,2,...,n-1\}$. In these cases, the off-diagonal elements indicate that the circulating current controllers of the parallel units will interact with each other in a similar fashion as the dq-axes circulating controllers will do within each unit, provided that the dq-axes are not decoupled. Decoupling of the dq-axes has been dealt with in the case of a single voltage source inverter for example in (Milosevic et al., 2006). Although the same principles can be applied also in the case of parallel voltage source inverters, it is not considered here.

Let us now consider the control effort needed to generate a certain amount of circulating current. Let us also assume, for simplicity, parallel connection of two units. Based on the preceding, we can write for the parallel inverters with separate direct voltage sources as

$$\mathbf{Y}''^{\text{sep,cc}}_{\text{dq0}}(s) = \begin{bmatrix} \frac{1}{2}\frac{Ls+R}{(Ls+R)^2+(\omega L)^2} & -\frac{1}{2}\frac{\omega L}{(Ls+R)^2+(\omega L)^2} \\ -\frac{1}{2}\frac{\omega L}{(Ls+R)^2+(\omega L)^2} & \frac{1}{2}\frac{Ls+R}{(Ls+R)^2+(\omega L)^2} \end{bmatrix} \mathbf{U}''^{\text{sep,cc}}_{\text{dq0}}(s) \tag{3.21}$$

and for the parallel inverters with a common direct voltage source as

$$\mathbf{Y}''^{\text{com,cc}}_{\text{dq0}}(s) = \begin{bmatrix} \frac{1}{2}\frac{Ls+R}{(Ls+R)^2+(\omega L)^2} & -\frac{1}{2}\frac{\omega L}{(Ls+R)^2+(\omega L)^2} & 0 \\ -\frac{1}{2}\frac{\omega L}{(Ls+R)^2+(\omega L)^2} & \frac{1}{2}\frac{Ls+R}{(Ls+R)^2+(\omega L)^2} & 0 \\ 0 & 0 & \frac{1}{2}\frac{1}{Ls+R} \end{bmatrix} \mathbf{U}''^{\text{com,cc}}_{\text{dq0}}(s) \tag{3.22}$$

Transforming (3.21) and (3.22) into the form (3.19) results in the case of parallel inverters with separate direct voltage sources in

$$\mathbf{U}''^{\mathrm{sep,cc}}_{\mathrm{dq0}}(s) = \begin{bmatrix} 2(Ls+R) & -2\omega L \\ 2\omega L & 2(Ls+R) \end{bmatrix} \mathbf{Y}''^{\mathrm{sep,cc}}_{\mathrm{dq0}}(s) \tag{3.23}$$

and in the case of parallel inverters with a common direct voltage source in

$$\mathbf{U}''^{\mathrm{com,cc}}_{\mathrm{dq0}}(s) = \begin{bmatrix} 2(Ls+R) & -2\omega L & 0 \\ 2\omega L & 2(Ls+R) & 0 \\ 0 & 0 & 2(Ls+R) \end{bmatrix} \mathbf{Y}''^{\mathrm{com,cc}}_{\mathrm{dq0}}(s) \tag{3.24}$$

Expressing the input vectors as $\mathbf{Y}''^{\mathrm{sep,cc}}_{\mathrm{dq0}}(s) = \begin{bmatrix} C_\mathrm{d}/s & C_\mathrm{q}/s \end{bmatrix}^\mathrm{T}$ and $\mathbf{Y}''^{\mathrm{com,cc}}_{\mathrm{dq0}}(s) = \begin{bmatrix} C_\mathrm{d}/s & C_\mathrm{q}/s & C_0/s \end{bmatrix}^\mathrm{T}$ where $C_\mathrm{d}, C_\mathrm{q}, C_0$ are the "desired" steady-state circulating currents and finding inverse Laplace transformations results in

$$\begin{bmatrix} u_\mathrm{d}(t) \\ u_\mathrm{q}(t) \end{bmatrix} = \begin{bmatrix} 2L\delta(t)+2R & -2\omega L \\ 2\omega L & 2L\delta(t)+2R \end{bmatrix} \begin{bmatrix} C_\mathrm{d} \\ C_\mathrm{q} \end{bmatrix} \tag{3.25}$$

and in

$$\begin{bmatrix} u_\mathrm{d}(t) \\ u_\mathrm{q}(t) \\ u_0(t) \end{bmatrix} = \begin{bmatrix} 2L\delta(t)+2R & -2\omega L & 0 \\ 2\omega L & 2L\delta(t)+2R & 0 \\ 0 & 0 & 2L\delta(t)+2R \end{bmatrix} \begin{bmatrix} C_\mathrm{d} \\ C_\mathrm{q} \\ C_0 \end{bmatrix} \tag{3.26}$$

where $\delta(t)$ is Dirac's delta function. Since Dirac's delta function has a zero value everywhere except at $t = 0$, we can write for $t > 0$ as

$$\begin{bmatrix} U_\mathrm{d} \\ U_\mathrm{q} \end{bmatrix} = \begin{bmatrix} 2R & -2\omega L \\ 2\omega L & 2R \end{bmatrix} \begin{bmatrix} C_\mathrm{d} \\ C_\mathrm{q} \end{bmatrix} \tag{3.27}$$

and

$$\begin{bmatrix} U_\mathrm{d} \\ U_\mathrm{q} \\ U_0 \end{bmatrix} = \begin{bmatrix} 2R & -2\omega L & 0 \\ 2\omega L & 2R & 0 \\ 0 & 0 & 2R \end{bmatrix} \begin{bmatrix} C_\mathrm{d} \\ C_\mathrm{q} \\ C_0 \end{bmatrix} \tag{3.28}$$

Now we have expressions that can be used to estimate the control effort needed to generate a certain amount of circulating current. As can be seen, the control effort needed increases, while the impedance between the parallel units increases. The expressions (3.27) and (3.28) also imply that increasing the impedance between the parallel units can help to keep circulating currents at a low value. This is because sensitivity to the variations in the inverter output voltages decreases. This property has been exploited in (Younis et al., 2009), where the current sharing between parallel units is improved by adding series resistors in the inverter outputs. The improved current sharing comes, however, at the expense of increased inverter losses.

3.4 Circulating currents caused by the dead-time effects

Contributions considering parallel-operating power semiconductor devices and modules (Hofer-Noser and Karrer, 1999; Nelson et al., 2002; Bortis et al., 2008) have identified that differences in finite turn-on and turn-off times of switching devices and forward voltage drops of switching devices and anti-parallel diodes cause unequal load current sharing between the modules. It has also been stated that differences in blanking times that are used to prevent short circuits in the inverter phase legs can cause circulating currents between the units (Zhang et al., 2005). The following concentrates on studying how the overall effects of these parameter variations, which are commonly called dead-time effects (Cichowski and Nieznanski, 2005), affect the circulating current generation between parallel two-level VSIs.

3.4.1 Average phase leg voltage formation

To facilitate the understanding of how the dead-time effects influence circulating current generation between parallel two-level VSIs, it is convenient first to consider phase leg voltage formation with the help of Figs. 3.1 and 3.2. The former shows a single phase leg of a two-level VSI feeding an inductive load, and possible paths for positive and negative phase currents. The current flowing from the phase leg to the load is defined as a positive phase current, and the current flowing from the load to the phase leg as a negative phase current. When the phase current is positive, the current flows either through the upper switching device T_a^+ or the lower anti-parallel diode D_a^- as shown in Fig. 3.1(a), and when the phase current is negative, the current flows either through the lower switching device T_a^- or the upper anti-parallel diode D_a^+ as illustrated in Fig. 3.1(b).

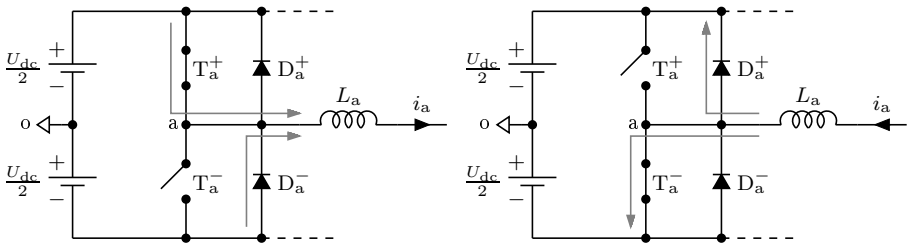

(a) Positive phase current. (b) Negative phase current.

Fig. 3.1: Single phase leg of a two-level voltage source inverter feeding an inductive load and possible paths for positive and negative phase currents.

Phase leg voltage formation is illustrated in Fig. 3.2 for both the positive and negative phase currents. In this context, phase leg voltage refers to the voltage between the output node a and the dc link midpoint o. For simplicity, it is assumed that the dc link voltage and the forward voltage drops of switching devices and anti-parallel diodes, which are denoted by U_dc, U_T, and U_D, are constant. T_on and T_off are the desired on- and off-times of the upper switching device, $t_\mathrm{on} > 0$ and $t_\mathrm{off} > 0$ are the finite turn-on and turn-off times of the upper and lower switching devices, and $t_\mathrm{d} > 0$ is the necessary blanking time used to prevent a short circuit in the phase leg.

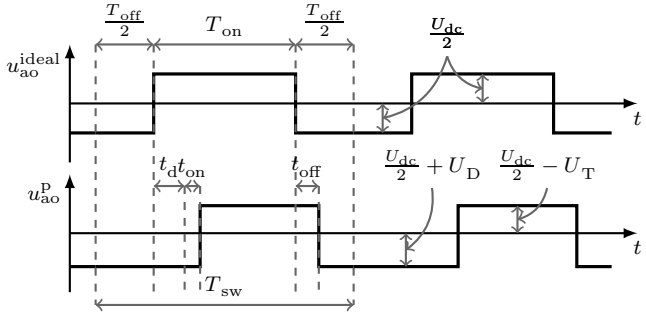

(a) Output voltage formation for a positive phase current.

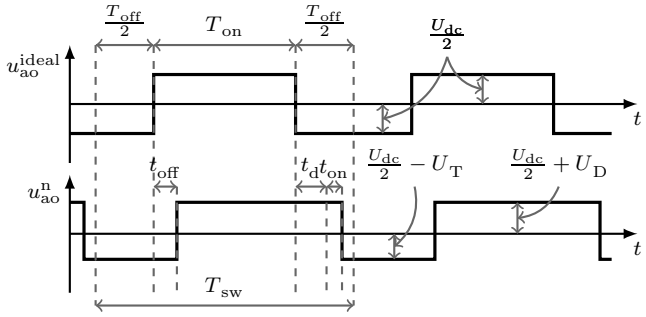

(b) Output voltage formation for a negative phase current.

Fig. 3.2: Inverter phase leg voltage formation for positive and negative phase currents. Ideal waveforms neglect the effects of the blanking time, the finite turn-on and turn-off times of the switching devices, and the forward voltage drops of the switching devices and the anti-parallel diodes.

Assuming that both the upper and lower switching devices are opened and closed, or vice versa, during the switching period as shown in Figs. 3.2(a) and 3.2(b), the phase leg voltages averaged with respect to the switching period $T_{\rm sw}$ can be defined as

$$\hat{u}_{\rm ao}^{\rm p} = \left(d - d_{\rm d} - \frac{1}{2}\right) U_{\rm dc} - (d - d_{\rm d})\ U_{\rm T} - (1 - d + d_{\rm d})\ U_{\rm D} \tag{3.29}$$

$$\hat{u}_{\rm ao}^{\rm n} = \left(d + d_{\rm d} - \frac{1}{2}\right) U_{\rm dc} + (1 - d - d_{\rm d})\ U_{\rm T} + (d + d_{\rm d})\ U_{\rm D} \tag{3.30}$$

where $\rm p$ and $\rm n$ in the superscripts denote positive and negative phase currents, respectively, the subscript indicates that the phase leg voltage is evaluated with respect to the midpoint of the direct voltage link, $d = T_{\rm on}/T_{\rm sw}$ is a phase duty cycle, and $d_{\rm d} = (t_{\rm d} + t_{\rm on} - t_{\rm off})/T_{\rm sw}$. Similarly, average phase leg voltages can be defined for the phases b and c. At this point it is pointed out that although the dead-time effects cause both the amplitude and phase distortion to the inverter phase leg voltages compared with the desired phase leg voltages, we will neglect the resulting phase distortion for the sake of simplicity.

3.4.2 Time-domain circulating current modeling

Let us now develop a time-domain circulating model that can be used to estimate circulating currents caused by the dead-time effects. Let us, however, consider only the case of parallel inverters with a common direct voltage source for the sake of a simplicity. The following is considered in more detail in (Itkonen et al., 2009a,c).

A Laplace domain circulating current model expressed in the abc coordinates can be written with the help of (3.7). Rewriting the right-hand side of the input-output model, which is of the similar form as (3.4), we can write

$$\mathbf{Y}_{\mathrm{abc}}^{\mathrm{cc}}(s) = \frac{1}{Ls+R}\Delta\mathbf{U}^{\mathrm{cc}}(s) \tag{3.31}$$

where the elements in the input vector $\Delta\mathbf{U}^{\mathrm{cc}}(s)$ are defined as

$$\begin{aligned}\Delta U_{\mathrm{ko},j}(s) &= \sum_{m=1}^{n}\frac{U_{\mathrm{ko},j}(s) - U_{\mathrm{ko},m}(s)}{n} \\ &= \sum_{m=1}^{n}\frac{\Delta U_{\mathrm{ko},jm}(s)}{n} \quad , \quad \begin{array}{l} k \in \{\mathrm{a},\mathrm{b},\mathrm{c}\} \\ m \in \{1,2,\ldots,n\}\end{array}\end{aligned} \tag{3.32}$$

The variables j and m are used to indicate the index of the parallel unit and k denotes the phase. Considering the formation of the phase leg voltage differences one switching period at a time, we can define average phase leg voltage differences as

$$\Delta\hat{U}_{\mathrm{ko},jm}(s) = \left(\hat{u}_{\mathrm{ko},j} - \hat{u}_{\mathrm{ko},m}\right)\frac{\left(e^{-as}-e^{-bs}\right)}{s} = \Delta\hat{u}_{\mathrm{ko},jm}\frac{\left(e^{-as}-e^{-bs}\right)}{s} \tag{3.33}$$

where $a = (q-1)\,T_{\mathrm{sw}}$, $b = qT_{\mathrm{sw}}$ and $q \in \{1,2,\ldots,\infty\}$. In the time-domain, the term in the right-hand side of (3.33) represents a voltage pulse, the amplitude of which equals $\Delta\hat{u}_{\mathrm{ko},jm} = \hat{u}_{\mathrm{ko},j} - \hat{u}_{\mathrm{ko},m}$. The values for $\hat{u}_{\mathrm{ko},j}$ and $\hat{u}_{\mathrm{ko},m}$ are obtained by (3.29) and (3.30).

The average phase leg voltage difference $\Delta\hat{u}_{\mathrm{ko},jm}$ is a function of dead-time effect parameters, phase duty cycles, directions of the phase currents, and dc link voltage. However, since the purpose is to study how the dead-time effects influence the circulating current generation, it is justified to assume that the parallel inverters are driven with similar switching patterns, that is, $d_k = d_{k,1} = d_{k,2} = \cdots = d_{k,n}$. Assuming further that the forward voltage drops of the switching devices and anti-parallel diodes are of the same value in each unit, that is, $U_{\mathrm{F},j} = U_{\mathrm{T},j} = U_{\mathrm{D},j}$, the phase leg voltage difference can be defined as

$$\Delta\hat{u}_{\mathrm{ko},jm} = \begin{cases} \Delta\hat{u}_{\mathrm{ko},jm}^{\mathrm{pp}} = \hat{u}_{\mathrm{ko},j}^{\mathrm{p}} - \hat{u}_{\mathrm{ko},m}^{\mathrm{p}} & \text{, when } i_{k,j} > 0, i_{k,m} > 0 \\ \Delta\hat{u}_{\mathrm{ko},jm}^{\mathrm{pn}} = \hat{u}_{\mathrm{ko},j}^{\mathrm{p}} - \hat{u}_{\mathrm{ko},m}^{\mathrm{n}} & \text{, when } i_{k,j} > 0, i_{k,m} < 0 \\ \Delta\hat{u}_{\mathrm{ko},jm}^{\mathrm{np}} = \hat{u}_{\mathrm{ko},j}^{\mathrm{n}} - \hat{u}_{\mathrm{ko},m}^{\mathrm{p}} & \text{, when } i_{k,j} < 0, i_{k,m} > 0 \\ \Delta\hat{u}_{\mathrm{ko},jm}^{\mathrm{nn}} = \hat{u}_{\mathrm{ko},j}^{\mathrm{n}} - \hat{u}_{\mathrm{ko},m}^{\mathrm{n}} & \text{, when } i_{k,j} < 0, i_{k,m} < 0 \end{cases} \tag{3.34}$$

where

$$\Delta\hat{u}_{\mathrm{ko},jm}^{\mathrm{pp}} = -\Delta\hat{u}_{\mathrm{ko},jm}^{\mathrm{nn}} = \left(-d_{\mathrm{d},j} + d_{\mathrm{d},m}\right)U_{\mathrm{dc}} + \left(-U_{\mathrm{F},j} + U_{\mathrm{F},m}\right) \tag{3.35}$$

$$\Delta\hat{u}_{\mathrm{ko},jm}^{\mathrm{pn}} = -\Delta\hat{u}_{\mathrm{ko},jm}^{\mathrm{np}} = -\left(d_{\mathrm{d},j} + d_{\mathrm{d},m}\right)U_{\mathrm{dc}} - \left(U_{\mathrm{F},j} + U_{\mathrm{F},m}\right) \tag{3.36}$$

Since (3.34) does not depend on the phase duty cycles, $\Delta\hat{u}_{\mathrm{ko},jm}$ is constant over sequential switching periods, where the directions of the phase currents do not change. Note also that when the directions of the phase currents are the same, the value of $\Delta\hat{u}_{\mathrm{ko},jm}$ depends on the differences in the dead-time effect parameters. However, when the directions of the phase currents are different, $\Delta\hat{u}_{\mathrm{ko},jm} \neq 0$ even if the dead-time effect parameters are the same. Furthermore, the magnitude is easily many times larger than in the cases where the phase currents are of the same direction and the value is such that the difference between the phase currents tends to decrease. Because of this, it is practical to consider only the cases where all phase currents are of the same direction (Itkonen et al., 2009a,c).

When all phase currents are positive, an average s-domain circulating current model corresponding to the phase k of the j^{th} inverter can be expressed as

$$\hat{C}^{\mathrm{p}}_{k,j} = \sum_{m=1}^{n} \frac{\Delta\hat{u}^{\mathrm{pp}}_{\mathrm{ko},jm}}{Ls+R} \frac{\left(e^{-as} - e^{-bs}\right)}{s} \quad , \quad \begin{matrix} k \in \{\mathrm{a},\mathrm{b},\mathrm{c}\} \\ m \in \{1,2,\ldots,n\} \end{matrix} \tag{3.37}$$

and when all phase currents are negative as

$$\hat{C}^{\mathrm{n}}_{k,j} = \sum_{m=1}^{n} \frac{\Delta\hat{u}^{\mathrm{nn}}_{\mathrm{ko},jm}}{Ls+R} \frac{\left(e^{-as} - e^{-bs}\right)}{s} \quad , \quad \begin{matrix} k \in \{\mathrm{a},\mathrm{b},\mathrm{c}\} \\ m \in \{1,2,\ldots,n\} \end{matrix} \tag{3.38}$$

Finding inverse Laplace transformations of (3.37) and (3.38) results in average time-domain circulating current models

$$\hat{c}^{\mathrm{p}}_{k,j} = \sum_{m=1}^{n} \left[\frac{\Delta\hat{u}^{\mathrm{pp}}_{\mathrm{ko},jm}}{nR} \left(H\left(t-t_a\right)\left(1-e^{-\frac{R}{L}(t)}\right) - H\left(t-t_b\right)\left(1-e^{-\frac{R}{L}(t)}\right)\right)\right] \tag{3.39}$$

$$\hat{c}^{\mathrm{n}}_{k,j} = \sum_{m=1}^{n} \left[\frac{\Delta\hat{u}^{\mathrm{nn}}_{\mathrm{ko},jm}}{nR} \left(H\left(t-t_c\right)\left(1-e^{-\frac{R}{L}(t)}\right) - H\left(t-t_d\right)\left(1-e^{-\frac{R}{L}(t)}\right)\right)\right] \tag{3.40}$$

where H is Heaviside's step function defined as

$$H\left(t-x\right) = \begin{cases} 1, & \text{when } t > x \\ 0, & \text{when } t < x \end{cases} \tag{3.41}$$

The time instants t_a, t_b and t_c, t_d, again, correspond to the time intervals during which all phase currents are assumed to be positive or negative, respectively.

3.4.3 Model verification

To verify the validity of the time-domain circulating current model given by (3.39) and (3.40), the calculated circulating current waveforms are compared both with the circuit simulation and the experimental results in this subsection. The circuit simulations were carried out with the model introduced in Appendix B, and the experimental setup is presented in Chapter 6. Therefore, neither of them are described here. The parameters used in the calculations correspond to the circuit simulation parameters given also in Appendix B. Furthermore, the time instants

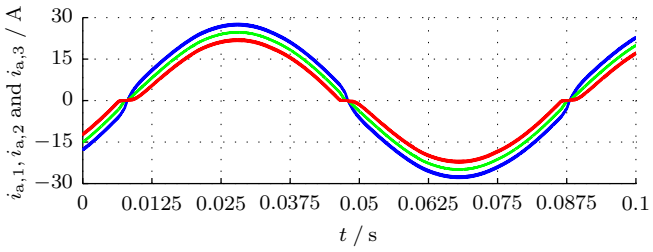

(a) Simulated phase currents.

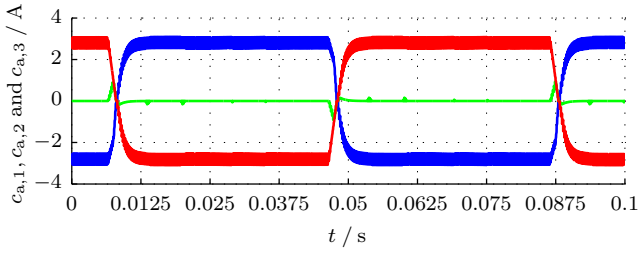

(b) Simulated circulating currents.

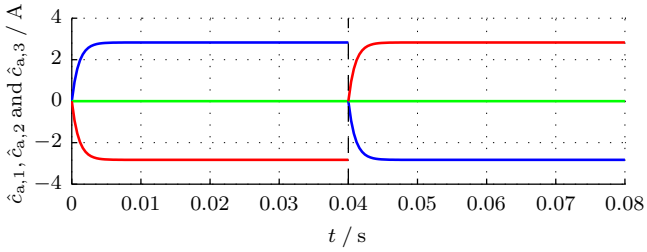

(c) Calculated circulating currents.

Fig. 3.3: Simulated phase currents and the corresponding circulating currents, and the calculated circulating currents when the phase leg voltage differences were generated by setting the blanking times as $t_{\mathrm{d},1} = 2.0\,\mu\mathrm{s}$, $t_{\mathrm{d},2} = 2.1\,\mu\mathrm{s}$ and $t_{\mathrm{d},3} = 2.2\,\mu\mathrm{s}$. Blue, green, and red lines indicate the first, second, and third inverter, respectively.

t_a, t_b, t_c, t_d in (3.39) and (3.40) were set as $t_a = 0, t_b = T_{\mathrm{f}}/2, t_c = T_{\mathrm{f}}/2, t_d = T_{\mathrm{f}}$ where $T_{\mathrm{f}} = 0.08\,\mathrm{ms}$ is the time of the fundamental period.

Let us first consider Fig. 3.3, which shows the simulated phase currents and the corresponding circulating currents, and the calculated circulating currents when the phase leg voltage differences were generated by setting the blanking times as $t_{\mathrm{d},1} = 2.0\,\mu\mathrm{s}$, $t_{\mathrm{d},2} = 2.1\,\mu\mathrm{s}$ and $t_{\mathrm{d},3} = 2.2\,\mu\mathrm{s}$. From Fig. 3.3(a) we can conclude that as a consequence of the blanking time differences, the load phase current that equals the sum of inverter phase currents is shared unequally between the units. The circulating current waveforms corresponding to the phase currents shown in Fig. 3.3(a) are presented in Fig. 3.3(b). The calculated circulating current waveforms, again, are illustrated in Fig. 3.3(c).

Comparing Figs. 3.3(b) and 3.3(c), we can see that the calculated waveforms are in good agreement with the circuit simulations. The most visible difference is that the calculated waveforms do not contain the switching ripple that is present in the simulated waveforms. This is, however, because the averaging procedure neglects the switching transients. The circuit simulated waveforms also show that as a consequence of the dead-time effects, the phase currents tend to cross the zero current level at the same time. Because of this property, the circulating currents generated during the positive and negative half cycles decrease rapidly to zero at the time intervals during which the phase currents cross the zero current level. This property was used in simplifying the time-domain circulating current model expression.

Let us now consider the simulated and calculated circulating current waveforms presented in Figs. 3.4, 3.5, and 3.6. The phase leg voltage differences were generated in the first case by setting the turn-on times as $t_{\mathrm{on},1} = 0\,\mathrm{ns}$, $t_{\mathrm{on},2} = 100\,\mathrm{ns}$ and $t_{\mathrm{on},3} = 200\,\mathrm{ns}$, in the second case by setting the turn-off times as $t_{\mathrm{off},1} = 0\,\mathrm{ns}$, $t_{\mathrm{off},2} = 100\,\mathrm{ns}$, and $t_{\mathrm{off},3} = 200\,\mathrm{ns}$, and in the third case by setting the forward voltage drops of the switches and diodes as $U_{\mathrm{F},1} = 2\ \mathrm{V}$, $U_{\mathrm{F},2} = 2.3\ \mathrm{V}$, and $U_{\mathrm{F},3} = 2.6\ \mathrm{V}$. In all three cases, the calculations give estimates that correspond well with the simulations. The preceding illustrations show that the presented time-domain circulating current model can be used to estimate the circulating currents that are caused by the dead-time effects.

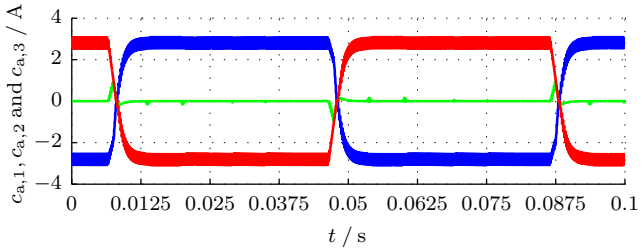

(a) Simulated circulating currents.

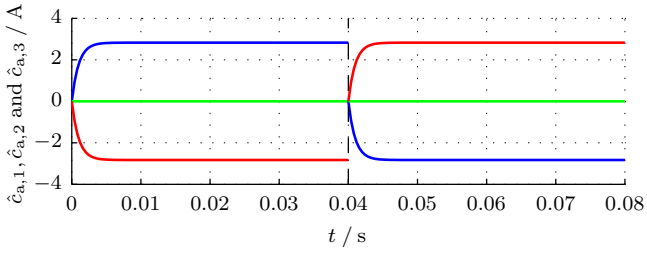

(b) Calculated circulating currents.

Fig. 3.4: Simulated and calculated circulating currents when the phase leg voltage differences were generated by setting the turn-on times as $t_{\mathrm{on},1} = 0\,\mathrm{ns}$, $t_{\mathrm{on},2} = 100\,\mathrm{ns}$ and $t_{\mathrm{on},3} = 200\,\mathrm{ns}$. Blue, green, and red lines indicate the first, second, and third inverter, respectively.

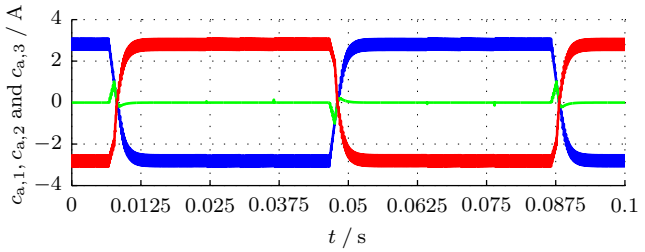

(a) Simulated circulating currents.

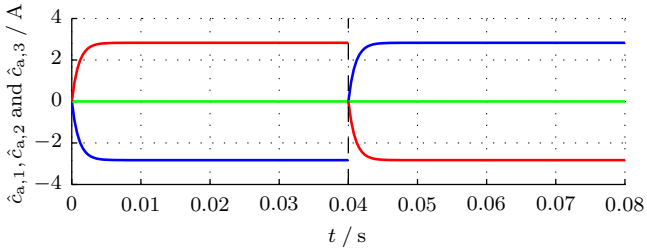

(b) Calculated circulating currents.

Fig. 3.5: Simulated and calculated circulating currents when the phase leg voltage differences were generated by setting the turn-off times as $t_{\mathrm{off},1} = 0$ ns, $t_{\mathrm{off},2} = 100ns$ and $t_{\mathrm{off},3} = 200ns$. Blue, green, and red lines indicate the first, second, and third inverter, respectively.

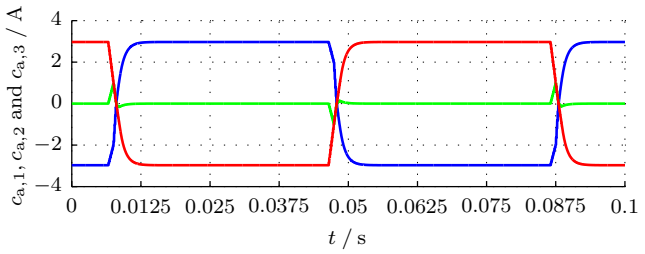

(a) Simulated circulating currents.

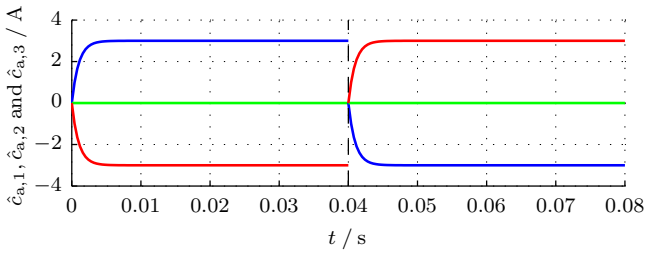

(b) Calculated circulating currents.

Fig. 3.6: Simulated and calculated circulating currents when the phase leg voltage differences were generated by setting the forward voltage drops of the inverters as $U_{\mathrm{F},1} = 2$ V, $U_{\mathrm{F},2} = 2.3$ V, and $U_{\mathrm{F},3} = 2.6$ V. Blue, green, and red lines indicate the first, second, and third inverter, respectively.

Let us now consider some experimental results. Figure 3.7 shows the phase currents and the corresponding circulating currents when the inverters were driven with the identical voltage commands. The presented waveforms show that there exist circulating currents even if the units are uniformly controlled. Because of this we cannot expect that the measured circulating current waveforms are similar to the ones obtained from the circuit simulations or the calculations.

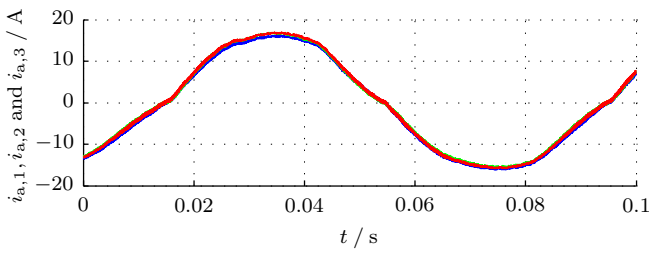

(a) Phase currents.

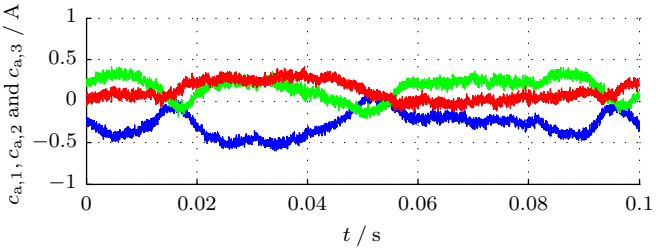

(b) Circulating currents.

Fig. 3.7: Measured phase currents and the corresponding circulating currents when the inverters were driven with identical voltage commands. Blue, green, and red lines indicate the first, second, and third inverter, respectively.

Consider Fig. 3.8, which presents the phase currents and the corresponding circulating currents when the turn-on times were set as $t_{\mathrm{on},1} \approx 0\,\mathrm{ns}$, $t_{\mathrm{on},2} \approx 100\,\mathrm{ns}$, and $t_{\mathrm{on},3} \approx 200\,\mathrm{ns}$. Although the resulting circulating current waveforms resemble only distantly the waveforms presented in Fig. 3.4, the result verifies that the phase currents tend to cross the zero current level at the same time as it was expected. Similar waveforms were presented in the case of two parallel units in (Itkonen et al., 2009c). In the case of two parallel units, the operation of the parallel units was more uniform yielding waveforms that correspond better with the predictions.

Let us now consider Fig. 3.9, which shows the phase currents and the corresponding circulating currents when the turn-off times were set as $t_{\mathrm{off},1} \approx 0\,\mathrm{ns}$, $t_{\mathrm{off},2} \approx 100\,\mathrm{ns}$, and $t_{\mathrm{off},3} \approx 200\,\mathrm{ns}$. As can be seen, the circulating current waveforms resemble distantly the waveforms presented in Fig. 3.5. However, also in this case, the most important observation to make is that the phase currents tend to cross the zero-current level at the same time at any circumstances. Based on the presented measurement results and (Itkonen et al., 2009c), we may conclude that the verification of the presented circulating current model in the case of several parallel units may be difficult or even impossible to perform experimentally. This is because we cannot distinguish the actual causes for the circulating currents.

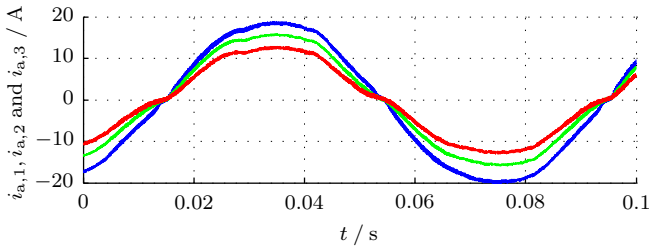

(a) Phase currents.

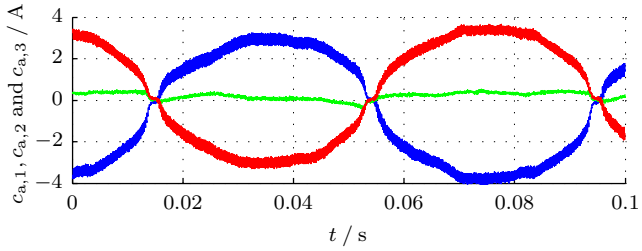

(b) Circulating currents.

Fig. 3.8: Measured phase currents and the corresponding circulating currents when the turn-on times were set as $t_{\mathrm{on},1} \approx 0\,\mathrm{ns}$, $t_{\mathrm{on},2} \approx 100\,\mathrm{ns}$, and $t_{\mathrm{on},3} \approx 200\,\mathrm{ns}$. Blue, green, and red lines indicate the first, second, and third inverter, respectively.

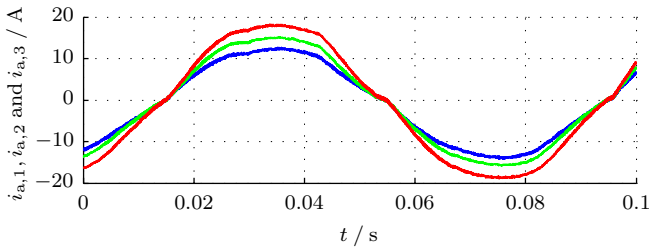

(a) Phase currents.

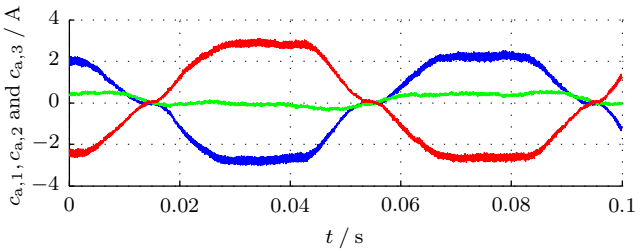

(b) Circulating currents.

Fig. 3.9: Measured phase currents and the corresponding circulating currents when the turn-off times were set as $t_{\mathrm{on},1} \approx 0\,\mathrm{ns}$, $t_{\mathrm{on},2} \approx 200\,\mathrm{ns}$, and $t_{\mathrm{on},3} \approx 400\,\mathrm{ns}$. Blue, green, and red lines indicate the first, second, and third inverter, respectively.

3.5 Discussion

This chapter addressed circulating current modeling of parallel three-phase two-level voltage source inverters. Circulating current models were developed for n parallel units and for both parallel inverter configurations considered in this dissertation.

The developed models showed that the main difference between the parallel inverter configurations from the circulating current point of view is that in the case of separate direct voltage sources, circulating currents in a certain unit can be controlled by controlling at least two phase leg voltages, while in the case of a common direct voltage source, circulating current control basically requires that all phase leg voltages are controlled. Furthermore, it was shown that we need to apply circulating current controllers in $n - 1$ parallel units to ensure that the current flow between the parallel units can be controlled. This holds true for both of the configurations. The difference is, however, that in the case of separate direct voltage sources, we need to apply controllers only in the dq-axes, while in the case of parallel inverters with a common direct voltage source, 0 axis current controllers must be used in addition to the dq-axes controllers.

Besides developing the circulating current models and considering some control related subjects, it was also considered how differences in blanking times, finite turn-on and turn-off times of switching devices, and forward voltage drops of switching devices and anti-parallel diodes affect the circulating current generation between the parallel units. For this purpose, a simplified time-domain circulating current model was developed. It was shown that the results obtained from the simplified model are in good agreement with the circuit simulations. Also some experimental results were presented. Although the experimental results confirmed some predictions, they also showed that it is rather difficult or even impossible to verify the model experimentally.

From the presented results we can, however, conclude that differences in blanking times, finite turn-on and turn-off times of switching devices, and forward voltage drops of switching devices and anti-parallel diodes result in a circulating current waveforms that are similar in all cases. It must, still, be emphasized that the circulating currents caused by the differences in blanking times and in finite turn-on and turn-off times of switching devices are dependent on the switching frequency, while the circulating currents caused by the forward voltage drops of switching devices and anti-parallel diodes are not.

Chapter 4

Dual modulator method for parallel three-phase voltage source inverters

This chapter considers application of space-vector-based modulation methods to the control of parallel two-level three-phase voltage source inverters. It is illustrated that the space-vector-based modulation methods may cause problems when applied to parallel inverters. The described problems are related to the fact that the differences in the stationary $\alpha\beta$-axes voltage components will reflect also to the zero-axis voltage components. In order to prevent these problems and to make it possible to control zero-sequence voltages separately from the $\alpha\beta$-axes voltages and vice versa, a dual modulator method is introduced.

4.1 Space-vector-based modulation

4.1.1 Basic principles

Space vector modulation (SVM) developed for the two-level three-phase inverters is based on the fact that such inverters can have eight different switching states (Holmes and Lipo, 2003), which are depicted in Fig. 4.1. Two of the states are known as zero states and the rest six as active states of the inverter. When either one upper and two lower or one lower and two upper switches are closed at the same time, the inverter is said to be in the active state. During the zero switching states either all lower or all upper switches are closed at the same time. The active switching states are denoted by numbers from 1 to 6 and the zero switching states by 0 and 7.

The state of the inverter can be mathematically expressed by a switching function space vector $\vec{r}^{\,\mathrm{s}}$, which is also called a switching vector, and a zero-sequence component r_0. The eight possible switching vectors and zero-sequence components can be obtained by applying (2.3), (2.7), and (2.8). The results are given in Table. 4.1. The table shows that there are only six nonzero switching vectors that correspond to the active states of the inverter, and four different zero-sequence component values that are at largest during the zero switching states. Further, the table indicates that it is impossible to control the inverter in such a fashion that no instantaneous zero-sequence voltage components are generated, since after all, the desired output voltages are realized by averaging the switching vectors over a switching period.

An output voltage vector and a zero-sequence voltage component of a three-phase VSI can be obtained with the help of the switching vector and the zero-sequence component as

$$\vec{u}^{\,\mathrm{s}} = \vec{r}^{\,\mathrm{s}} u_{\mathrm{dc}} \tag{4.1}$$

$$u_0 = r_0 u_{\mathrm{dc}} \tag{4.2}$$

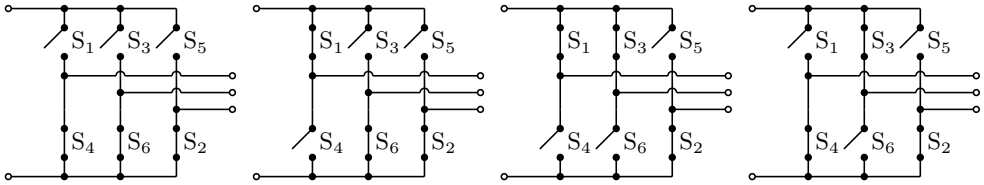

(a) State 0. (b) State 1. (c) State 2. (d) State 3.

(e) State 4. (f) State 5. (g) State 6. (h) State 7.

Fig. 4.1: Eight possible switching states of a three-phase two-level inverter. The states 0 and 7 are known as zero states, while the states 1–6 represent active states of the inverter.

Table 4.1: Eight possible switching states represented by the switching vector $\vec{r}^{\,\mathrm{s}}$ and the zero-sequence component r_0. The variables r_a, r_b and r_c are the phase switching functions of the inverter.

State	r_a	r_b	r_c	$\vec{r}^{\,\mathrm{s}}$	r_0
0	$-1/2$	$-1/2$	$-1/2$	0	$-1/2$
1	$+1/2$	$-1/2$	$-1/2$	$+2/3e^{j0\pi/3}$	$-1/6$
2	$+1/2$	$+1/2$	$-1/2$	$+2/3e^{j1\pi/3}$	$+1/6$
3	$-1/2$	$+1/2$	$-1/2$	$+2/3e^{j2\pi/3}$	$-1/6$
4	$-1/2$	$+1/2$	$+1/2$	$+2/3e^{j3\pi/3}$	$+1/6$
5	$-1/2$	$-1/2$	$+1/2$	$+2/3e^{j4\pi/3}$	$-1/6$
6	$+1/2$	$-1/2$	$+1/2$	$+2/3e^{j5\pi/3}$	$+1/6$
7	$+1/2$	$+1/2$	$+1/2$	0	$+1/2$

where u_dc is the direct voltage of the inverter. The orientation of the output voltage vectors in the $\alpha\beta$ plane is illustrated in Fig. 4.2(a). As can be seen, the active vectors divide the plane into six equal sectors, which are denoted by $m \in \{1, 2, \cdots, 6\}$. The instantaneous lengths of active voltage vectors equal $|\vec{u}_i^{\,\mathrm{s}}| = 2/3u_\mathrm{dc}$, $i \in \{1, 2, \cdots, 6\}$. The hexagon obtained by connecting the tips of the active vectors shows the boundary inside of which any voltage vector can be realized by appropriately averaging the active and zero voltage vectors. The circle inside the hexagon shows the limit of a linear modulation region. The radius of this circle is equal to $u_\mathrm{dc}/\sqrt{3}$. Within the linear modulation region, the average line-to-line voltages remain sinusoidal, but the average phase leg voltages may be distorted.

The formation of the average output voltage vector, which is referred to as a voltage reference vector from this point forward, is illustrated in Fig. 4.2(b). As shown, the voltage reference vector

$$\vec{u}_\mathrm{ref}^{\,\mathrm{s}} = u_{\mathrm{ref},\alpha} + ju_{\mathrm{ref},\beta} \tag{4.3}$$

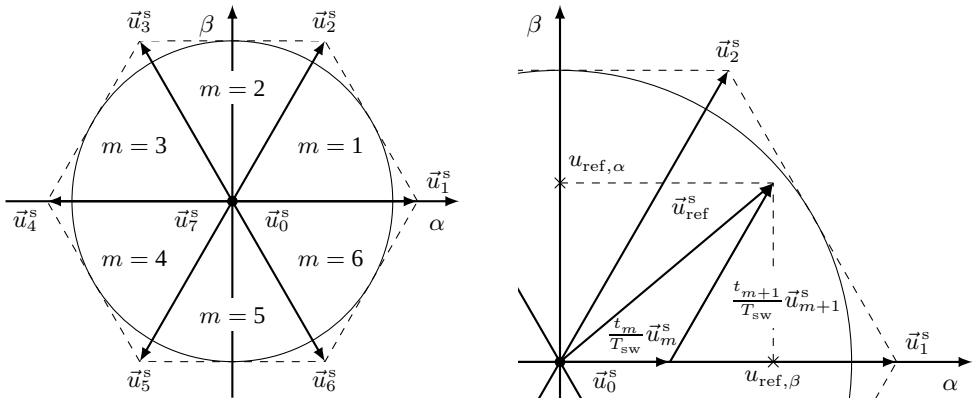

(a) Eight discrete space vectors. (b) Formation of average space vector.

Fig. 4.2: Eight discrete space vectors $\vec{u}_i^{\mathrm{s}}$, $i \in \{0, 1, 2, \cdots, 7\}$ and formation of the average space vector $\vec{u}^{\mathrm{s}}$ as a result of averaging two adjacent active space vectors. Note that the active space vectors $\vec{u}_{1-6}^{\mathrm{s}}$ divide the $\alpha\beta$ plane into six equal sectors denoted by m.

is obtained by averaging two adjacent voltage vectors as

$$\vec{u}_{\mathrm{ref}}^{\mathrm{s}} = \frac{t_m}{T_{\mathrm{sw}}}\vec{u}_m^{\mathrm{s}} + \frac{t_{m+1}}{T_{\mathrm{sw}}}\vec{u}_{m+1}^{\mathrm{s}} \tag{4.4}$$

where t_m and t_{m+1} are time durations of the active vectors

$$\vec{u}_m^{\mathrm{s}} = \frac{2}{3}u_{\mathrm{dc}}e^{j\left((m-1)\frac{\pi}{3}\right)} \tag{4.5}$$

and

$$\vec{u}_{m+1}^{\mathrm{s}} = \frac{2}{3}u_{\mathrm{dc}}e^{j\left(m\frac{\pi}{3}\right)} \tag{4.6}$$

and T_{sw} is the time of a switching period. By equating the real and imaginary parts of (4.4), one can solve the durations for the active vectors. The solutions can be given in a matrix form as (Sarén, 2005)

$$\begin{bmatrix} t_m \\ t_{m+1} \end{bmatrix} = \frac{\sqrt{3}T_{\mathrm{sw}}}{u_{\mathrm{dc}}} \begin{bmatrix} \sin\left(m\frac{\pi}{3}\right) & -\cos\left(m\frac{\pi}{3}\right) \\ -\sin\left((m-1)\frac{\pi}{3}\right) & \cos\left((m-1)\frac{\pi}{3}\right) \end{bmatrix} \begin{bmatrix} u_{\mathrm{ref},\alpha} \\ u_{\mathrm{ref},\beta} \end{bmatrix} \tag{4.7}$$

The durations of the active vectors are limited as

$$t_m + t_{m+1} \leq T_{\mathrm{sw}} \tag{4.8}$$

When the sum of active vector durations does not exceed the switching period time, zero vector(s) are applied for the time remaining. The total duration of the zero vector can be calculated as

$$t_{\mathrm{z}} = t_0 + t_7 = T_{\mathrm{sw}} - \left(t_m + t_{m+1}\right) \tag{4.9}$$

which shows that t_{z} can be divided between the zero voltage vectors $\vec{u}_0^{\mathrm{s}}$ and $\vec{u}_7^{\mathrm{s}}$, the durations of which are denoted by t_0 and t_7, respectively. From the calculated active and zero vector times, (4.7) and (4.9), one can determine phase leg references for the inverter.

4.1.2 Phase leg references

According to Holmes and Lipo (2003), the placement of the zero vector can be considered to be the primary difference between PWM strategies, and in alternative implementations, the positions of active space vectors are simply varied within the switching period. This basically means that phase leg references for various PWM methods can be obtained by dividing the active and zero vector times into the phase legs differently. Let us consider a conventional space vector PWM (van der Broeck et al., 1988) as an example.

The conventional space vector PWM uses two active vectors adjacent to the voltage reference vector and two zero vectors within each switching period. Although van der Broeck et al. (1988) suggested that each switching period should be started and ended with different zero vectors, an alternative way is to divide each switching period into two subintervals, the length of which equals a half switching period and which align the applied space vectors as depicted in Fig. 4.3. The space vector sequences depicted in Figs. 4.3(a) and 4.3(b) are for the odd $m = \{1, 2, 3\}$ and even $m = \{2, 4, 6\}$ sectors, respectively. The order of the active space vectors in the odd and even sectors is reversed to obtain a minimum switching frequency of each phase leg.

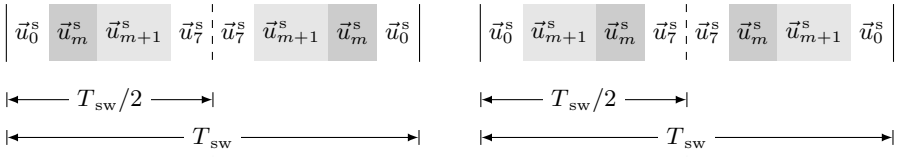

(a) Odd sectors $m = \{1, 2, 3\}$. (b) Even sectors $m = \{2, 4, 6\}$.

Fig. 4.3: Space vector sequences for the odd $m = \{1, 2, 3\}$ and even $m = \{2, 4, 6\}$ sectors in the case of conventional space vector PWM.

With the help of the space vector sequence illustrated in Fig. 4.3(a) and Table 4.1, we can sketch phase switching function waveforms depicted in Fig. 4.4, which correspond to the odd sector $m = 1$. Similar phase switching function waveforms can be obtained also for the other sectors. In each subinterval, the durations of active vectors $\vec{u}_m^{\,\mathrm{s}}$ and $\vec{u}_{m+1}^{\,\mathrm{s}}$ are equal to $t_m/2$ and $t_{m+1}/2$, respectively, and the durations of zero vectors to $t_{\mathrm{z}}/4$. This is because the overall zero vector duration t_{z} is divided equally between the zero vectors $\vec{u}_0^{\,\mathrm{s}}$ and $\vec{u}_7^{\,\mathrm{s}}$, that is, $t_0 = t_7 = t_{\mathrm{z}}/2$.

From the sketched phase switching function waveforms, one can define on-time durations of the upper switching devices $T_{\mathrm{on,a}}$, $T_{\mathrm{on,b}}$, and $T_{\mathrm{on,c}}$ for each sector. Averaging the on-time durations with respect to the switching period gives phase duty cycles

$$d_{\mathrm{a}} = T_{\mathrm{on,a}}/T_{\mathrm{sw}} \tag{4.10}$$

$$d_{\mathrm{b}} = T_{\mathrm{on,b}}/T_{\mathrm{sw}} \tag{4.11}$$

$$d_{\mathrm{c}} = T_{\mathrm{on,c}}/T_{\mathrm{sw}} \tag{4.12}$$

The phase duty cycle waveforms are illustrated in Fig. 4.5(a) assuming that the magnitude of the constantly rotating voltage reference vector equals $|\vec{u}_{\mathrm{ref}}^{\,\mathrm{s}}| = 1/\sqrt{3}$, which, again, corresponds to the limit of the achievable linear modulation region. Note, however, that the phase duty cycles are given in the interval $[-1/2\ 1/2]$, instead of $[0\ 1]$. Thus, the phase duty cycle values $-1/2$ and $1/2$ correspond to the situations where the lower and upper switches are closed for the whole switching period, respectively.

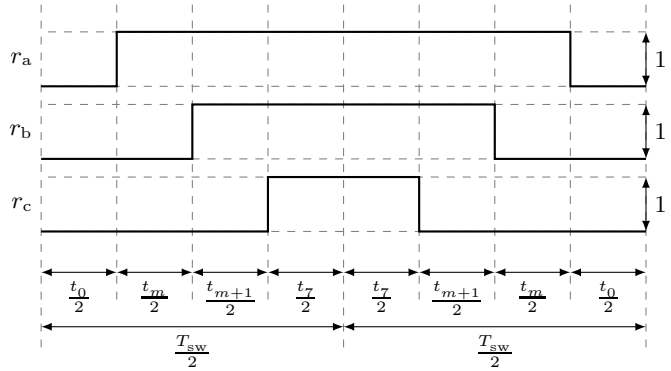

Fig. 4.4: Formation of the phase switching functions r_a, r_b, and r_c in the sector $m = 1$ for the conventional space vector PWM.

By transforming the phase duty cycles into the stationary $\alpha\beta 0$ coordinates by applying (2.9), one obtains duty cycle waveforms shown in Fig. 4.5(b). The magnitudes of the sinusoidal $\alpha\beta$ plane components denoted by d_α and d_β equal $1/\sqrt{3}$, as it was commanded, but as a consequence of the principles that the space-vector-based modulation methods apply, also a zero-sequence duty cycle component d_0 is generated. If the zero-sequence duty cycle component is subtracted from the phase duty cycles as

$$d'_\mathrm{a} = d_\mathrm{a} - d_0 \tag{4.13}$$

$$d'_\mathrm{b} = d_\mathrm{b} - d_0 \tag{4.14}$$

$$d'_\mathrm{c} = d_\mathrm{c} - d_0 \tag{4.15}$$

sinusoidal phase duty cycle waveforms shown in Fig. 4.5(c) are obtained. As can be seen, the amplitudes of these waveforms exceed the maximum realizable phase duty cycle values. This shows the main advantage of the space-vector-based modulation methods over a sinusoidal PWM where a low-frequency sinusoidal target reference waveform is compared against a high-frequency carrier waveform; see for example Holmes and Lipo (2003). In other words, the linear modulation region of the sinusoidal PWM is less than the linear modulation region of the space-vector-based modulation methods. The increase in the linear modulation region comes, however, at the expense of the introduced zero-sequence component.

4.2 Space-vector-modulated parallel inverters

Active current balancing techniques presented for parallel three-phase VSCs and VSIs manipulate the phase leg references to achieve the desired goal, which is to share load current with the specified ratios; see for example (Shi and Venkataramanan, 2004; Pan and Liao, 2007). When parallel inverters apply space-vector-based modulation methods, the phase leg references are indirectly manipulated by manipulating the voltage vectors fed to the modulators. When parallel inverters apply different voltage vectors, the targeted difference is generated in terms of $\alpha\beta$-plane components, but as a consequence of the principles that the space-vector-based modulation methods apply, the difference is also generated in zero-sequence components. Thus, it is possible that the zero-sequence circulating currents are excited as a consequence of the active current balancing (Chen, 2009b). Let us illustrate this with an example.

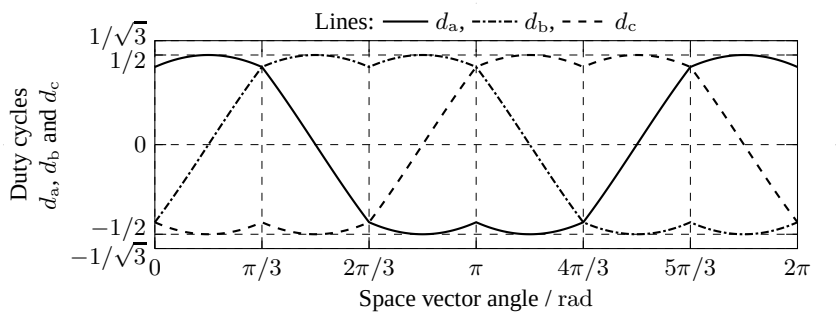

(a) Duty cycles in the stationary abc reference frame.

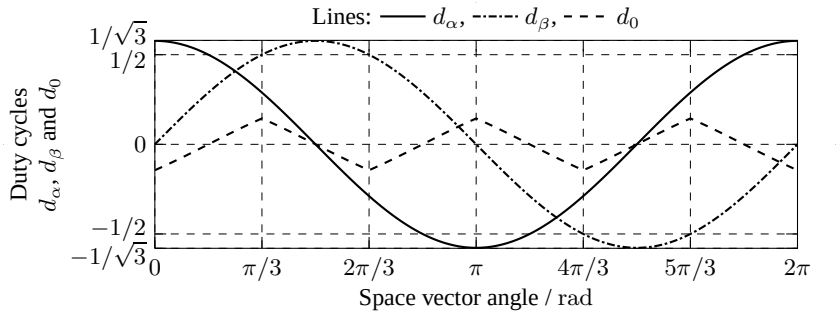

(b) Duty cycles in the stationary $\alpha\beta0$ reference frame.

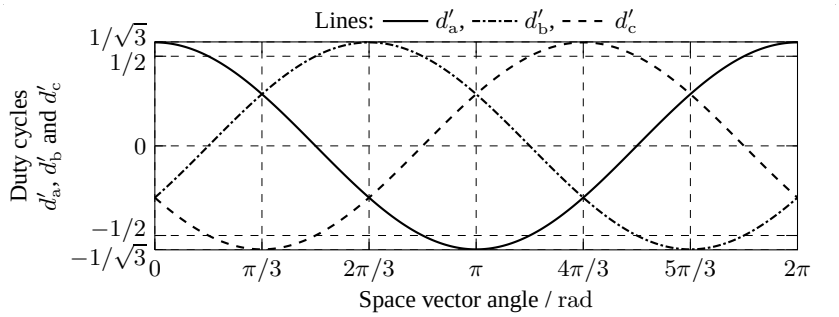

(c) Duty cycles without zero-sequence components.

Fig. 4.5: Duty cycle waveforms obtained by applying the conventional space vector PWM. The magnitude of the constantly rotating voltage reference vector was set as $|\vec{u}^{\,\mathrm{s}}_{\mathrm{ref}}| = 1/\sqrt{3}$, which corresponds to the limit of the linear modulation region of the space-vector-based modulation methods.

Let us consider a parallel connection of two inverters and assume that the inverters apply different voltage vectors to achieve the desired goal from the load current sharing point of view. The duty cycle waveforms that were obtained assuming that there is both an amplitude and phase difference between the applied voltage vectors are depicted in Fig. 4.6. From Figs. 4.6(a) and 4.6(b) one can see that the amplitudes and phases of the $\alpha\beta$-axes components diverge as expected. However, a difference is also generated into the zero-sequence components as

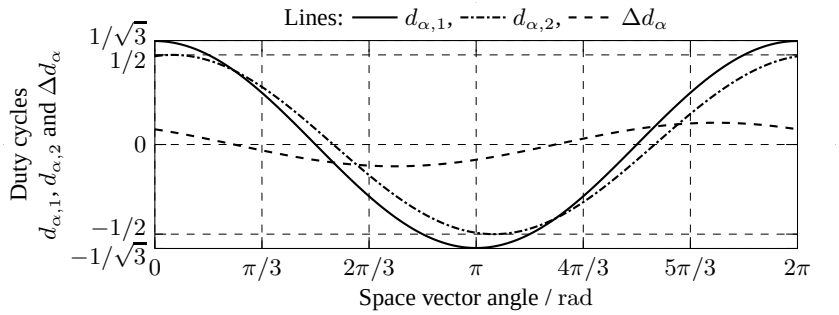

(a) α-axis duty cycles.

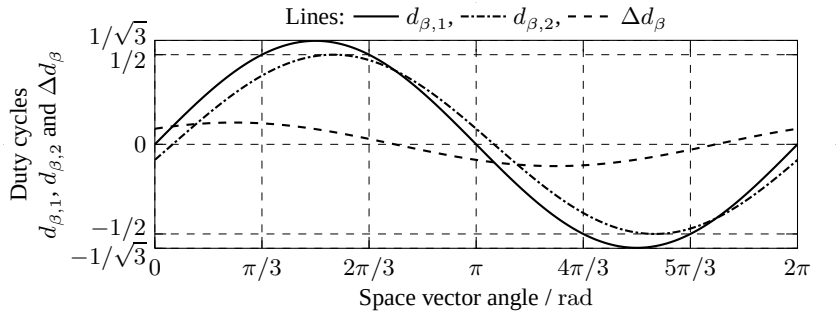

(b) β-axis duty cycles..

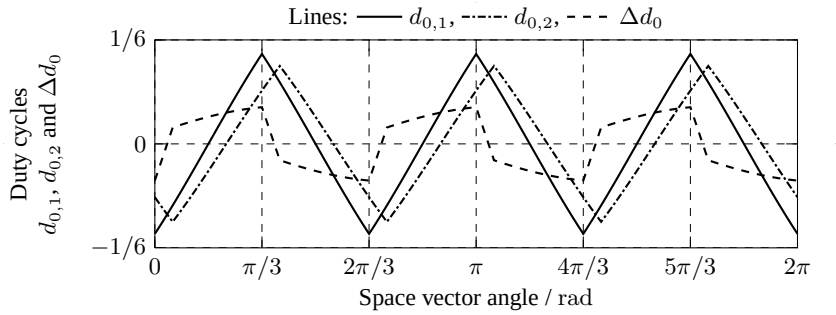

(c) 0-axis duty cycles.

Fig. 4.6: Duty cycle waveforms of two parallel inverters when there is both an amplitude and phase difference between the applied voltage vectors.

can be seen from Fig. 4.6(c). Because of this property, the space vector modulation methods may inherently cause zero-sequence circulating currents in the case of parallel inverters with a common direct voltage source. This, again, is because in such parallel connections, the zero-sequence circuit does not appear as an open-circuit as in the case of parallel inverters with separate direct voltage sources.

4.3 Dual modulator principle

Based on the previous sections, the space-vector-based modulation methods generate low-frequency zero-sequence voltage components, which, in turn, can result in low-frequency zero-sequence circulating currents in the parallel inverter configurations where zero-sequence current paths exist. To deal with this problem and to make it possible to control zero-sequence voltages independently from the $\alpha\beta$-axes voltages, and vice versa, a dual modulator method is proposed in the following.

A block diagram of the proposed dual modulator is depicted in Fig. 4.7. The dual modulator basically consists of two independently operating modulators, which are referred to as primary and secondary modulators. The primary modulator can be, in principle, any type of a modulator. The primary modulator can, for example, apply the principles of the conventional space vector PWM. The secondary modulator, again, is realized applying the inverse of the transformation matrix

$$\mathbf{T}_{\alpha\beta0} = \frac{2}{3}\begin{bmatrix} 1 & -1/2 & -1/2 \\ 0 & \sqrt{3}/2 & -\sqrt{3}/2 \\ 1/2 & 1/2 & 1/2 \end{bmatrix} \tag{4.16}$$

The inverse is defined as

$$\mathbf{T}^{-1}_{\alpha\beta0} = \begin{bmatrix} 1 & 0 & 1 \\ -1/2 & \sqrt{3}/2 & 1 \\ -1/2 & -\sqrt{3}/2 & 1 \end{bmatrix} \tag{4.17}$$

As depicted in Fig. 4.7, the matrix (4.17) is used to convert both scaled $\alpha\beta$-axes and 0-axis components into phase duty cycles. The components are also scaled with the instantaneous direct voltages u_{dc}. The advantage of this kind of an arrangement is that the $\alpha\beta$-axes voltages can be controlled independently from the 0-axis voltages. In its intented application, similar voltage vectors are fed to each primary modulator of each parallel-connected unit, and the secondary modulators are fed by the voltage vector and zero-sequence voltage components, which are obtained from the circulating current controllers.

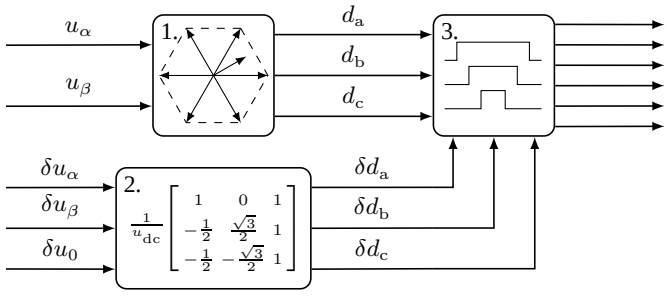

Fig. 4.7: Block diagram of the proposed dual modulator. The dual modulator basically consists of two independently operating modulators known as primary and secondary modulators. Modulating waveforms of the primary and secondary modulators are produced in the block 1 and 2, respectively.

4.4 Discussion

In this chapter, the basic principles of space-vector-based modulation methods were outlined. Then application of the space-vector-based modulation methods in the control of parallel inverters was considered. It was explained why the space-vector-based modulation methods may inherently excite low-frequency zero-sequence circulating currents in the parallel inverter configurations where zero-sequence current paths exist. The reason for such circulating current generation is the zero-sequence voltages that are added to the inverter phase leg references to increase the linear modulation to its maximum. To deal with this problem and to enable independent control of both the $\alpha\beta$-axes and 0-axis voltage components, a dual modulator principle was introduced.

Although the dual modulator principle can be applied both in the control of parallel inverters with separate direct voltage sources and in the control of parallel inverters with a common direct voltage source, it is intended to be used only with the latter case. This is because in the former case there is no path for the zero-sequence current to flow between the inverters.

Chapter 5

Space vector and zero-sequence component limitation

A dual modulator principle was introduced in the previous chapter. The dual modulator basically consists of two independently operating modulators, the outputs of which eventually constitute the switching commands of the inverter. In its intended usage, the same voltage vector is fed to the primary modulators of each parallel unit and the inputs of the secondary modulators are obtained from the circulating current controllers. It is obvious that when the inverters are driven into saturation, we cannot exactly realize the commanded voltages. Therefore, if we want to guarantee that the voltage commands obtained from the circulating current controllers can be realized, we must make sure that the inverter is not driven into saturation by the primary modulator. This problem can be dealt with by limiting the inputs of the primary and secondary modulators.

The inputs of the primary modulator can be limited by applying existing space vector limitation methods. The limitation of the secondary modulator inputs is not as straightforward. This is because one has to limit both the voltage reference vector and the zero-sequence voltage component so that the resulting phase leg references do not exceed the maximum allowed values at any time. To deal with this problem, an algorithm that combines the space vector and zero-sequence component limitation methods is introduced in this chapter. The algorithm basically adjusts the voltage vector and zero-sequence voltage component limits according to the current values of these components. Three combinations are presented to show that the algorithm can be used with different types of space vector limitation methods. Further, an application example is given to illustrate the intended usage of the proposed algorithm.

5.1 Some space vector limitation methods

Based on the review presented by Ottersten and Svensson (2002), voltage reference vectors can be limited at least in three different ways without the knowledge of plant parameters. These methods, which are known as the circular limit method, the space vector limit method, and the minimum amplitude error method are presented in the following. The methods are presented since they will be applied later on in this chapter. There are also some limitation methods that take plant parameters into account, but are not considered here.

5.1.1 Circular limit method

In the circular limit method, an overlong voltage reference vector $\vec{u}^{\,\mathrm{s}}_{\mathrm{ref}}$ is limited to the maximum circle within the hexagon as depicted in Fig. 5.1. In this context, the hexagon refers to the

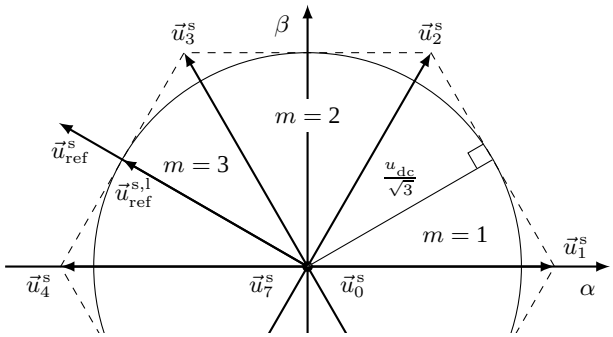

Fig. 5.1: Principle of the circular limit method. The circular limit method limits the voltage reference vector $\vec{u}_{\mathrm{ref}}^{\,\mathrm{s}}$ to the maximum circle within the hexagon, which represents the boundary of realizable voltage vectors. The limitation distorts the vector amplitude.

boundary of realizable voltage vectors. The detection of whether the vector is within the circle or not is performed by comparing the length of the vector to the radius of the maximum circle as

$$|\vec{u}_{\mathrm{ref}}^{\,\mathrm{s}}| = \sqrt{u_{\mathrm{ref},\alpha}^2 + u_{\mathrm{ref},\beta}^2} > \frac{u_{\mathrm{dc}}}{\sqrt{3}} \tag{5.1}$$

If the condition (5.1) holds true, a limited space vector is calculated as

$$\vec{u}_{\mathrm{ref}}^{\,\mathrm{s,l}} = \frac{u_{\mathrm{dc}}}{\sqrt{3}} \frac{\vec{u}_{\mathrm{ref}}^{\,\mathrm{s}}}{|\vec{u}_{\mathrm{ref}}^{\,\mathrm{s}}|} \tag{5.2}$$

The limited voltage vector is oriented in the same direction as the original vector, but the amplitude is distorted. The main drawback of this method is that it does not make use of all available voltage.

5.1.2 Space vector limit method

In the space vector limit method, an overlong voltage vector is limited to the hexagon as illustrated in Fig. 5.2. The detection of whether the vector is outside the hexagon or not is performed in two stages. In the first stage, the vector is transformed into xy coordinates as

$$\vec{u}_{\mathrm{ref,xy}}^{\,\mathrm{s}} = \vec{u}_{\mathrm{ref}}^{\,\mathrm{s}} e^{-j\theta_{\mathrm{xy}}} = \left(u_{\mathrm{ref},\alpha} + j u_{\mathrm{ref},\beta}\right) e^{-j\theta_{\mathrm{xy}}} \tag{5.3}$$

where

$$\theta_{\mathrm{xy}} = \left(1 + 2\,(m-1)\right) \frac{\pi}{6} \tag{5.4}$$

is the angle between the α- and x-axes and the variable $m \in \{1, 2, \cdots, 6\}$ denotes the sector in which the voltage vector $\vec{u}_{\mathrm{ref}}^{\,\mathrm{s}}$ lies. In other words, the x-axis is oriented so that it lies in the middle of the sector in which the voltage vector $\vec{u}_{\mathrm{ref}}^{\,\mathrm{s}}$ lies. Then, in the second stage, the vector outside the hexagon is detected by

$$\mathrm{Re}\left\{\vec{u}_{\mathrm{ref,xy}}^{\,\mathrm{s}}\right\} > \frac{u_{\mathrm{dc}}}{\sqrt{3}} \tag{5.5}$$

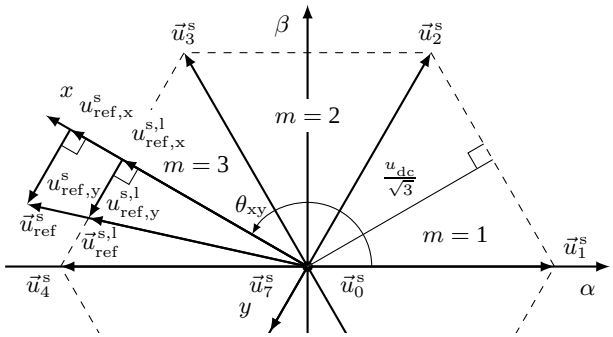

Fig. 5.2: Principle of the space vector limit method. The space vector limit method limits the voltage reference vector $\vec{u}_{\mathrm{ref}}^{\,\mathrm{s}}$ to the boundary of realizable voltage vectors. The limitation distorts the vector amplitude.

If the condition (5.5) holds true, the real and imaginary parts of a limited voltage vector $\vec{u}_{\mathrm{ref,xy}}^{\,\mathrm{s,l}}$ are calculated as

$$u_{\mathrm{ref,x}}^{\mathrm{s,l}} = \frac{u_{\mathrm{dc}}}{\sqrt{3}} \tag{5.6}$$

$$u_{\mathrm{ref,y}}^{\mathrm{s,l}} = u_{\mathrm{ref,x}}^{\mathrm{s,l}} \frac{u_{\mathrm{ref,y}}^{\mathrm{s}}}{u_{\mathrm{ref,x}}^{\mathrm{s}}} \tag{5.7}$$

The limited voltage vector $\vec{u}_{\mathrm{ref,xy}}^{\,\mathrm{s,l}}$ is transformed back into $\alpha\beta$ coordinates as follows

$$\vec{u}_{\mathrm{ref}}^{\,\mathrm{s,l}} = \vec{u}_{\mathrm{ref,xy}}^{\,\mathrm{s,l}} e^{j\theta_{\mathrm{xy}}} = \left(u_{\mathrm{ref,x}}^{\mathrm{s,l}} + j u_{\mathrm{ref,y}}^{\mathrm{s,l}} \right) e^{j\theta_{\mathrm{xy}}} \tag{5.8}$$

Also in this method, the limited vector is oriented in the same direction as the original vector, but the amplitude is distorted. The advantage of the space vector limit method compared with the circular limit method is that all available voltage can be utilized.

5.1.3 Minimum amplitude error method

The minimum amplitude error method limits an overlong voltage vector to the hexagon as shown in Fig. 5.3. The limitation is basically realized by calculating the vector on the hexagon that is nearest to the vector to be limited. The need for limitation is determined as in the case of the space vector limit method, that is, by first transforming the voltage vector into xy coordinates applying (5.3) and then detecting the vector outside the hexagon by (5.5). If a limitation is needed, the real and imaginary parts of the limited voltage vector $\vec{u}_{\mathrm{ref,xy}}^{\,\mathrm{s,l}}$ are calculated as

$$u_{\mathrm{ref,x}}^{\mathrm{s,l}} = \frac{u_{\mathrm{dc}}}{\sqrt{3}} \tag{5.9}$$

$$u_{\mathrm{ref,y}}^{\mathrm{s,l}} = \begin{cases} u_{\mathrm{ref,y}}^{\mathrm{s}} & \text{, when } \left| u_{\mathrm{ref,y}}^{\mathrm{s}} \right| \leq \frac{u_{\mathrm{dc}}}{3} \\ \mathrm{sign}\left(u_{\mathrm{ref,y}}^{\mathrm{s}} \right) \frac{u_{\mathrm{dc}}}{3} & \text{, when } \left| u_{\mathrm{ref,y}}^{\mathrm{s}} \right| > \frac{u_{\mathrm{dc}}}{3} \end{cases} \tag{5.10}$$

The limited voltage vector $\vec{u}_{\mathrm{ref,xy}}^{\,\mathrm{s,l}}$ is transformed back into $\alpha\beta$ coordinates by applying (5.8). The difference between the minimum amplitude error method and the space vector limit method

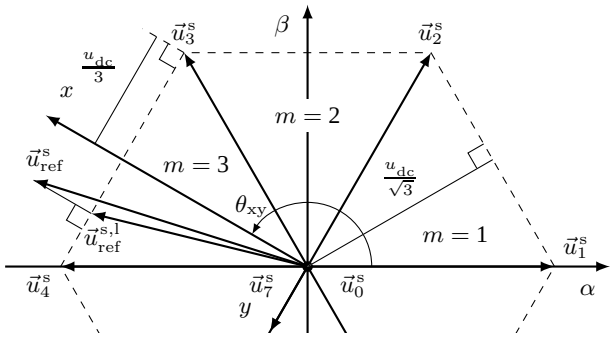

Fig. 5.3: Principle of the minimum amplitude error method. The minimum amplitude error method limits the voltage reference vector $\vec{u}_{\mathrm{ref}}^{\,\mathrm{s}}$ to the boundary of realizable voltage vectors. Besides distorting the vector amplitude, the limitation may also distort the vector angle.

is that in the former case both the vector amplitude and the angle may be distorted, while in the latter case only the vector amplitude is distorted.

5.2 Limits of the space vector limitation methods

The presented space vector limitation methods limit the voltage vectors to the outer hexagon or to the maximum circle within the outer hexagon, which are depicted in Fig. 5.4. These boundaries cannot, however, be applied when a voltage reference vector $\vec{u}_{\mathrm{ref}}^{\,\mathrm{s}}$ is to be transformed into realizable phase leg references by applying the transformation matrix (2.10). This is because the transformation results in symmetric phase leg references and only voltage vectors within the inner hexagon, which is depicted in Fig. 5.4, can be realized using symmetric phase leg voltages (Rodriguez et al., 2005).

From above it follows that when voltage vectors are transformed into phase leg references applying (2.10), the vectors must be limited to the inner hexagon or to the maximum circle within the inner hexagon depending on the space vector limitation method applied. Since this affects the detection and limitation of overlong vectors, the presented space vector limitation methods cannot be directly applied. In the case of the circular limit method this means that the length of the voltage vector is compared with the inradius of the inner hexagon r instead of the inradius of the outer hexagon R. Mathematically this is expressed as

$$|\vec{u}_{\mathrm{ref}}^{\,\mathrm{s}}| = \sqrt{u_{\mathrm{ref},\alpha}^2 + u_{\mathrm{ref},\beta}^2} > r \tag{5.11}$$

If the condition (5.11) holds true, a limited voltage vector is calculated as

$$\vec{u}_{\mathrm{ref}}^{\,\mathrm{s,l}} = r\frac{\vec{u}_{\mathrm{ref}}^{\,\mathrm{s}}}{|\vec{u}_{\mathrm{ref}}^{\,\mathrm{s}}|} \tag{5.12}$$

When the space vector limit method or the minimum amplitude error method is applied, overlong voltage vectors cannot be directly detected by applying (5.3)–(5.4). This is because the inner hexagon is rotated 30° with respect to the outer hexagon. One way to deal with this problem is to define the sectors that divide the $\alpha\beta$ plane into six equal segments as illustrated in Fig. 5.5.

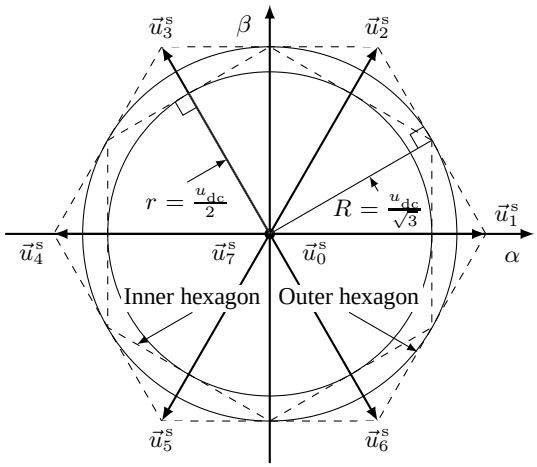

Fig. 5.4: Limitation boundaries. The outer hexagon shows the boundary of realizable voltage vectors, while the inner hexagon shows the boundary within which any voltage vector can be realized by using symmetric phase leg voltages.

Then, the voltage vector can be transformed into xy coordinates by applying (5.3) and

$$\theta_{\mathrm{xy}} = (m-1)\,\frac{\pi}{3} \tag{5.13}$$

After the transformation, the real-axis component of the transformed vector is compared with the inradius of the inner hexagon as

$$\mathrm{Re}\left\{\vec{u}^{\,\mathrm{s}}_{\mathrm{ref,xy}}\right\} > r \tag{5.14}$$

If the condition (5.14) holds true, the voltage vector is limited. In the case of the space vector limit method, the limitation is performed as

$$u^{\mathrm{s,l}}_{\mathrm{ref,x}} = r \tag{5.15}$$

$$u^{\mathrm{s,l}}_{\mathrm{ref,y}} = u^{\mathrm{s,l}}_{\mathrm{ref,x}} \frac{u^{\mathrm{s}}_{\mathrm{ref,y}}}{u^{\mathrm{s}}_{\mathrm{ref,x}}} \tag{5.16}$$

and in the case of the minimum amplitude error method as

$$u^{\mathrm{s,l}}_{\mathrm{ref,x}} = r \tag{5.17}$$

$$u^{\mathrm{s,l}}_{\mathrm{ref,y}} = \begin{cases} u^{\mathrm{s}}_{\mathrm{ref,y}} & \text{, when } \left|u^{\mathrm{s}}_{\mathrm{ref,y}}\right| \leq \frac{1}{\sqrt{3}} r \\ \mathrm{sign}\left(u^{\mathrm{s}}_{\mathrm{ref,y}}\right) \frac{1}{\sqrt{3}} r & \text{, when } \left|u^{\mathrm{s}}_{\mathrm{ref,y}}\right| > \frac{1}{\sqrt{3}} r \end{cases} \tag{5.18}$$

5.3 Zero-sequence voltage component limitation method

The transformation of the zero-sequence voltage component $u_{\mathrm{ref},0}$ into phase leg references applying the transformation matrix (2.10) results in $u_{\mathrm{ref,a}} = u_{\mathrm{ref,b}} = u_{\mathrm{ref,c}} = u_{\mathrm{ref},0}$. Thus, the

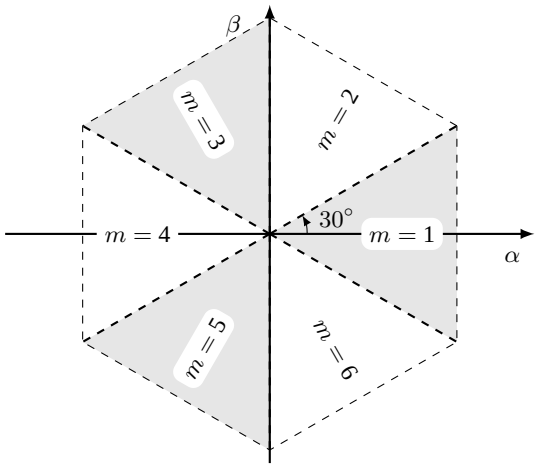

Fig. 5.5: Alternative way of dividing the $\alpha\beta$ plane into six equal sectors denoted by $m \in \{1, 2, \cdots, 6\}$.

need for zero-sequence component limitation can be determined as

$$\left|u_{\mathrm{ref},0}\right| > r_0 \tag{5.19}$$

where r_0 denotes the applied zero-sequence component limit. If the condition (5.19) holds true, a limited zero-sequence voltage component is calculated as

$$u^{\mathrm{l}}_{\mathrm{ref},0} = \mathrm{sign}\left(u_{\mathrm{ref},0}\right) r_0 \tag{5.20}$$

5.4 Proposed limitation algorithm

The limitation of a voltage reference vector $\vec{u}^{\,\mathrm{s}}_{\mathrm{ref}}$ and a zero-sequence voltage component $u_{\mathrm{ref},0}$ were separately dealt with in the previous sections. When both of these components are nonzero, the phase leg references that are obtained by applying the transformation matrix (2.10) are composed of both of them. Thus, if we want to guarantee that the resulting phase leg references are always realizable, the applied limits cannot be independently defined.

When the zero-sequence voltage component equals zero, the minimum length of the voltage reference vector that can result in unrealizable phase leg references equals $|\vec{u}^{\,\mathrm{s}}_{\mathrm{ref}}| = u_{\mathrm{dc}}/2$. This occurs when the voltage vector is oriented in the same direction as any of the active voltage vectors $\vec{u}^{\,\mathrm{s}}_i$, $i \in \{1, 2, \cdots, 6\}$. Similarly, when the length of the voltage reference vector equals zero, the magnitude of the minimum zero-sequence voltage component that results in unrealizable phase leg references also equals $\left|u_{\mathrm{ref},0}\right| = u_{\mathrm{dc}}/2$. Thus, the maximum voltage vector and zero-sequence voltage component limits are equal to

$$r_{\max} = r_{0,\max} = u_{\mathrm{dc}}/2 \tag{5.21}$$

The previous also implies that the sum of the voltage vector length and the zero-sequence voltage component magnitude should not exceed the value of $u_{\mathrm{dc}}/2$. Thus, if the condition

$$|\vec{u}^{\,\mathrm{s}}_{\mathrm{ref}}| + \left|u_{\mathrm{ref},0}\right| \leq \frac{u_{\mathrm{dc}}}{2} \tag{5.22}$$

does not hold true, the voltage vector and zero-sequence voltage component must be limited. The limits to be applied can be obtained by scaling the maximum limits according to the current voltage vector length and the zero-sequence voltage component magnitude. If we treat the length and magnitude equally, the voltage vector limit can be given as

$$r = r_{\max} \frac{|\vec{u}^{\mathrm{s}}_{\mathrm{ref}}|}{|\vec{u}^{\mathrm{s}}_{\mathrm{ref}}| + \left|u_{\mathrm{ref},0}\right|} \tag{5.23}$$

and the zero-sequence voltage component limit as

$$r_0 = r_{0,\max} \frac{\left|u_{\mathrm{ref},0}\right|}{|\vec{u}^{\mathrm{s}}_{\mathrm{ref}}| + \left|u_{\mathrm{ref},0}\right|} \tag{5.24}$$

Combining the determination of the voltage vector and zero-sequence component limits with the limitation methods presented in the previous sections results in a limitation algorithm that can be used to limit both the voltage vector and zero-sequence voltage component so that the resulting phase leg references are always realizable. The algorithm consists of three major steps, which can be described as follows:

1. Define the voltage vector and zero-sequence component limits. If the condition (5.22) holds true, set the limits as $r = r_0 = u_{\mathrm{dc}}/2$. Otherwise, the limits are defined applying (5.23) and (5.24).
2. Apply the zero-sequence component limitation method. If the condition (5.19) holds true, limit the zero-sequence component applying (5.20). Otherwise, the zero-sequence component remains the same.
3. Apply the space vector limitation method.
   (a) If the circular limit method is applied, first detect the overlong voltage vectors by applying (5.11). If the condition (5.11) holds true, limit the voltage vector by applying (5.12). Otherwise, the voltage vector remains the same.
   (b) If the space vector limit method is applied, first transform the voltage vector into xy coordinates by applying (5.3) and (5.16), and detect the overlong voltage vector by using (5.14). If the condition (5.14) holds true, limit the voltage vector by applying (5.7) and transform the limited vector back into the $\alpha\beta$ coordinates using (5.8). Otherwise, the voltage vector remains the same.
   (c) If the minimum amplitude error method is applied, the detection of the overlong voltage vector is performed by applying (5.3), (5.16) and (5.14). If the condition (5.14) holds true, the voltage vector is limited by applying (5.18) and transformed back into the $\alpha\beta$ coordinates by using (5.8). Otherwise, the voltage vector remains the same.

5.5 Limitation examples

To illustrate the operation of the proposed limitation algorithm, it is convenient to define a three-dimensional voltage vector in Cartesian coordinates, which is comprised of the voltage

reference vector $\vec{u}^{\mathrm{s}}_{\mathrm{ref}} = u_{\mathrm{ref},\alpha} + ju_{\mathrm{ref},\beta}$ and the zero-sequence voltage component $u_{\mathrm{ref},0}$ as

$$\vec{u}^{\mathrm{s}}_{\alpha\beta 0} = u_{\mathrm{ref},\alpha}\mathbf{i} + u_{\mathrm{ref},\beta}\mathbf{j} + u_{\mathrm{ref},0}\mathbf{k} \tag{5.25}$$

Vectors **i**, **j**, and **k** are unit vectors. Similarly, a limited three-dimensional voltage vector is defined

$$\vec{u}^{\mathrm{s,l}}_{\alpha\beta 0} = \vec{u}^{\mathrm{l}}_{\mathrm{ref},\alpha}\mathbf{i} + \vec{u}^{\mathrm{l}}_{\mathrm{ref},\beta}\mathbf{j} + u^{\mathrm{l}}_{\mathrm{ref},0}\mathbf{k} \tag{5.26}$$

where $\vec{u}^{\mathrm{l}}_{\mathrm{ref},\alpha}$ and $\vec{u}^{\mathrm{l}}_{\mathrm{ref},\beta}$ are components of the limited voltage reference vector $\vec{u}^{\mathrm{s,l}}_{\mathrm{ref}}$ and $u^{\mathrm{l}}_{\mathrm{ref},0}$ is the limited zero-sequence voltage component. By varying the length of the voltage reference vector $|\vec{u}^{\mathrm{s}}_{\mathrm{ref}}|$ and the zero-sequence component magnitude $\left|u_{\mathrm{ref},0}\right|$ such that the condition (5.22) does not hold true, one can obtain limited voltage vector trajectories that, again, can be used to depict the shape of the area within which the voltage vector is limited. When the zero-sequence voltage component limitation method is used together with the circular limit method, $\vec{u}^{\mathrm{s}}_{\alpha\beta 0}$ is limited to the surface of the area shown in Fig. 5.6(a). In the case of the space vector limit method or the minimum amplitude error method, $\vec{u}^{\mathrm{s}}_{\alpha\beta 0}$ is limited to the surface of the area shown in Fig. 5.6(b).

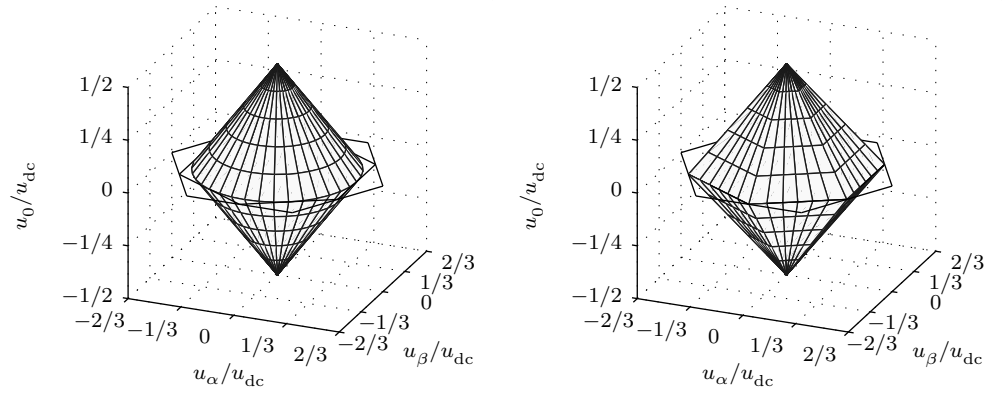

(a) (b)

Fig. 5.6: Areas within which the voltage vector $\vec{u}^{\mathrm{s}}_{\alpha\beta 0}$ is limited when the zero-sequence component limitation method is used together with (a) the circular limit method and (b) the space vector or minimum amplitude error method.

Let us now consider the voltage vector and zero-sequence voltage component limitation assuming that the length of the constantly rotating voltage vector equals $|\vec{u}^{\mathrm{s}}_{\mathrm{ref}}| = 2u_{\mathrm{dc}}/3$ and that the zero-sequence voltage component is equal to $u_{\mathrm{ref},0} = u_{\mathrm{dc}}/3$. With these assumptions, the applied voltage vector and zero-sequence component limits are equal to $r = u_{\mathrm{dc}}/3$ and $r_0 = u_{\mathrm{dc}}/6$, respectively. The limits were obtained by applying (5.23) and (5.24). Some voltage vectors that correspond with these values are shown together with the limited voltage vectors in Fig. 5.7. The limitation was performed by applying the circular limit and zero-sequence voltage component limitation methods. The limited zero-sequence component equals $u^{\mathrm{l}}_{\mathrm{ref},0} = u_{\mathrm{dc}}/6$ and the length of the constantly rotating voltage vector is limited to the circle in the $\alpha\beta$ plane. The length of the vector equals $|\vec{u}^{\mathrm{s}}_{\mathrm{ref}}| = r = u_{\mathrm{dc}}/3$ as expected.

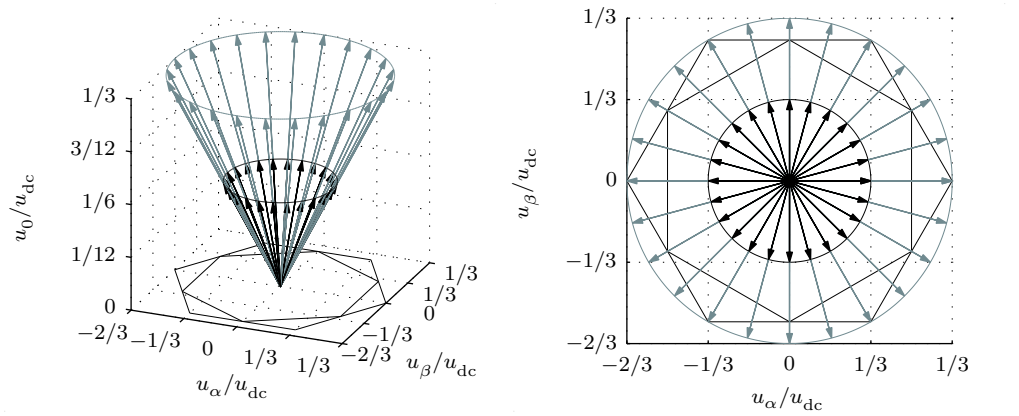

(a) $\alpha\beta 0$-space. (b) $\alpha\beta$-plane.

Fig. 5.7: Trajectories of the desired and limited voltage vectors when the limitation was performed applying the circular limit and zero-sequence component limitation methods. The desired zero-sequence component was $u_{\mathrm{ref},0} = u_{\mathrm{dc}}/3$ and the length of the constantly rotating voltage reference vector $|\vec{u}^{\,\mathrm{s}}_{\mathrm{ref}}| = 2u_{\mathrm{dc}}/3$.

When the space vector limit and minimum amplitude error methods were applied with the zero-sequence component limitation method, the voltage reference vector and the zero-sequence voltage component were limited as illustrated in Figs. 5.8 and 5.9. In both cases, the zero-sequence component $u_{\mathrm{ref},0}$ was limited to the value of $u^{\mathrm{l}}_{\mathrm{ref},0} = u_{\mathrm{dc}}/6$ as expected. Further, the voltage reference vector was limited to the hexagon that is oriented similarly as the inner hexagon shown in Fig. 5.5. The inradius of this hexagon equals $r = u_{\mathrm{dc}}/3$ as expected.

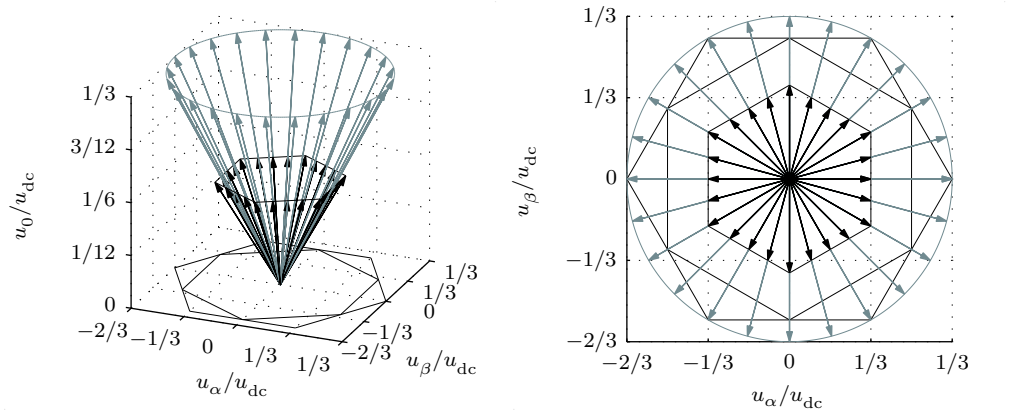

(a) $\alpha\beta 0$-space. (b) $\alpha\beta$-plane.

Fig. 5.8: Trajectories of the desired and limited voltage vectors when the limitation was performed applying the space vector limit and zero-sequence component limitation methods. The desired zero-sequence component was $u_{\mathrm{ref},0} = u_{\mathrm{dc}}/3$ and the length of the constantly rotating voltage reference vector $|\vec{u}^{\,\mathrm{s}}_{\mathrm{ref}}| = 2u_{\mathrm{dc}}/3$.

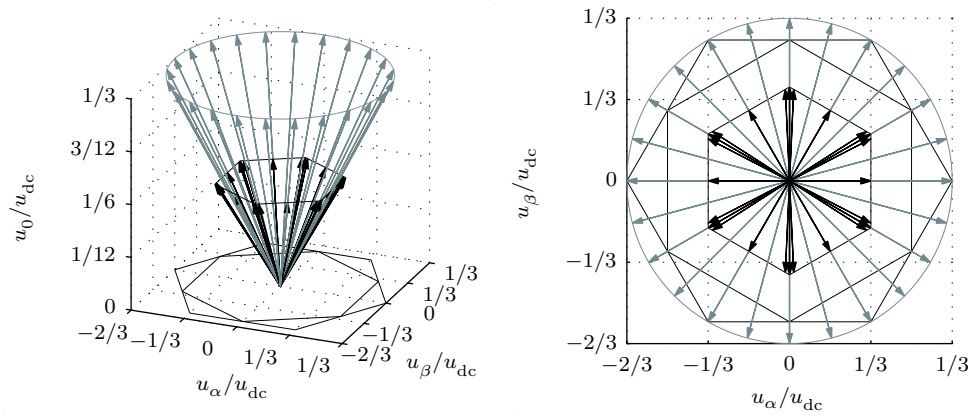

(a) $\alpha\beta 0$-space. (b) $\alpha\beta$-plane.

Fig. 5.9: Trajectories of the desired and limited voltage vectors when the limitation was performed applying the minimum amplitude error and zero-sequence component limitation methods. The desired zero-sequence component was $u_{\mathrm{ref},0} = u_{\mathrm{dc}}/3$ and the length of the constantly rotating voltage reference vector $|\vec{u}^{\,\mathrm{s}}_{\mathrm{ref}}| = u_{\mathrm{dc}}/3$.

Transforming the limited voltage reference vectors $\vec{u}^{\,\mathrm{s,l}}_{\mathrm{ref}}$ and the limited zero-sequence components $u^{\mathrm{l}}_{\mathrm{ref},0}$ into phase leg references applying the transformation matrix (2.10) results in the waveforms shown in Fig. 5.10. The maximum phase leg reference magnitude equals in each case $u_{\mathrm{dc}}/2$, which is the maximum realizable phase leg reference value. The effect of the added zero-sequence voltage component can be seen as a bias, the value of which equals $u_{\mathrm{dc}}/6$.

5.6 Application example

The limitation algorithm presented in this chapter was developed to be used in conjunction with the dual modulator that was introduced in the previous chapter. In this section, we will illustrate how to apply the proposed limitation algorithm with the dual modulator.

A block diagram of the dual modulator, the inputs of which are limited, is presented in Fig. 5.11. The limitation of the primary modulator inputs is performed in the block number 4. The limitation can be performed using any of the space vector limitation methods presented in Section 5.1. The limitation of the secondary modulator inputs is performed in the block number 5. In this case, the limitation is performed applying the proposed limitation algorithm that was introduced in Section 5.4. However, it has to be pointed out that we cannot directly set the applied limits as instructed in the above-mentioned sections. This is because the available voltage must be distributed between the primary and secondary modulators.

The limits that are to be applied with the proposed limitation algorithm can be expressed as

$$r_{\max} = r_{0,\max} = k u_{\mathrm{dc}}/2 \tag{5.27}$$

where $k \in \begin{bmatrix} 0 & 1 \end{bmatrix}$ is a scaling factor. Typically, the scaling factor can be set to a low value, since the circulating current generation is sensitive to the output voltage differences. The limit that is

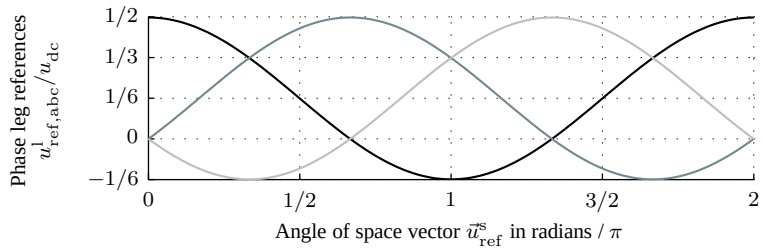

(a) Circular limit method with the zero-sequence component limitation.

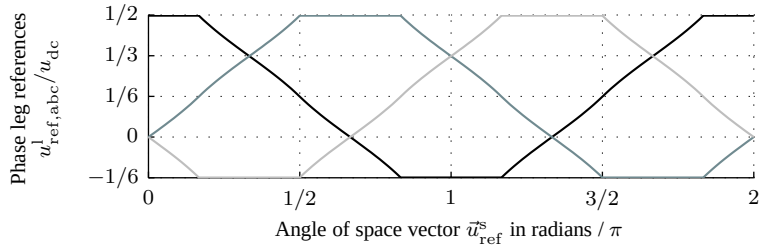

(b) Space vector limit method with the zero-sequence component limitation.

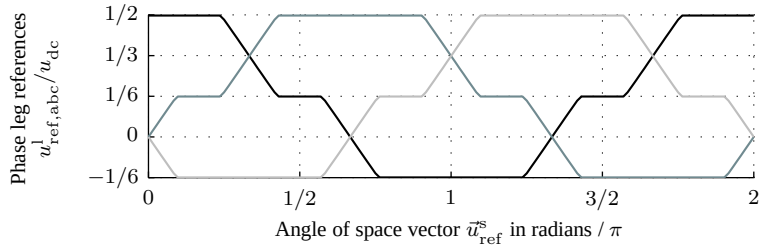

(c) Minimum amplitude error method with the zero-sequence component limitation.

Fig. 5.10: Limited phase leg references. Limitations were performed by applying the zero-sequence component limitation method together with the (a) circular limit method, (b) space vector limit method, and (c) minimum amplitude error method. The desired zero-sequence component was $u_{\mathrm{ref},0} = u_{\mathrm{dc}}/3$ and the length of the constantly rotating voltage reference vector $|\vec{u}^{\mathrm{s}}_{\mathrm{ref}}| = u_{\mathrm{dc}}/3$

.

to be applied with the space vector limitation method can be given with the help of the scaling factor as

$$r = (1-k)\,\frac{u_{\mathrm{dc}}}{\sqrt{3}} \tag{5.28}$$

It is pointed out here that the scaling factor distributes the available voltage between the primary and secondary modulators. Therefore, we may conclude that the main disadvantage of this approach is that the voltage available is reduced from the load point of view. The advantage, however, is that we can ensure that the voltage commands obtained from the circulating current controllers can always be realized within the applied limits.

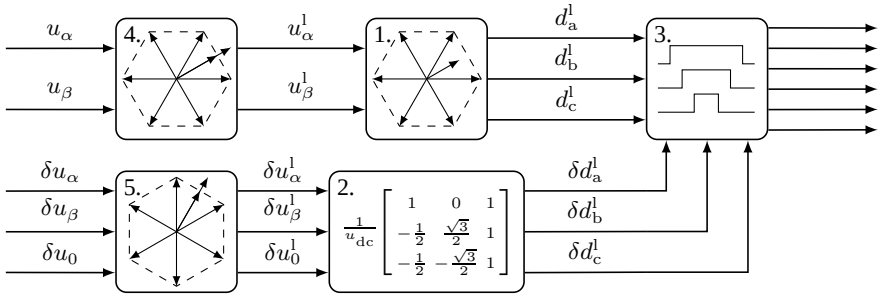

Fig. 5.11: Block diagram of the proposed dual modulator with proper limitations. The inputs of the primary and secondary modulators are limited in the blocks 4 and 5, respectively.

5.7 Discussion

In this chapter, limitation of space vector and zero-sequence components was considered. The contribution of this chapter is a limitation algorithm that combines the space vector and zero-sequence component limitation methods so that the maximum allowed phase leg reference values, which are comprised of both the space vector and zero-sequence components, are not exceeded at any time. Three different combinations were presented to show that the algorithm can be used to combine different space vector limitation methods with the zero-sequence limitation method.

Since the proposed limitation algorithm was developed to be used in conjunction with the dual modulator proposed in the previous chapter, an application example was also given. While presenting the application example, it was also discussed that as a consequence of the limitation, the voltage available is reduced from the load point of view. The limitation, however, guarantees that the voltage commands obtained from the circulating current controllers can always be realized within the applied limits.

Chapter 6

Verification of the dual modulator method and the limitation algorithm

In this chapter, experimental results are presented to verify the operation of both the proposed dual modulator and the limitation algorithm. The results are also used to verify the main difference between the studied parallel inverter configurations from the circulating current point of view. Before the results are given, the main components of the laboratory prototype and the measurement setup are described in brief.

6.1 Description of the experimental setup

The main components of the laboratory prototype are depicted in Fig. 6.1. The prototype consisted of a personal computer (PC), a dSPACE real-time controller, a field programmable gate array (FPGA) based control board, three customized commercial low-voltage frequency converters, and an induction motor, the nominal parameters of which are given in Table. 6.1. In all measurements, the motor was operating in no-load condition. This is because the operation point is not essential when the operation of the dual modulator or the limitation algorithm is illustrated.

Table 6.1: Nominal parameters of the induction motor used in the experiments.

Parameter	Value	Unit
Nominal power P_n	22	kW
Nominal voltage U_n	380	V
Nominal current I_n	43	A
Nominal frequency f_n	50	Hz
Nominal speed n_n	1460	$\mathrm{r/min}$
Power factor $\cos\phi$	0.86	

The main circuit of a single commercial frequency converter was comprised of line-side inductors, a full-wave diode rectifier bridge, a direct voltage link capacitor, and a three-phase inverter bridge. The main circuits were customized by adding single-phase reactors of $100\,\mu\mathrm{H}$ to the inverter outputs. Additional cabling was also provided to enable connection between the direct voltage buses of the converters.

The control parts of the frequency converters were customized by replacing the original control cards with custom FPGA-based control cards to enable fiber-optic connection to the FPGA-based

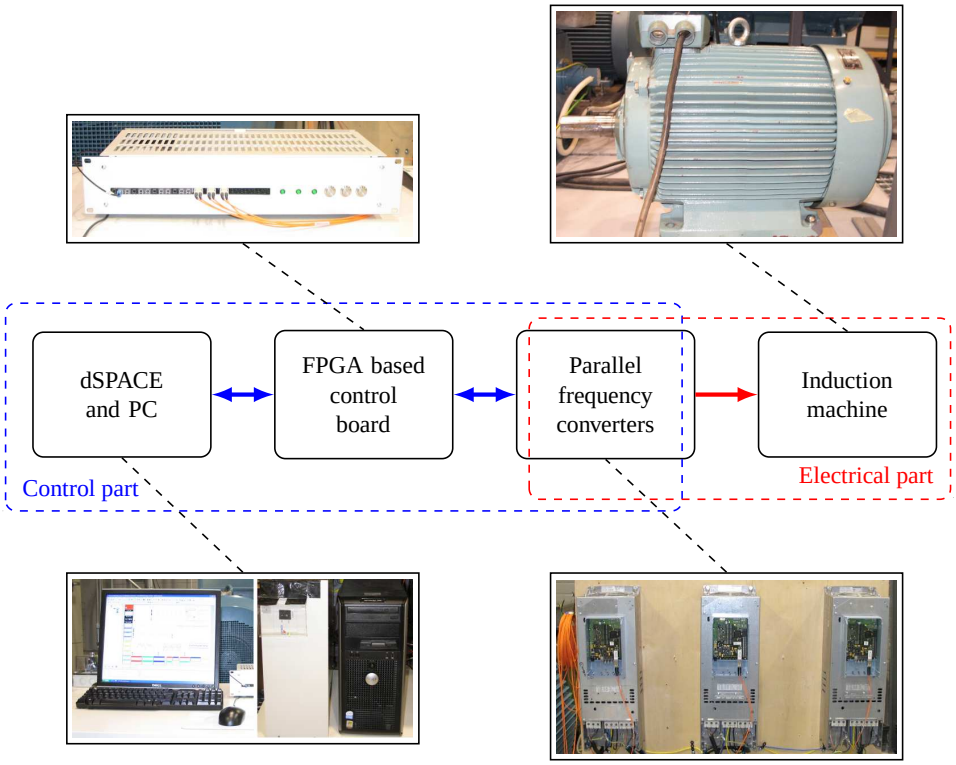

Fig. 6.1: Main components of the laboratory prototype. The prototype consisted of a PC, a dSPACE real-time controller, an FPGA-based control board, customized commercial frequency converters, and an induction motor operating in no-load condition.

control board. The function of the FPGA-based control board was to operate as an interface between the converters and the dSPACE real-time controller and to synchronize the operation of parallel units. The principle of the synchronization method applied has been presented and its performance analyzed in (Laakkonen et al., 2009).

The converter control algorithms developed using Matlab/Simulink were implemented in the dSPACE real-time controller. These included an open-loop scalar control, the proposed limitation algorithm, and the proposed dual modulator. The actual pulse pattern formation was realized in the FPGA-based control cards located at each converter unit. The conventional space vector PWM was applied as the primary modulation method.

An overview of the measurement setup is shown in Fig. 6.2. The measurement equipment consisted of two Agilent DSO6104A four-channel digital oscilloscopes and eight Fluke 80i110s current probes. All output phase currents of the first and second inverter and two output phase currents of the third inverter were measured. The third output phase current of the third inverter was eventually calculated from the measured phase currents as

$$i_{\mathrm{c},3} = -\left(i_{\mathrm{a},1} + i_{\mathrm{b},1} + i_{\mathrm{c},1} + i_{\mathrm{a},2} + i_{\mathrm{b},2} + i_{\mathrm{c},2} + i_{\mathrm{a},3} + i_{\mathrm{b},3}\right) \tag{6.1}$$

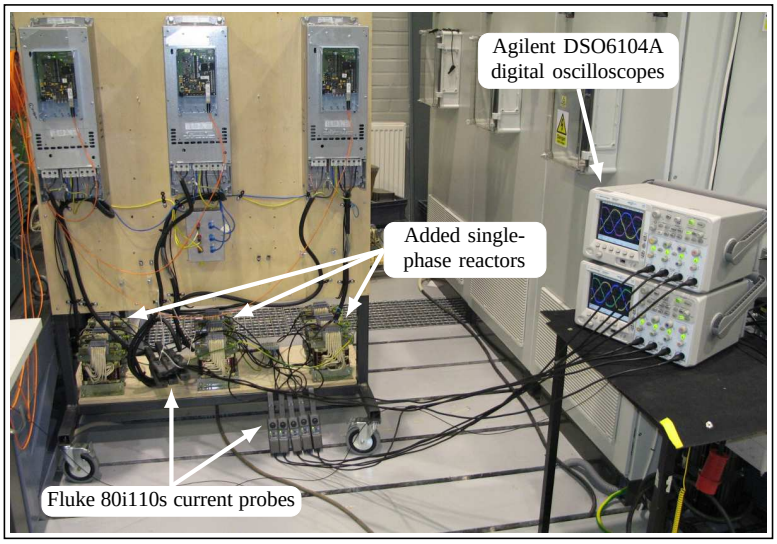

Fig. 6.2: Overview of the measurement setup. Eight of nine output phase currents of the inverters were measured using Fluke 80i110s current probes. The measured signals were viewed and captured using Agilent DSO6104A digital oscilloscopes.

This is possible since the sum of load phase currents must satisfy

$$i_{\mathrm{a,L}} + i_{\mathrm{b,L}} + i_{\mathrm{c,L}} = 0 \tag{6.2}$$

and the load phase currents can be expressed as

$$i_{\mathrm{a,L}} = i_{\mathrm{a},1} + i_{\mathrm{a},2} + i_{\mathrm{a},3} \tag{6.3}$$
$$i_{\mathrm{b,L}} = i_{\mathrm{b},1} + i_{\mathrm{b},2} + i_{\mathrm{b},3} \tag{6.4}$$
$$i_{\mathrm{c,L}} = i_{\mathrm{c},1} + i_{\mathrm{c},2} + i_{\mathrm{c},3} \tag{6.5}$$

Besides measuring the output phase currents of the inverters, voltage vectors fed to the primary and secondary modulators were captured from the ControlDesk, which is a graphical interface between the operator and the dSPACE real-time controller.

6.2 Verification of the dual modulator method

The operation of the proposed dual modulator was verified both in the case of parallel inverters with common and separate direct voltage sources. Basically, two types of tests were carried out. The first tests were performed to verify the ability to control the average $\alpha\beta$-axes voltage components without affecting the average 0-axis voltage components. The second tests were performed to verify the ability to control the average 0-axis voltage components without the affecting average $\alpha\beta$-axes voltage components. These tests were also used to verify the main differences between the parallel inverter configurations.

Before the results from the above-described tests are presented, let us consider for comparison the results that were obtained when the parallel inverters were driven with identical voltage

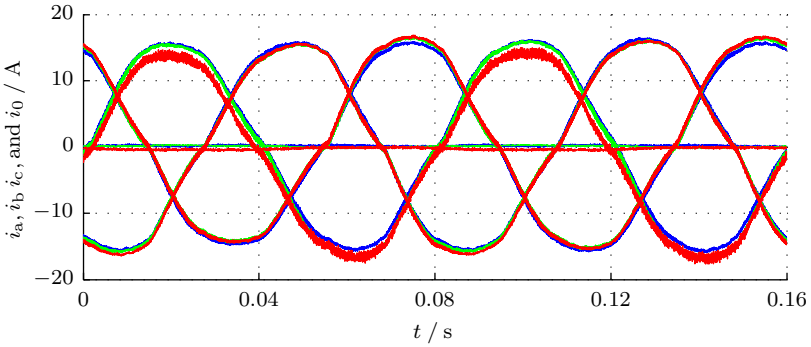

(a) Parallel inverters with a common direct voltage source.

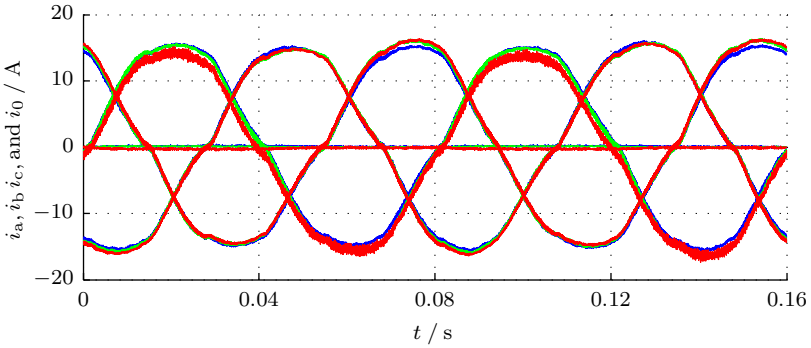

(b) Parallel inverters with separate direct voltage sources.

Fig. 6.3: Measured phase and zero-sequence currents in the case of parallel inverters with common and separate direct voltage sources. In both cases, the parallel inverters were driven with identical voltage commands. Blue, green, and red lines indicate the first, second, and third inverter, respectively.

commands. These results are shown in Fig. 6.3. Both in the case of parallel inverters with common and separate direct voltage sources, the phase currents were well in balance although neither the frequency converter components nor the added output reactors were matched in any way. The zero-sequence currents were also approximately zero in both cases.

Let us now consider Fig. 6.4, which shows phase currents and current vector trajectories in the case of parallel inverters with a common direct voltage source when identical voltage vectors were fed to each primary modulator and the voltage vectors fed to the secondary modulators were moving along the trajectories depicted in Figs. 6.4(a) and 6.4(b). As a consequence of the voltage vector differences, which were generated by adjusting the $\alpha\beta$-axes voltage components, mainly the $\alpha\beta$-axes currents were affected as expected. This can be concluded from Figs. 6.4(c) and 6.4(d). The minor zero-sequence currents were probably a consequence of the fact that instantaneous zero-sequence voltages have always nonzero values. Similar behavior was observed also in the case of parallel inverters with separate direct voltage sources. These results are shown in Fig. 6.5. The main difference was that the zero-sequence currents were maintained approximately at zero values as expected.

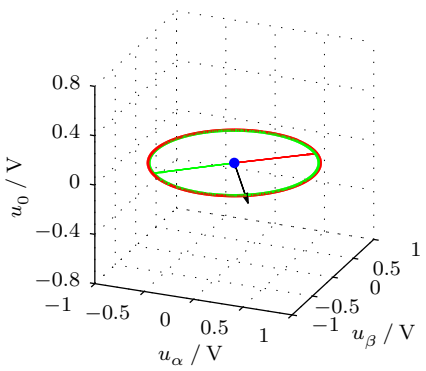

(a) Trajectories of the voltage vectors fed to the secondary modulators in the $\alpha\beta 0$ space.

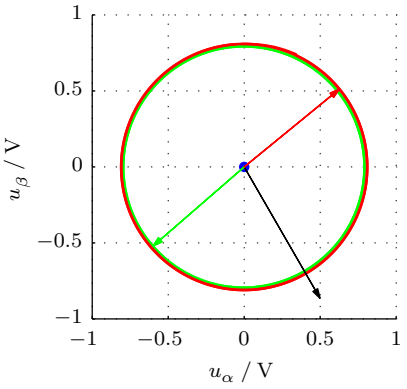

(b) Trajectories of the voltage vectors projected on the $\alpha\beta$ plane.

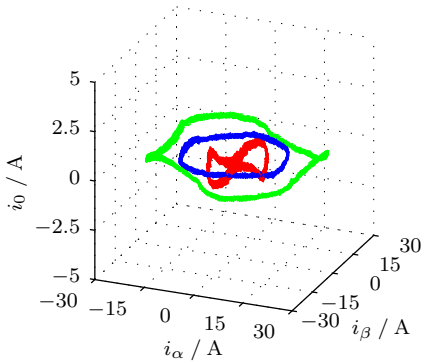

(c) Current vector trajectories in the $\alpha\beta 0$ space.

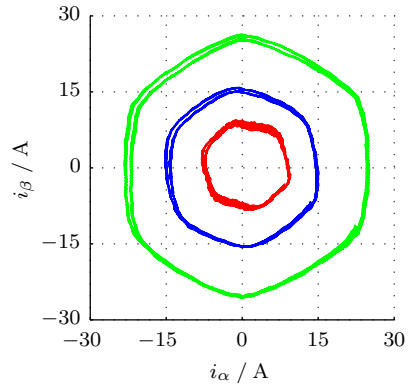

(d) Current vector trajectories projected on the $\alpha\beta$ plane.

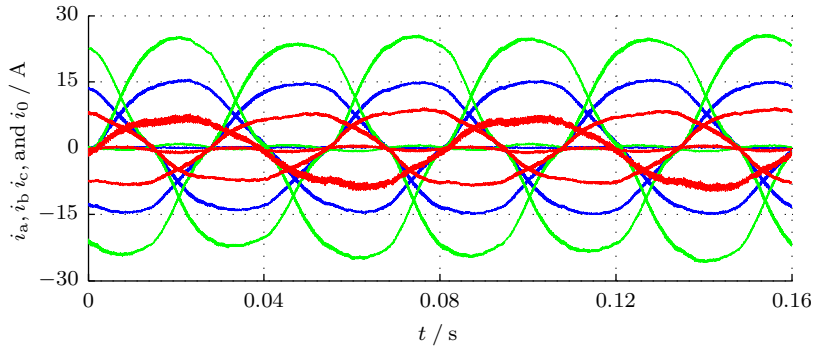

(e) Phase and zero-sequence currents.

Fig. 6.4: Captured trajectories of the voltage vectors fed to the secondary modulators, measured phase currents, and current vector trajectories in the case of parallel inverters with a common direct voltage source. Identical voltage vectors were fed to each primary modulator. Blue, green, and red lines indicate the first, second, and third inverter, respectively. The vector drawn in black shows the instantaneous orientation of the voltage vector fed to the primary modulators.

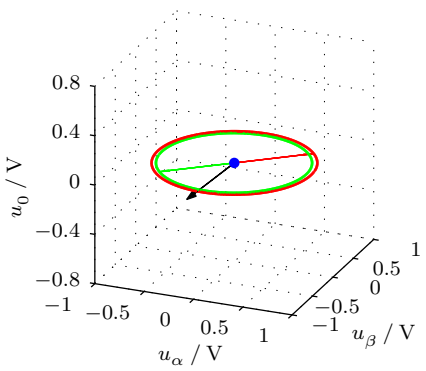

(a) Trajectories of the voltage vectors fed to the secondary modulators in the $\alpha\beta 0$ space.

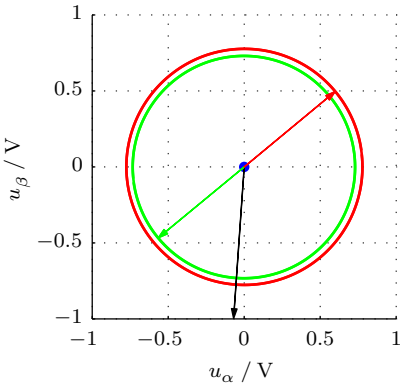

(b) Trajectories of the voltage vectors projected on the $\alpha\beta$ plane.

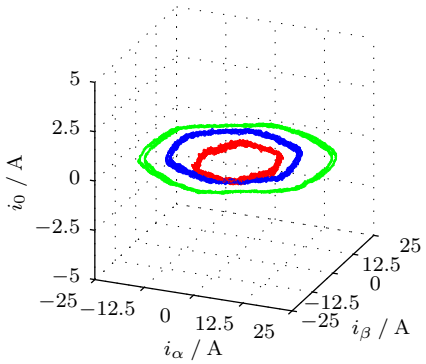

(c) Current vector trajectories in the $\alpha\beta 0$ space.

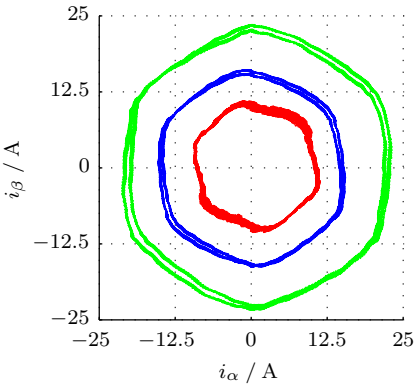

(d) Current vector trajectories projected on the $\alpha\beta$ plane.

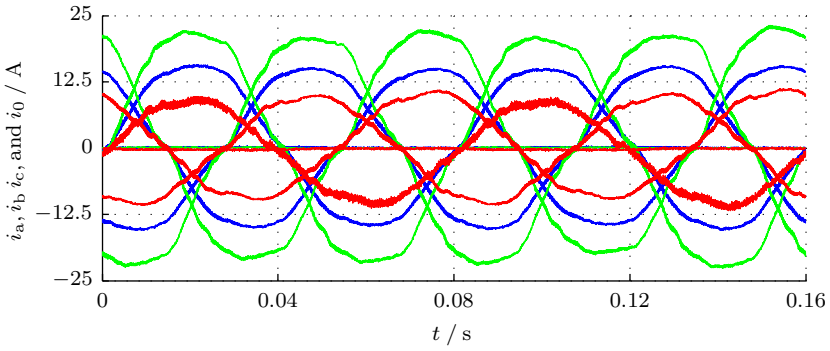

(e) Phase and zero-sequence currents.

Fig. 6.5: Captured trajectories of the voltage vectors fed to the secondary modulators, measured phase currents, and current vector trajectories in the case of parallel inverters with separate direct voltage sources. Identical voltage vectors were fed to each primary modulator. Blue, green, and red lines indicate the first, second, and third inverter, respectively. The vector drawn in black shows the instantaneous orientation of the voltage vector fed to the primary modulators.

Let us next consider the results presented in Figs. 6.6 and 6.7. In these cases, the voltage vectors fed to the secondary modulators were set as depicted in Figs. 6.6(a) and 6.7(a). In other words, only the 0-axis voltage components were adjusted and the $\alpha\beta$-axes voltage components were set to zero. In the case of parallel inverters with a common direct voltage source, such a difference resulted in low-frequency zero-sequence currents as expected. In addition, the $\alpha\beta$-axes current components were distorted as shown in Fig. 6.6(d). The main reasons for this kind of distortion are the required blanking time, the finite turn-on and turn-off times of switching devices, and the forward voltage drops of switching devices and anti-parallel diodes. As a consequence of these nonidealities, phase currents tend to cross the zero-current level at the same time (Itkonen et al., 2009c). This kind of behavior is visible in Fig. 6.6(e), which shows the phase and zero-sequence currents of the inverters.

In the case of parallel inverters with separate direct voltage sources, zero-sequence voltage component differences introduced minor high-frequency zero-sequence currents as can be seen from Figs. 6.7(c) and 6.7(e). This is mainly because the generated switching differences were such that the upper and lower switching devices in the parallel phase legs were not conducting simultaneously at any time. In other words, no current paths closing through the frequency converters were generated, although the inputs were not isolated. The formation of such current paths has been illustrated in (Itkonen et al., 2008).

6.3 Verification of the limitation algorithm

The operation of the proposed limitation algorithm was verified in the case of a common direct voltage source. Some of the results are shown in Figs. 6.8, 6.9, and 6.10 which correspond to the cases where the limitation was performed by applying the circular limit, space vector limit, and minimum amplitude error methods together with the zero-sequence component limitation method. In each presented case, the maximum space vector and zero-sequence component limits were set at $r_{\max} = r_{0,\max} \approx 0.5\,\mathrm{V}$.

Let us first consider the results shown in Fig. 6.8. Figures 6.8(a) and 6.8(b) show the trajectories of the commanded and limited voltage vectors when the circular limit method was used together with the zero-sequence component limitation method. As shown, both the $\alpha\beta$-axes and 0-axis voltage components were limited. The projections of the commanded and limited voltage vectors on the $\alpha\beta$ plane show that the limitation was performed so that only the amplitude of the vector that is comprised of the $\alpha\beta$-axes voltage components was distorted, as expected.

Consider next the results shown in Fig. 6.9. In this case, the limitation was performed applying the space vector limit method together with the zero-sequence component limitation method. Also in this case, the projections of the commanded and limited voltage vectors on the $\alpha\beta$ plane show that the limitation was performed so that only the amplitude of the vector that is comprised of the $\alpha\beta$-axes voltage components was distorted, as expected.

The results in the case where the limitation was realized applying the minimum amplitude error method together with the zero-sequence component limitation method are illustrated in Fig. 6.10. The projections of the commanded and limited voltage vectors on the $\alpha\beta$ plane show that the limited vector lies on the hexagon and that this vector is approximately closest to the vector to be limited, as expected.

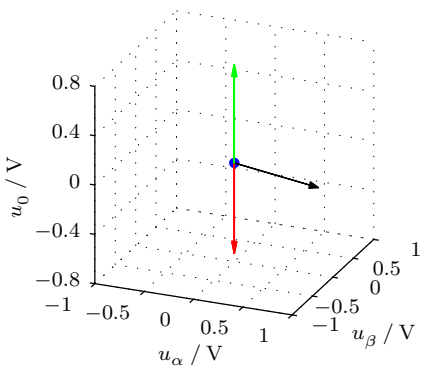

(a) Voltage vectors fed to the secondary modulators in the $\alpha\beta 0$ pace.

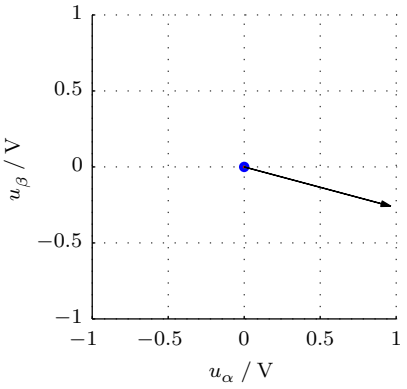

(b) Voltage vectors projected on the $\alpha\beta$ plane.

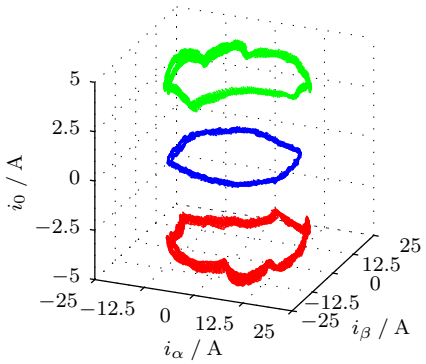

(c) Current vector trajectories in the $\alpha\beta 0$ space.

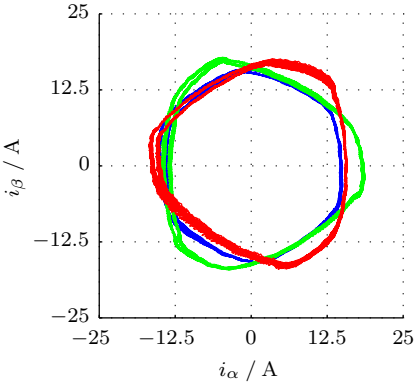

(d) Current vector trajectories projected on the $\alpha\beta$ plane.

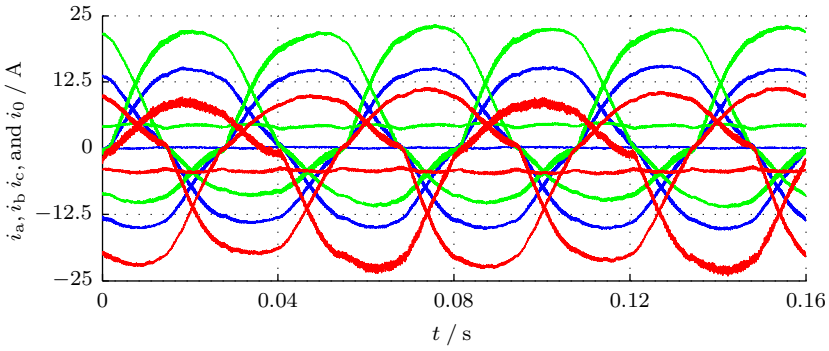

(e) Phase and zero-sequence currents.

Fig. 6.6: Captured voltage vectors fed to the secondary modulators, measured phase currents, and current vector trajectories in the case of parallel inverters with a common direct voltage source. Identical voltage vectors were fed to each primary modulator. Blue, green, and red lines indicate the first, second, and third inverter, respectively. The vector drawn in black shows the instantaneous orientation of the voltage vector fed to the primary modulators.

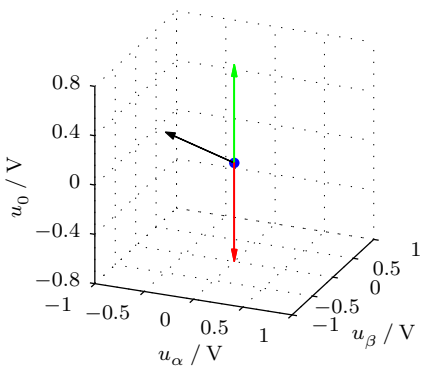

(a) Voltage vectors fed to the secondary modulators in the $\alpha\beta 0$ space.

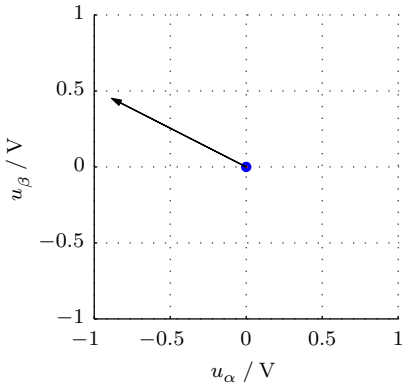

(b) Voltage vectors projected on the $\alpha\beta$ plane.

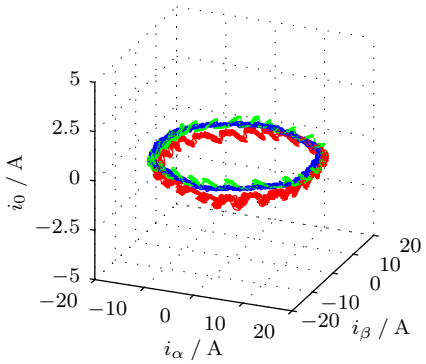

(c) Current vector trajectories in the $\alpha\beta 0$ space.

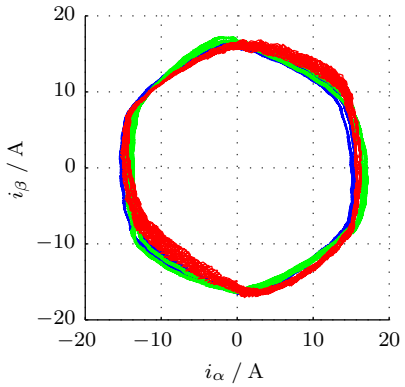

(d) Current vector trajectories projected on the $\alpha\beta$ plane.

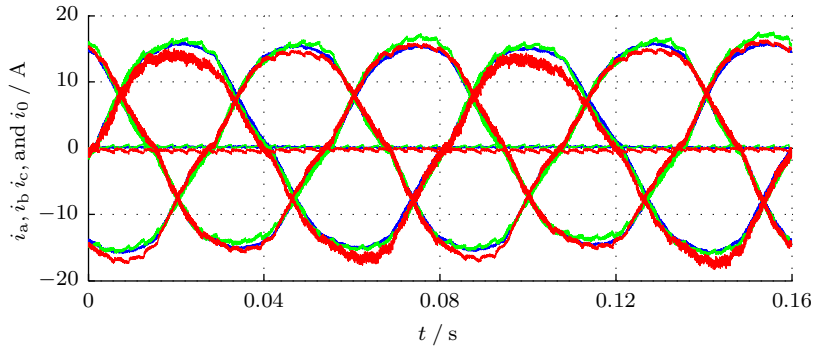

(e) Phase and zero-sequence currents.

Fig. 6.7: Captured voltage vectors fed to the secondary modulators, measured phase currents, and current vector trajectories in the case of parallel inverters with separate direct voltage sources. Identical voltage vectors were fed to each primary modulator. Blue, green, and red lines indicate the first, second, and third inverter, respectively. The vector drawn in black shows the instantaneous orientation of the voltage vector fed to the primary modulators.

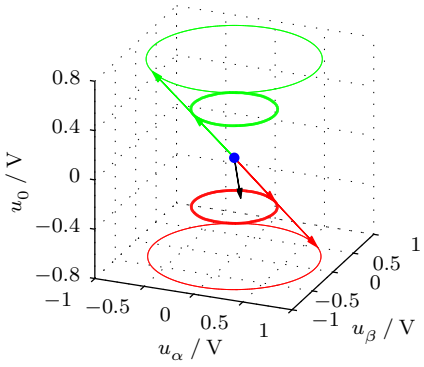

(a) Trajectories of the limited voltage vectors fed to the secondary modulators in the $\alpha\beta 0$ space.

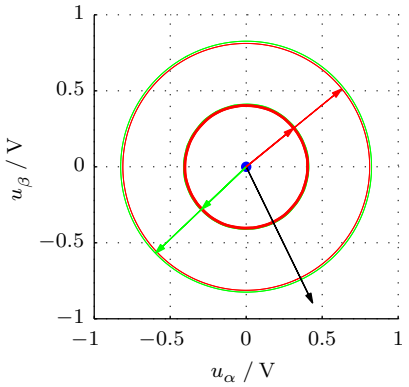

(b) Trajectories of the limited voltage vectors projected on the $\alpha\beta$ plane.

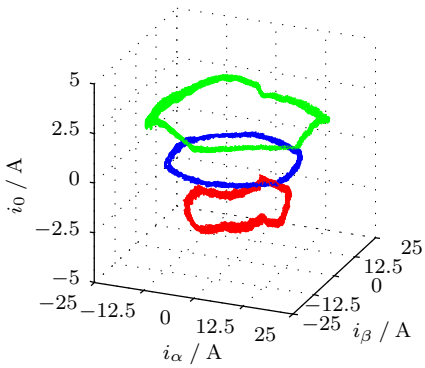

(c) Current vector trajectories in the $\alpha\beta 0$ space.

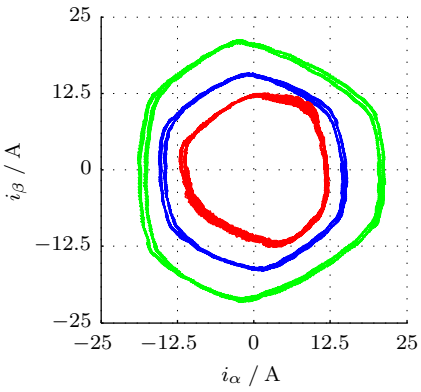

(d) Current vector trajectories in the $\alpha\beta$ plane.

Fig. 6.8: Captured trajectories of the limited voltage vectors fed to the secondary modulators and corresponding current vector trajectories in the case of parallel inverters with a common direct voltage source. The same voltage vectors were fed to each primary modulator. The limitation was performed applying the circular limit and zero-sequence component limitation methods. Blue, green, and red lines indicate the first, second, and third inverter, respectively. The vector drawn in black shows the instantaneous orientation of the voltage vector fed to the primary modulators.

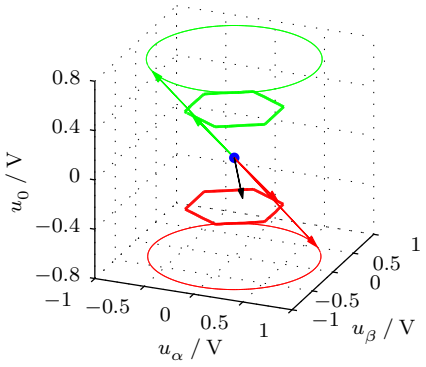

(a) Trajectories of the limited voltage vectors fed to the secondary modulators in the $\alpha\beta 0$ space.

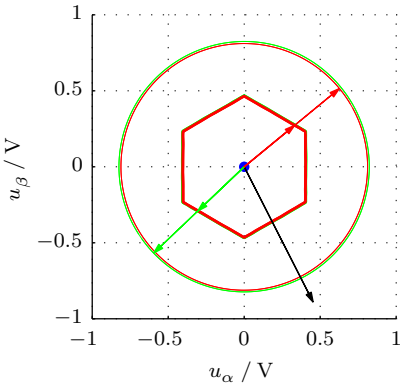

(b) Trajectories of the limited voltage vectors projected on the $\alpha\beta$ plane.

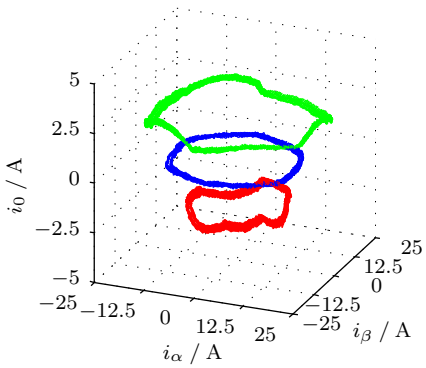

(c) Current vector trajectories in the $\alpha\beta 0$ space.

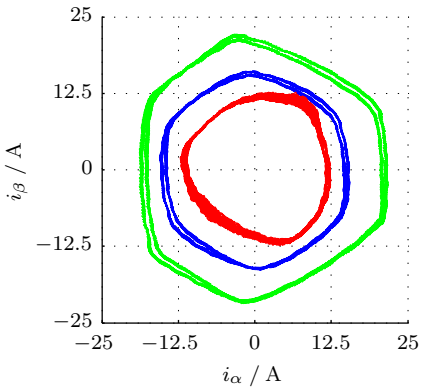

(d) Current vector trajectories in the $\alpha\beta$ plane.

Fig. 6.9: Captured trajectories of the limited voltage vectors fed to the secondary modulators and corresponding current vector trajectories in the case of parallel inverters with a common direct voltage source. The same voltage vectors were fed to each primary modulator. The limitation was performed applying the space vector limit and zero-sequence component limitation methods. Blue, green, and red lines indicate the first, second, and third inverter, respectively. The vector drawn in black shows the instantaneous orientation of the voltage vector fed to the primary modulators.

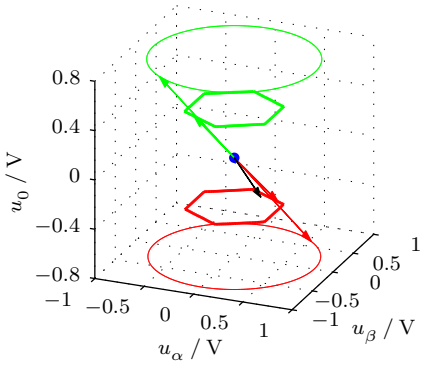

(a) Trajectories of the limited voltage vectors fed to the secondary modulators in the $\alpha\beta 0$ space.

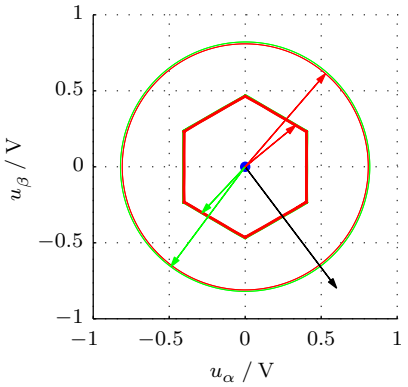

(b) Trajectories of the limited voltage vectors projected on the $\alpha\beta$ plane.

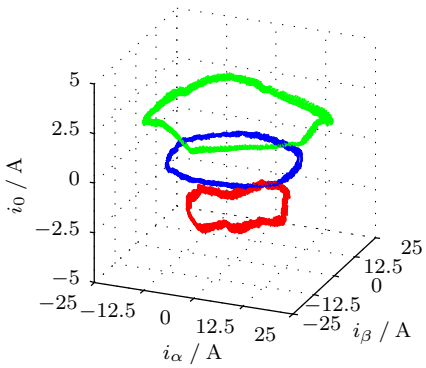

(c) Current vector trajectories in the $\alpha\beta 0$ space.

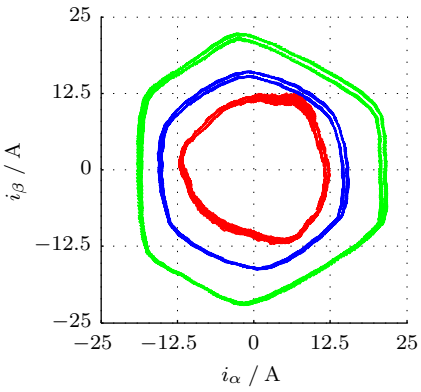

(d) Current vector trajectories on the $\alpha\beta$ plane.

Fig. 6.10: Captured trajectories of the limited voltage vectors fed to the secondary modulators and corresponding current vector trajectories in the case of parallel inverters with a common direct voltage source. The same voltage vectors were fed to each primary modulator. The limitation was performed applying the minimum amplitude error limit and zero-sequence component limitation methods. Blue, green, and red lines indicate the first, second, and third inverter, respectively. The vector drawn in black shows the instantaneous orientation of the voltage vector fed to the primary modulators.

6.4 Discussion

In this chapter, several measurement results were presented to verify the operation of both the proposed dual modulator method and the limitation algorithm. The operation of the dual modulator was verified both in the case of parallel inverters with a common direct voltage source and in the case of separate direct voltage sources. The results showed that with the proposed dual modulator method, it is possible to control the $\alpha\beta$-axes and 0-axis voltage components independently. The presented results also showed the main difference between the studied parallel inverter configurations; in the case of a common direct voltage source, zero-sequence currents can flow between the inverters, while in the case of separate direct voltage sources they cannot.

The proposed limitation algorithm was verified in the case of parallel inverters with a common direct voltage source. All presented combinations were verified. In other words, limitations were performed applying the circular limit, space vector limit, and minimum amplitude error methods together with the zero-sequence component limitation method. In all cases, the limitations were realized as expected.

Chapter 7

Conclusions

This chapter discusses and summarizes the main results of this dissertation and provides suggestions for future work.

7.1 Summary and main results of the work

Parallel connection of power converter units is commonly used to increase the current carrying capacity of power converter systems beyond the ratings of individual power semiconductor devices. High-power converters realized by using parallel connection are needed for example in multimegawatt wind power generation systems. Besides the parallel connection can be used to increase the current carrying capacity, the number of applications requiring parallel connection of several power converters units are growing. These include for example photovoltaic and fuel cell applications.

Parallel-operating power converters are, however, subject to overcurrent and thermal stresses that are caused by unequal load current sharing and currents circulating between the units. The unequal load current sharing and the currents circulating between the parallel units are commonly described with the term circulating current. Circulating currents are caused by component tolerances and asynchronous operation of the parallel units.

The main objective of this dissertation was to study and compare two different parallel three-phase voltage source inverter configurations from the circulating current point of view. The target was met by first developing mathematical models for both parallel inverter configurations, then deriving circulating current models from the developed parallel inverter models, and finally, performing a circulating current analysis. Both the parallel inverter and circulating current models were derived for an arbitrary number of parallel units. Most of the existing contributions dealing with the modeling of parallel three-phase power converters consider only parallel connection of two units, which is a special case.

The circulating current analysis showed that the main difference between the studied parallel inverter configurations, from the circulating current point of view, is that in the case of parallel inverters with a common direct voltage source, a zero-sequence circulating current may flow between the inverters, while in the case of parallel inverters with separate direct voltage sources there is no path for such a circulating current. This, however, holds true only when the separate direct voltage sources are isolated.

The circulating current analysis also demonstrated that circulating currents in a certain unit can be controlled by controlling at least two of three phase leg voltages in the case of parallel inverters with separate direct voltage sources, while in the case of a common direct voltage source, it is required that all three phase leg voltages are controlled if the circulating currents are to be

maintained near the zero level. Furthermore, the analysis showed that the current flow between the inverters can be controlled provided that $n - 1$ units are equipped with proper circulating current controllers.

Besides comparing the studied parallel inverter configuration from the circulating current point of view, it was also considered how differences in blanking times, finite turn-on and turn-off times of switching devices, and forward voltage drops of switching devices and anti-parallel diodes affect circulating current generation between the parallel units. The considerations were based on a simplified time-domain circulating current model. It was, however, shown that the results obtained from the simplified model were well in agreement with the circuit simulations. Moreover, some experimental results were presented. Although the experimental results verified some of the predictions, it was concluded that the verification of the simplified model is difficult or even impossible to perform experimentally.

The secondary objective of this dissertation was to develop a modulation method that allows to control zero-sequence voltages separately from the $\alpha\beta$-axes voltages, and vice versa. The target was met in the form of a dual modulator method. The dual modulator basically consists of two independently operating modulators, the outputs of which eventually constitute the switching commands of the inverter. The two independently operating modulators were referred to as primary and secondary modulators.

In its intended usage, the same voltage vector is fed to the primary modulators of each parallel unit and the inputs of the secondary modulators are obtained from the circulating current controllers. To ensure that the voltage commands obtained from the circulating current controllers can be realized, the inputs of the primary and secondary modulators must be limited. The inputs of primary modulator can be limited with the existing space vector limitation methods. The limitation of secondary modulator inputs is not as straightforward. This is because one has to limit both the voltage reference vector and zero-sequence voltage components so that the allowed phase leg reference values are not exceeded at any time. To deal with this problem, a limitation algorithm that can be used to combine the existing space vector limitation methods with the zero-sequence component limitation method was introduced.

The feasibility of both the proposed dual modulator method and the limitation algorithm was verified experimentally. Experimental results also verified some of the circulating current analysis results. These included for example that zero-sequence circulating currents exist in the case of parallel inverters with a common direct voltage source.

7.2 Suggestions for future work

Circulating current models for two different parallel three-phase voltage source inverter configurations have been presented in this dissertation. The models were used to show the main difference between the studied configurations from the circulating current point of view and to study circulating generation mechanisms. It was also briefly demonstrated that the presented circulating current models can be used in designing circulating current controllers. The design of circulating current control system was not, however, included in this dissertation. Thus, the future work will concentrate on developing and analyzing such a circulating current control system.

The feasibility of both the proposed dual modulator method and the limitation algorithm was verified experimentally. The experiments were, however, carried out under steady-state operation

conditions. Thus, dynamic tests should be carried out to investigate the benefits and drawbacks of the proposed methods. It is also pointed out here that information obtained from the voltage vector and zero-sequence component limitation can be used to avoid integrator windup. Thus, the future work should also focus on combining the proposed limitation algorithm with the integrator wind-up prevention provided that the circulating current controllers are integrative.

References

Antsaklis, P.J. and Michel, A.N. (2006), *Linear Systems*, Birkhäuser Boston, ISBN 10 0-8176-4434-2.

Azar, R., Udrea, R., Ng, W.T., Dawson, F., Findlay, W., and Waind, P. (2008), "The Current Sharing Optimization of Paralleled IGBTs in a Power Module Tile Using a PSpice Frequency Dependent Impedance Model," *IEEE Transactions on Power Electronics*, vol. 23, no. 1, pp. 206–217.

Baumann, M. and Kolar, J. (2007), "Parallel Connection of Two Three-Phase Three-Switch Buck-Type Unity-Power-Factor Rectifier Systems With DC-Link Current Balancing," *IEEE Transactions on Industrial Electronics*, vol. 54, no. 6, pp. 3042–3053.

Boroyevich, D. and Burgos, R. (2003), "PEBB-Oriented Generalized Representation of Switching Power Converters," in *IEEE Power Engineering Society General Meeting, 2003*, pp. 1344–1349.

Bortis, D., Biela, J., and Kolar, J.W. (2008), "Active Gate Control for Current Balancing of Parallel-Connected IGBT Modules in Solid-State Modulators," *IEEE Transactions on Plasma Science*, vol. 36, no. 5, pp. 2632–2637.

Bose, B.K. (2009), "Power Electronics and Motor Drives Recent Progress and Perspective," *IEEE Transactions on Industrial Electronics*, vol. 56, no. 2, pp. 581–588.

van der Broeck, H., Skudelny, H.C., and Stanke, G. (1988), "Analysis and Realization of a Pulsewidth Modulator Based on Voltage Space Vectors," *IEEE Transactions on Industry Applications*, vol. 24, no. 1, pp. 142–150.

Cai, H., Zhao, R., and Yang, H. (2008), "Study on Ideal Operation Status of Parallel Inverters," *IEEE Transactions on Power Electronics*, vol. 23, no. 6, pp. 2964–2969.

Chen, Q., Yang, X., and an Wang, Z. (2006), "Active Balancing Temperature Control Strategy for the Parallel IPEM-based Converters," in *IEEE Power Electronics Specialists Conference PESC, 2006*.

Chen, T.P. (2006), "Circulating Zero-Sequence Current Control of Parallel Three-Phase Inverters," *IEE Proceedings - Electric Power Applications*, vol. 153, no. 2, pp. 282–288.

Chen, T.P. (2009a), "Common-Mode Ripple Current Estimator for Parallel Three-Phase Inverters," *IEEE Transactions on Power Electronics*, vol. 24, no. 5, pp. 1330–1339.

Chen, T.P. (2009b), "Dual-Modulator Compensation Technique for Parallel Inverters Using Space-Vector Modulation," *IEEE Transactions on Industrial Electronics*, vol. 56, no. 8, pp. 3004–3012.

Chen, Y. and Smedley, K. (2008), "One-Cycle-Controlled Three-Phase Grid-Connected Inverters and Their Parallel Operation," *IEEE Transactions on Industry Applications*, vol. 44, no. 2, pp. 663–671.

Cichowski, A. and Nieznanski, J. (2005), "Self-Tuning Dead-Time Compensation Method for Voltage-Source Inverters," *IEEE Power Electronics Letters*, vol. 3, no. 2, pp. 72–75.

Fu, X., Chunliang, E., Li, J., and Xu, H. (2008), "Modeling and Simulation of Parallel-Operation Grid-Connected Inverter," in *IEEE International Conference on Industrial Technology ICIT, 2008*.

Hiti, S., Boroyevich, D., and Cuadros, C. (1994), "Small-Signal Modeling and Control of Three-Phase PWM Converters," in *Conference Record of the IEEE Industry Applications Society Annual Meeting, 1994*, pp. 1143–1150.

Hofer-Noser, P. and Karrer, N. (1999), "Monitoring of Paralleled IGBT/Diode Modules," *IEEE Transactions on Power Electronics*, vol. 14, no. 3, pp. 438–444.

Holmes, D.G. and Lipo, T.A. (2003), *Pulse Width Modulation For Power Converters Principles And Practice*, A John Wiley & Sons, Inc., Publication, ISBN 0-471-20814-0.

Holtz, J. (1996), "On the Spatial Propagation of Transient Magnetic Fields in AC Machines," *IEEE Transactions on Industry Applications*, vol. 32, no. 4, pp. 927–937.

Itkonen, T. and Luukko, J. (2008), "Switching-Function-Based Simulation Model for Three-Phase Voltage Source Inverter Taking Dead-Time Effects into Account," in *34th Annual Conference of IEEE Industrial Electronics Society IECON, 2008*, pp. 992–997.

Itkonen, T., Luukko, J., Laakkonen, T., Silventoinen, P., and Pyrhönen, O. (2008), "Switching Effects in Directly Paralleled Three-Phase AC/DC/AC Converters with Separate DC Links," in *IEEE Power Electronics Specialists Conference PESC, 2008*, pp. 1937–1943.

Itkonen, T., Luukko, J., and Pöllänen, R. (2009a), "Modeling and Analysis of the Dead-Time Effects in Parallel Two-Level Voltage Source Inverters," in *IEEE Energy Conversion Congress and Exposition ECCE, 2009*, pp. 3211–3217.

Itkonen, T., Luukko, J., and Pollanen, R. (2009b), "Analysis of Current Characteristics of Parallel Three-Phase Voltage Source Inverters," in *European Conference on Power Electronics and Applications EPE, 2009*.

Itkonen, T., Luukko, J., Sankala, A., Laakkonen, T., and Pöllänen, R. (2009c), "Modeling and Analysis of the Dead-Time Effects in Parallel PWM Two-Level Three-Phase Voltage-Source Inverters," *IEEE Transactions on Power Electronics*, vol. 24, no. 11, pp. 2446–2455.

Itkonen, T., Rauma, K., Sarén, H., Laakkonen, O., Pyrhönen, O., and Silventoinen, P. (2006), "Parallel Connected Voltage Source Inverters without Intermodule Reactors," in *12th International Power Electronics and Motion Control Conference EPE-PEMC, 2006*, pp. 641–646.

Jin, H. (1997), "Behavior-Mode Simulation of Power Electronic Circuits," *IEEE Transactions on Power Electronics*, vol. 12, no. 3, pp. 443–452.

Joseph, C.J.J., Zolghadri, M.R., Homaifar, A., Lee, F.C., and Lorenz, R.D. (2004), "Novel Thermal Based Current Sharing Control of Parallel Converters," in *26th Annual International Telecommunications Energy Conference INTELEC, 2004*, pp. 647–653.

Kovács, P.K. and Rácz, E. (1959), *Transient Phenomena in Electrical Machines*, Verlag der Ungarischen Akademie der Wissenschaften. 1959. Budapest, Amsterdam.

Kreyszig, E. (1999), *Advanced Engineering Mathematics*, JOHN WILEY & SONS, INC., eight edn., ISBN 0-471-33328-X.

Laakkonen, T., Luukko, J., Ahola, J., and Silventoinen, P. (2009), "Analysis of Time-Stamping-Based Synchronization of a PEBB System," in *IEEE International Symposium on Industrial Electronics ISIE, 2009*, pp. 12–17.

Luniewski, P. and Jansen, U. (2007), "Benefits of System-Oriented IGBT Module Design for High Power Inverters," in *European Conference on Power Electronics and Applications EPE, 2007*.

Mazumder, S.K. (2005), "Continuous and Discrete Variable-Structure Controls for Parallel Three-Phase Boost Rectifier," *IEEE Transactions on Industrial Electronics*, vol. 52, no. 2, pp. 340–354.

Milosevic, M., Andersson, G., and Grabic, S. (2006), "Decoupling Current Control and Maximum Power Point Control in Small Power Network with Photovoltaic Source," in *IEEE Power Systems Conference and Exposition PES, 2006*.

Naumanen, V., Luukko, J., Itkonen, T., Pyrhonen, O., and Pyrhonen, J. (2009), "Modulation Technique for Series-Connected H-Bridge Multilevel Converters with Equal Load Sharing," *IET Power Electronics*, vol. 2, no. 3, pp. 275–286.

Neacsu, D., Wagner, E., and Borowy, B. (2008), "A Simulation Benchmark for Selection of the PWM Algorithms for Three-Phase Interleaved Converters," *IEEE Transactions on Industrial Electronics*, vol. 55, no. 4, pp. 1628–1636.

Nelson, J., Venkataramanan, G., and Beihoff, B. (2002), "Investigation of Parallel Operation of IGBTs," in *IEEE 37th Annual Industry Applications Conference IAS, 2002*, pp. 2585–2591.

Ottersten, R. and Svensson, J. (2002), "Vector Current Controlled Voltage Source Converter-Deadbeat Control and Saturation Strategies," *IEEE Transactions on Power Electronics*, vol. 17, no. 2, pp. 279–285.

Pan, C.T. and Liao, Y.H. (2007), "Modeling and Coordinate Control of Circulating Currents in Parallel Three-Phase Boost Rectifiers," *IEEE Transactions on Industrial Electronics*, vol. 54, no. 2, pp. 825–838.

Pan, C.T. and Liao, Y.H. (2008), "Modeling and Control of Circulating Currents for Parallel Three-Phase Boost Rectifiers With Different Load Sharing," *IEEE Transactions on Industrial Electronics*, vol. 55, no. 7, pp. 2776–2785.

Pöllänen, R., Tarkiainen, A., Niemelä, M., and Pyrhönen, J. (2005), "Control of Zero-Sequence Current in Parallel Connected Voltage Source PWM Rectifiers Using Converter-Flux-Based Control," in *European Conference on Power Electronics and Applications EPE, 2005*.

Råde, L. and Westergren, B. (2001), *Mathematical Handbook for Science and Engineering BETA*, Studentlitteratur, fourth edn., ISBN 91-44-00839-2.

Rodriguez, P., Pou, J., Luna, A., Ghizoni, D., Guo, J., Francis, G., Burgos, R., and Boroyevich, D. (2005), "Three-Dimensional SVM for Modular Power Electronics Systems," in *31st Annual Conference of IEEE Industrial Electronics Society IECON, 2005*.

Roubal, J., Husek, P., and Stecha, J. (2009), "Linearization: Students Forget the Operating Point," *IEEE Transactions on Education*, vol. XX, no. XX, Date of Publication: September 28, 2009.

Sao, C. and Lehn, P.W. (2006), "A Block Diagram Approach to Reference Frame Transformation of Converter Dynamic Models," in *Canadian Conference on Electrical and Computer Engineering CCECE, 2006*, pp. 2270–2274.

Sarén, H. (2005), *Analysis of the Voltage Source Inverter with Small DC-Link Capacitor*, Ph.D. thesis, Lappeenranta University of Technology.

Sasagawa, K., Abe, Y., and Matsuse, K. (2004), "Voltage-Balancing Method for IGBTs Connected in Series," *IEEE Transactions on Industry Applications*, vol. 40, no. 4, pp. 1025–1030.

Shi, B. and Venkataramanan, G. (2004), "Parallel Operation of Voltage Source Inverters with Minimal Intermodule Reactors," in *IEEE 39th Annual Industry Applications Conference IAS, 2004*.

Sun, J. (2009), "Small-Signal Methods for AC Distributed Power Systems A Review," *IEEE Transactions on Power Electronics*, vol. 24, no. 11, pp. 2545–2554.

Wester, G. and Middlebrook, R. (1973), "Low-Frequency Characterization of Switched dc-dc Converters," *IEEE Transactions on Aerospace and Electronic Systems*, vol. 9, no. 3, pp. 376–385.

Wilson, T.G. (2000), "The Evolution of Power Electronics," *IEEE Transactions on Power Electronics*, vol. 15, no. 3, pp. 439–446.

Xing, K., Lee, F., Borojevic, D., Ye, Z., and Mazumder, S. (1999), "Interleaved PWM with Discontinuous Space-Vector Modulation," *IEEE Transactions on Power Electronics*, vol. 14, no. 5, pp. 906–917.

Ye, Z. and Boroyevich, D. (2001), "A Novel Modeling and Control Approach for Parallel Three-Phase Buck Rectifiers," in *IEEE 36th Annual Industry Applications Conference IAS, 2001*, pp. 350–356.

Ye, Z., Boroyevich, D., Choi, J.Y., and Lee, F.C. (2002), "Control of Circulating Current in Two Parallel Three-Phase Boost Rectifiers," *IEEE Transactions on Power Electronics*, vol. 17, no. 5, pp. 609–615.

Ye, Z., Boroyevich, D., and Lee, F.C. (2000), "Modeling and Control of Zero-Sequence Current in Parallel Multi-Phase Converters," in *IEEE Power Electronics Specialists Conference PESC, 2000*, pp. 680–685.

Younis, M.A.A., Rahim, N.A., and Mekhilef, S. (2009), "Distributed Generation with Parallel Connected Inverter," in *4th IEEE Conference on Industrial Electronics and Applications ICIEA, 2009*.

Yu, X., Jiang, Z., and Zhang, Y. (2008), "Control of Parallel Inverter-Interfaced Distributed Energy Resources," in *IEEE Energy 2030 Conference, 2008*.

Zhang, D., Wang, F., Burgos, R., and Boroyevich, D. (2009a), "Common Mode Circulating Current Control of Interleaved Three-Phase Two-Level Voltage-Source Converters with Discontinuous Space-Vector Modulation," in *IEEE Energy Conversion Congress and Exposition ECCE, 2009*, pp. 2801–2807.

Zhang, Y., Chen, X., Kang, Y., and Chen, J. (2005), "The Restrain of the Dead Time Effects in Parallel Inverters," in *IEEE International Conference on Electric Machines and Drives, 2005*, pp. 797–802.

Zhang, Y., Jiang, Z., and Yu, X. (2009b), "Small-Signal Modeling and Analysis of Parallel-Connected Voltage Source Inverters," in *IEEE 6th International Power Electronics and Motion Control Conference IPEMC, 2009*, pp. 377–383.

Zorngiebel, V., Spahn, E., Buderer, G., Welleman, A., and Fleischmann, W. (2009), "Compact High Voltage IGBT Switch for Pulsed Power Applications," *IEEE Transactions on Magnetics*, vol. 45, no. 1, pp. 531–535.

Appendix A

Factorization of transfer function matrices using singular value decomposition

Singular value decomposition (SVD) can be used to factorize any $m \times n$ matrix $\mathbf{A}$ into (Råde and Westergren, 2001)

$$\mathbf{A} = \mathbf{QSP}^{\mathrm{T}} \tag{A.1}$$

where $\mathbf{Q}$ is an $m \times m$ orthogonal matrix, $\mathbf{S}$ is an $m \times n$ diagonal type matrix, and $\mathbf{P}$ is an $n \times n$ orthogonal matrix. The orthogonal matrices $\mathbf{Q}$ and $\mathbf{P}$ satisfy $\mathbf{Q}^{\mathrm{T}}\mathbf{Q} = \mathbf{I}$ and $\mathbf{P}^{\mathrm{T}}\mathbf{P} = \mathbf{I}$ where $\mathbf{I}$ is an identity matrix with the appropriate dimensions. The real and positive diagonal elements of $\mathbf{S}$ are singular values of $\mathbf{A}$. The properties of SVD include that the number of singular values equals the rank of $\mathbf{A}$.

The columns of $\mathbf{P}$ are orthonormal eigenvectors corresponding to the eigenvalues of $\mathbf{A}^{\mathrm{T}}\mathbf{A}$. To obtain the orthonormal eigenvectors, we first need to apply a characteristic equation (Kreyszig, 1999), which can be expressed as

$$\det\left(\mathbf{A}^{\mathrm{T}}\mathbf{A} - \lambda\mathbf{I}\right) = \begin{vmatrix} a_{11} - \lambda & a_{12} & \cdots & a_{1n} \\ a_{21} & a_{22} - \lambda & \ddots & \vdots \\ \vdots & \cdots & \cdots & a_{(n-1)n} \\ a_{n1} & \cdots & a_{n(n-1)} & a_{nn} - \lambda \end{vmatrix} = 0 \tag{A.2}$$

The term λ is called an eigenvalue of $\mathbf{A}^{\mathrm{T}}\mathbf{A}$ and $\mathbf{I}$ is an identity matrix with the dimensions of $n \times n$. It is worth emphasizing that the eigenvalues of $\mathbf{A}^{\mathrm{T}}\mathbf{A}$ are the roots of (A.2) and that there are at least one eigenvalue and at most n distinct eigenvalues. After determining the eigenvalues, eigenvectors are obtained by

$$\left(\mathbf{A}^{\mathrm{T}}\mathbf{A} - \lambda\mathbf{I}\right)\vec{g} = 0 \tag{A.3}$$

where $\vec{g} \neq 0$ is a non-zero eigenvector corresponding to the eigenvalue λ. The resulting eigenvectors can be expressed in the matrix form as

$$\mathbf{G} = \begin{bmatrix} \vec{g}_1 & \vec{g}_2 & \cdots & \vec{g}_n \end{bmatrix} \tag{A.4}$$

The orthogonal matrix $\mathbf{P}$ is now obtained by orthogonalizing the matrix of eigenvectors (A.4). The orthogonalization can be performed by applying the Gram-Schmidt orthogonalization, see for example (Råde and Westergren, 2001). The orthogonal matrix $\mathbf{P}$ can be given as

$$\mathbf{P} = \begin{bmatrix} \vec{p}_1 & \vec{p}_2 & \cdots & \vec{p}_n \end{bmatrix} \tag{A.5}$$

To obtain the diagonal type matrix $\mathbf{S}$, we need to determine the singular values of $\mathbf{A}$. Assuming that the eigenvalues obtained by (A.2) are as $\lambda_1, \ldots, \lambda_r > 0$ and $\lambda_{r+1}, \ldots, \lambda_n = 0$, the singular values can be given as

$$\mu_i = \sqrt{\lambda_i}, \quad i = 1, 2, \ldots, r \tag{A.6}$$

The singular values (A.6) are put into the diagonal of $\mathbf{S}$ as

$$s_{ii} = \mu_i, \quad i = 1, 2, \ldots, r \tag{A.7}$$

and the rest of the elements are set to zero.

The construction of the orthogonal matrix $\mathbf{Q}$ can be described as follows. First set

$$\vec{h}_i = \frac{1}{\mu_i}\mathbf{A}\vec{g}_i, \quad i = 1, 2, \ldots, r \tag{A.8}$$

and if $r < m$, complete by $\vec{h}_{r+1}, \ldots, \vec{h}_m$ which, again, are obtained by

$$\left(\mathbf{A}\mathbf{A}^{\mathrm{T}} - \lambda\mathbf{I}\right)\vec{h} = 0 \tag{A.9}$$

It is pointed out that (A.9) is basically used only to obtain eigenvectors corresponding to the eigenvalues $\lambda_{r+1}, \ldots, \lambda_m = 0$. Now we can write

$$\mathbf{H} = \begin{bmatrix} \vec{h}_1 & \vec{h}_2 & \cdots & \vec{h}_m \end{bmatrix} \tag{A.10}$$

The orthogonal matrix $\mathbf{Q}$ is obtained from (A.10) by applying the Gram-Schmidt orthogonalization. The result can be expressed as

$$\mathbf{Q} = \begin{bmatrix} \vec{q}_1 & \vec{q}_2 & \cdots & \vec{q}_n \end{bmatrix} \tag{A.11}$$

A.1 Factorization of transfer function matrices

Let us apply SVD to the transfer function matrices (3.6) and (3.8), which correspond to the parallel inverters with separate and common dc voltage sources, respectively. For the sake of a convenient representation, let us assume parallel connection of two units and that $s = 0$. Although only the special case $n = 2$ is considered, the same procedure can be applied to any number of parallel units.

A.1.1 Parallel inverters with separate direct voltage sources

Assuming $s = 0$ and parallel connection of two units ($n = 2$), the transfer function matrix (3.6) reduces into

$$\mathbf{G}_{\mathrm{dq0}}^{\mathrm{sep}}(0) = \begin{bmatrix} \frac{1}{2}\frac{R}{R^2+\omega^2L^2} & \frac{1}{2}\frac{\omega L}{R^2+\omega^2L^2} & 0 & -\frac{1}{2}\frac{R}{R^2+\omega^2L^2} & -\frac{1}{2}\frac{\omega L}{R^2+\omega^2L^2} & 0 \\ -\frac{1}{2}\frac{\omega L}{R^2+\omega^2L^2} & \frac{1}{2}\frac{R}{R^2+\omega^2L^2} & 0 & \frac{1}{2}\frac{\omega L}{R^2+\omega^2L^2} & -\frac{1}{2}\frac{R}{R^2+\omega^2L^2} & 0 \\ 0 & 0 & 0 & 0 & 0 & 0 \\ -\frac{1}{2}\frac{R}{R^2+\omega^2L^2} & -\frac{1}{2}\frac{\omega L}{R^2+\omega^2L^2} & 0 & \frac{1}{2}\frac{R}{R^2+\omega^2L^2} & \frac{1}{2}\frac{\omega L}{R^2+\omega^2L^2} & 0 \\ \frac{1}{2}\frac{\omega L}{R^2+\omega^2L^2} & -\frac{1}{2}\frac{R}{R^2+\omega^2L^2} & 0 & -\frac{1}{2}\frac{\omega L}{R^2+\omega^2L^2} & \frac{1}{2}\frac{R}{R^2+\omega^2L^2} & 0 \\ 0 & 0 & 0 & 0 & 0 & 0 \end{bmatrix} \tag{A.12}$$

Let us denote $\mathbf{G}_{\mathrm{dq0}}^{\mathrm{sep}}(0) = \mathbf{A}$. Multiplying the matrix $\mathbf{A}$ with the transpose of $\mathbf{A}$ results in

$$\mathbf{A}^{\mathrm{T}}\mathbf{A} = \begin{bmatrix} \frac{1}{2}\frac{1}{R^2+\omega^2L^2} & 0 & 0 & -\frac{1}{2}\frac{1}{R^2+\omega^2L^2} & 0 & 0 \\ 0 & \frac{1}{2}\frac{1}{R^2+\omega^2L^2} & 0 & 0 & -\frac{1}{2}\frac{1}{R^2+\omega^2L^2} & 0 \\ 0 & 0 & 0 & 0 & 0 & 0 \\ -\frac{1}{2}\frac{1}{R^2+\omega^2L^2} & 0 & 0 & \frac{1}{2}\frac{1}{R^2+\omega^2L^2} & 0 & 0 \\ 0 & -\frac{1}{2}\frac{1}{R^2+\omega^2L^2} & 0 & 0 & \frac{1}{2}\frac{1}{R^2+\omega^2L^2} & 0 \\ 0 & 0 & 0 & 0 & 0 & 0 \end{bmatrix} \tag{A.13}$$

Applying the characteristic equation (A.2) to (A.13) results in a characteristic polynomial

$$\lambda^4\left(\lambda^2 - \frac{2}{R^2+\omega^2L^2}\lambda + \frac{1}{\left(R^2+\omega^2L^2\right)^2}\right) = 0 \tag{A.14}$$

from which we can solve the eigenvalues

$$\lambda_1 = \frac{1}{R^2+\omega^2L^2} \tag{A.15a}$$

$$\lambda_2 = \frac{1}{R^2+\omega^2L^2} \tag{A.15b}$$

$$\lambda_3 = 0 \tag{A.15c}$$

$$\lambda_4 = 0 \tag{A.15d}$$

$$\lambda_5 = 0 \tag{A.15e}$$

$$\lambda_6 = 0 \tag{A.15f}$$

Eigenvectors corresponding to the eigenvalues (A.15) are determined by (A.3). For example, for the eigenvalue λ_1 we can write

$$\begin{aligned} &\left(\mathbf{A}^{\mathrm{T}}\mathbf{A} - \lambda_1\mathbf{I}\right)\vec{g}_1 = \\ &\begin{bmatrix} -\frac{1}{2}\frac{1}{R^2+\omega^2L^2} & 0 & 0 & -\frac{1}{2}\frac{1}{R^2+\omega^2L^2} & 0 & 0 \\ 0 & -\frac{1}{2}\frac{1}{R^2+\omega^2L^2} & 0 & 0 & -\frac{1}{2}\frac{1}{R^2+\omega^2L^2} & 0 \\ 0 & 0 & -\frac{1}{R^2+\omega^2L^2} & 0 & 0 & 0 \\ -\frac{1}{2}\frac{1}{R^2+\omega^2L^2} & 0 & 0 & -\frac{1}{2}\frac{1}{R^2+\omega^2L^2} & 0 & 0 \\ 0 & -\frac{1}{2}\frac{1}{R^2+\omega^2L^2} & 0 & 0 & -\frac{1}{2}\frac{1}{R^2+\omega^2L^2} & 0 \\ 0 & 0 & 0 & 0 & 0 & -\frac{1}{R^2+\omega^2L^2} \end{bmatrix}\vec{g}_1 \\ &= 0 \end{aligned} \tag{A.16}$$

A non-zero eigenvector that satisfies (A.16) can be given as $\vec{g}_1 = \begin{bmatrix} 1 & 0 & 0 & -1 & 0 & 0 \end{bmatrix}^{\mathrm{T}}$. Similarly, we can define eigenvectors for the rest of the eigenvalues (A.15). The resulting eigenvectors can be given in the matrix form (A.4) as

$$\begin{aligned} \mathbf{G} &= \begin{bmatrix} \vec{g}_1 & \vec{g}_2 & \vec{g}_3 & \vec{g}_4 & \vec{g}_5 & \vec{g}_6 \end{bmatrix} \\ &= \begin{bmatrix} 1 & 0 & 0 & 1 & 0 & 0 \\ 0 & 1 & 0 & 0 & 1 & 0 \\ 0 & 0 & 1 & 0 & 0 & 0 \\ -1 & 0 & 0 & 1 & 0 & 0 \\ 0 & -1 & 0 & 0 & 1 & 0 \\ 0 & 0 & 0 & 0 & 0 & 1 \end{bmatrix} \end{aligned} \tag{A.17}$$

Applying the Gram-Schmidt orthogonalization to (A.17) yields

$$\begin{aligned}\mathbf{P} &= \begin{bmatrix}\vec{p}_1 & \vec{p}_2 & \vec{p}_3 & \vec{p}_4 & \vec{p}_5 & \vec{p}_6\end{bmatrix} \\ &= \begin{bmatrix} \frac{1}{\sqrt{2}} & 0 & 0 & \frac{1}{\sqrt{2}} & 0 & 0 \\ 0 & \frac{1}{\sqrt{2}} & 0 & 0 & \frac{1}{\sqrt{2}} & 0 \\ 0 & 0 & 1 & 0 & 0 & 0 \\ -\frac{1}{\sqrt{2}} & 0 & 0 & \frac{1}{\sqrt{2}} & 0 & 0 \\ 0 & -\frac{1}{\sqrt{2}} & 0 & 0 & \frac{1}{\sqrt{2}} & 0 \\ 0 & 0 & 0 & 0 & 0 & 1 \end{bmatrix}\end{aligned} \tag{A.18}$$

The transpose of $\mathbf{P}$ equals

$$\begin{aligned}\mathbf{P}^{\mathrm{T}} &= \begin{bmatrix}\vec{p}_1 & \vec{p}_2 & \vec{p}_3 & \vec{p}_4 & \vec{p}_5 & \vec{p}_6\end{bmatrix}^{\mathrm{T}} \\ &= \begin{bmatrix} \frac{1}{\sqrt{2}} & 0 & 0 & -\frac{1}{\sqrt{2}} & 0 & 0 \\ 0 & \frac{1}{\sqrt{2}} & 0 & 0 & -\frac{1}{\sqrt{2}} & 0 \\ 0 & 0 & 1 & 0 & 0 & 0 \\ \frac{1}{\sqrt{2}} & 0 & 0 & \frac{1}{\sqrt{2}} & 0 & 0 \\ 0 & \frac{1}{\sqrt{2}} & 0 & 0 & \frac{1}{\sqrt{2}} & 0 \\ 0 & 0 & 0 & 0 & 0 & 1 \end{bmatrix}\end{aligned} \tag{A.19}$$

The diagonal type matrix $\mathbf{S}$ is obtained with the eigenvalues (A.15) and (A.6)–(A.7). This results in

$$\mathbf{S} = \begin{bmatrix} \frac{1}{\sqrt{R^2+\omega^2L^2}} & 0 & 0 & 0 & 0 & 0 \\ 0 & \frac{1}{\sqrt{R^2+\omega^2L^2}} & 0 & 0 & 0 & 0 \\ 0 & 0 & 0 & 0 & 0 & 0 \\ 0 & 0 & 0 & 0 & 0 & 0 \\ 0 & 0 & 0 & 0 & 0 & 0 \\ 0 & 0 & 0 & 0 & 0 & 0 \end{bmatrix} \tag{A.20}$$

The matrix $\mathbf{H}$ is obtained by (A.8) and (A.9). This results in

$$\begin{aligned}\mathbf{H} &= \begin{bmatrix}\vec{h}_1 & \vec{h}_2 & \vec{h}_3 & \vec{h}_4 & \vec{h}_5 & \vec{h}_6\end{bmatrix} \\ &= \begin{bmatrix} \frac{R}{\sqrt{R^2+\omega^2L^2}} & \frac{\omega L}{\sqrt{R^2+\omega^2L^2}} & 0 & 1 & 0 & 0 \\ -\frac{\omega L}{\sqrt{R^2+\omega^2L^2}} & \frac{R}{\sqrt{R^2+\omega^2L^2}} & 0 & 0 & 1 & 0 \\ 0 & 0 & 1 & 0 & 0 & 0 \\ -\frac{R}{\sqrt{R^2+\omega^2L^2}} & -\frac{\omega L}{\sqrt{R^2+\omega^2L^2}} & 0 & 1 & 0 & 0 \\ \frac{\omega L}{\sqrt{R^2+\omega^2L^2}} & -\frac{R}{\sqrt{R^2+\omega^2L^2}} & 0 & 0 & 1 & 0 \\ 0 & 0 & 0 & 0 & 0 & 1 \end{bmatrix}\end{aligned} \tag{A.21}$$

Now the orthogonal matrix $\mathbf{Q}$ is obtained from (A.21) by applying the Gram-Schmidt orthogonalization. This results in

$$\begin{aligned}\mathbf{Q} &= \begin{bmatrix}\vec{q}_1 & \vec{q}_2 & \vec{q}_3 & \vec{q}_4 & \vec{q}_5 & \vec{q}_6\end{bmatrix} \\ &= \begin{bmatrix} \frac{1}{\sqrt{2}}\frac{R}{\sqrt{R^2+\omega^2L^2}} & \frac{1}{\sqrt{2}}\frac{\omega L}{\sqrt{R^2+\omega^2L^2}} & 0 & \frac{1}{\sqrt{2}} & 0 & 0 \\ -\frac{1}{\sqrt{2}}\frac{\omega L}{\sqrt{R^2+\omega^2L^2}} & \frac{1}{\sqrt{2}}\frac{R}{\sqrt{R^2+\omega^2L^2}} & 0 & 0 & \frac{1}{\sqrt{2}} & 0 \\ 0 & 0 & 1 & 0 & 0 & 0 \\ -\frac{1}{\sqrt{2}}\frac{R}{\sqrt{R^2+\omega^2L^2}} & -\frac{1}{\sqrt{2}}\frac{\omega L}{\sqrt{R^2+\omega^2L^2}} & 0 & \frac{1}{\sqrt{2}} & 0 & 0 \\ \frac{1}{\sqrt{2}}\frac{\omega L}{\sqrt{R^2+\omega^2L^2}} & -\frac{1}{\sqrt{2}}\frac{R}{\sqrt{R^2+\omega^2L^2}} & 0 & 0 & \frac{1}{\sqrt{2}} & 0 \\ 0 & 0 & 0 & 0 & 0 & 1 \end{bmatrix}\end{aligned} \tag{A.22}$$

Now the SVD of (A.12) can be given by (A.22), (A.20) and (A.19).

A.1.2 Parallel inverters with a common direct voltage source

Let us now apply SVD to the transfer function matrix (3.8) and assume, again, parallel connection of two units ($n = 2$) and that $s = 0$. As a consequence of these assumptions, the transfer function matrix (3.8) reduces into

$$\mathbf{G}_{\mathrm{dq0}}^{\mathrm{com}}(0) = \begin{bmatrix} \frac{1}{2}\frac{R}{R^2+\omega^2L^2} & \frac{1}{2}\frac{\omega L}{R^2+\omega^2L^2} & 0 & -\frac{1}{2}\frac{R}{R^2+\omega^2L^2} & -\frac{1}{2}\frac{\omega L}{R^2+\omega^2L^2} & 0 \\ -\frac{1}{2}\frac{\omega L}{R^2+\omega^2L^2} & \frac{1}{2}\frac{R}{R^2+\omega^2L^2} & 0 & \frac{1}{2}\frac{\omega L}{R^2+\omega^2L^2} & -\frac{1}{2}\frac{R}{R^2+\omega^2L^2} & 0 \\ 0 & 0 & \frac{1}{2}\frac{1}{R} & 0 & 0 & -\frac{1}{2}\frac{1}{R} \\ -\frac{1}{2}\frac{R}{R^2+\omega^2L^2} & -\frac{1}{2}\frac{\omega L}{R^2+\omega^2L^2} & 0 & \frac{1}{2}\frac{R}{R^2+\omega^2L^2} & \frac{1}{2}\frac{\omega L}{R^2+\omega^2L^2} & 0 \\ \frac{1}{2}\frac{\omega L}{R^2+\omega^2L^2} & -\frac{1}{2}\frac{R}{R^2+\omega^2L^2} & 0 & -\frac{1}{2}\frac{\omega L}{R^2+\omega^2L^2} & \frac{1}{2}\frac{R}{R^2+\omega^2L^2} & 0 \\ 0 & 0 & -\frac{1}{2}\frac{1}{R} & 0 & 0 & \frac{1}{2}\frac{1}{R} \end{bmatrix} \tag{A.23}$$

Let us denote $\mathbf{G}_{\mathrm{dq0}}^{\mathrm{com}}(0) = \mathbf{A}$. Multiplying the matrix $\mathbf{A}$ with the transpose of $\mathbf{A}$ results in

$$\mathbf{A}^{\mathrm{T}}\mathbf{A} = \begin{bmatrix} \frac{1}{2}\frac{1}{R^2+\omega^2L^2} & 0 & 0 & -\frac{1}{2}\frac{1}{R^2+\omega^2L^2} & 0 & 0 \\ 0 & \frac{1}{2}\frac{1}{R^2+\omega^2L^2} & 0 & 0 & -\frac{1}{2}\frac{1}{R^2+\omega^2L^2} & 0 \\ 0 & 0 & \frac{1}{2}\frac{1}{R^2} & 0 & 0 & -\frac{1}{2}\frac{1}{R^2} \\ -\frac{1}{2}\frac{1}{R^2+\omega^2L^2} & 0 & 0 & \frac{1}{2}\frac{1}{R^2+\omega^2L^2} & 0 & 0 \\ 0 & -\frac{1}{2}\frac{1}{R^2+\omega^2L^2} & 0 & 0 & \frac{1}{2}\frac{1}{R^2+\omega^2L^2} & 0 \\ 0 & 0 & -\frac{1}{2}\frac{1}{R^2} & 0 & 0 & \frac{1}{2}\frac{1}{R^2} \end{bmatrix} \tag{A.24}$$

Applying the characteristic equation (A.2) to (A.24) results in a characteristic polynomial

$$\lambda^3\left(\left(\lambda - \frac{1}{R^2}\right)\left(\lambda^2 - \frac{2}{R^2+\omega^2L^2}\lambda + \frac{1}{(R^2+\omega^2L^2)^2}\right)\right) = 0 \tag{A.25}$$

from which we can obtain the eigenvalues

$$\lambda_1 = \frac{1}{R^2} \tag{A.26a}$$

$$\lambda_2 = \frac{1}{R^2 + \omega^2 L^2} \tag{A.26b}$$

$$\lambda_3 = \frac{1}{R^2 + \omega^2 L^2} \tag{A.26c}$$

$$\lambda_4 = 0 \tag{A.26d}$$

$$\lambda_5 = 0 \tag{A.26e}$$

$$\lambda_6 = 0 \tag{A.26f}$$

Eigenvectors corresponding to the eigenvalues (A.26) are determined by (A.3). For example, for the eigenvalue λ_1 we can write

$$\left(\mathbf{A}^{\mathrm{T}}\mathbf{A} - \lambda_1 \mathbf{I}\right)\vec{g}_1 = \begin{bmatrix} \frac{1}{2}\frac{1}{R^2+\omega^2L^2} - \frac{1}{R^2} & 0 & 0 & -\frac{1}{2}\frac{1}{R^2+\omega^2L^2} & 0 & 0 \\ 0 & \frac{1}{2}\frac{1}{R^2+\omega^2L^2} - \frac{1}{R^2} & 0 & 0 & -\frac{1}{2}\frac{1}{R^2+\omega^2L^2} & 0 \\ 0 & 0 & -\frac{1}{2}\frac{1}{R^2} & 0 & 0 & -\frac{1}{2}\frac{1}{R^2} \\ -\frac{1}{2}\frac{1}{R^2+\omega^2L^2} & 0 & 0 & \frac{1}{2}\frac{1}{R^2+\omega^2L^2} - \frac{1}{R^2} & 0 & 0 \\ 0 & -\frac{1}{2}\frac{1}{R^2+\omega^2L^2} & 0 & 0 & \frac{1}{2}\frac{1}{R^2+\omega^2L^2} - \frac{1}{R^2} & 0 \\ 0 & 0 & -\frac{1}{2}\frac{1}{R^2} & 0 & 0 & -\frac{1}{2}\frac{1}{R^2} \end{bmatrix}\vec{g}_1 = 0 \tag{A.27}$$

A non-zero eigenvector that satisfies (A.27) can be given as $\vec{g}_1 = \begin{bmatrix} 0 & 0 & 1 & 0 & 0 & -1 \end{bmatrix}^{\mathrm{T}}$. Similarly, we can define eigenvectors for the rest of the eigenvalues (A.26). The resulting eigenvectors can be given in the matrix form (A.4) as

$$\mathbf{G} = \begin{bmatrix} \vec{g}_1 & \vec{g}_2 & \vec{g}_3 & \vec{g}_4 & \vec{g}_5 & \vec{g}_6 \end{bmatrix} = \begin{bmatrix} 0 & 0 & 1 & 0 & 0 & 1 \\ 0 & 1 & 0 & 0 & 1 & 0 \\ 1 & 0 & 0 & 1 & 0 & 0 \\ 0 & 0 & -1 & 0 & 0 & 1 \\ 0 & -1 & 0 & 0 & 1 & 0 \\ -1 & 0 & 0 & 1 & 0 & 0 \end{bmatrix} \tag{A.28}$$

Applying the Gram-Schmidt orthogonalization to (A.28) yields

$$\mathbf{P} = \begin{bmatrix} \vec{p}_1 & \vec{p}_2 & \vec{p}_3 & \vec{p}_4 & \vec{p}_5 & \vec{p}_6 \end{bmatrix} = \begin{bmatrix} 0 & 0 & \frac{1}{\sqrt{2}} & 0 & 0 & \frac{1}{\sqrt{2}} \\ 0 & \frac{1}{\sqrt{2}} & 0 & 0 & \frac{1}{\sqrt{2}} & 0 \\ \frac{1}{\sqrt{2}} & 0 & 0 & \frac{1}{\sqrt{2}} & 0 & 0 \\ 0 & 0 & -\frac{1}{\sqrt{2}} & 0 & 0 & \frac{1}{\sqrt{2}} \\ 0 & -\frac{1}{\sqrt{2}} & 0 & 0 & \frac{1}{\sqrt{2}} & 0 \\ -\frac{1}{\sqrt{2}} & 0 & 0 & \frac{1}{\sqrt{2}} & 0 & 0 \end{bmatrix} \tag{A.29}$$

The transpose of $\mathbf{P}$ equals

$$\begin{aligned}\mathbf{P}^{\mathrm{T}} &= \begin{bmatrix}\vec{p}_1 & \vec{p}_2 & \vec{p}_3 & \vec{p}_4 & \vec{p}_5 & \vec{p}_6\end{bmatrix}^{\mathrm{T}} \\ &= \begin{bmatrix} 0 & 0 & \frac{1}{\sqrt{2}} & 0 & 0 & -\frac{1}{\sqrt{2}} \\ 0 & \frac{1}{\sqrt{2}} & 0 & 0 & -\frac{1}{\sqrt{2}} & 0 \\ \frac{1}{\sqrt{2}} & 0 & 0 & -\frac{1}{\sqrt{2}} & 0 & 0 \\ 0 & 0 & \frac{1}{\sqrt{2}} & 0 & 0 & \frac{1}{\sqrt{2}} \\ 0 & \frac{1}{\sqrt{2}} & 0 & 0 & \frac{1}{\sqrt{2}} & 0 \\ \frac{1}{\sqrt{2}} & 0 & 0 & \frac{1}{\sqrt{2}} & 0 & 0 \end{bmatrix}\end{aligned} \tag{A.30}$$

The diagonal type matrix $\mathbf{S}$ is obtained with the eigenvalues (A.26) and (A.6)–(A.7). This results in

$$\mathbf{S} = \begin{bmatrix} \frac{1}{\sqrt{R^2}} & 0 & 0 & 0 & 0 & 0 \\ 0 & \frac{1}{\sqrt{R^2+\omega^2L^2}} & 0 & 0 & 0 & 0 \\ 0 & 0 & \frac{1}{\sqrt{R^2+\omega^2L^2}} & 0 & 0 & 0 \\ 0 & 0 & 0 & 0 & 0 & 0 \\ 0 & 0 & 0 & 0 & 0 & 0 \\ 0 & 0 & 0 & 0 & 0 & 0 \end{bmatrix} \tag{A.31}$$

The matrix $\mathbf{H}$ is obtained by (A.8) and (A.9). This results in

$$\begin{aligned}\mathbf{H} &= \begin{bmatrix}\vec{h}_1 & \vec{h}_2 & \vec{h}_3 & \vec{h}_4 & \vec{h}_5 & \vec{h}_6\end{bmatrix} \\ &= \begin{bmatrix} 0 & \frac{\omega L}{\sqrt{R^2+\omega^2L^2}} & \frac{R}{\sqrt{R^2+\omega^2L^2}} & 0 & 0 & 1 \\ 0 & \frac{R}{\sqrt{R^2+\omega^2L^2}} & -\frac{\omega L}{\sqrt{R^2+\omega^2L^2}} & 0 & 1 & 0 \\ 1 & 0 & 0 & 1 & 0 & 0 \\ 0 & -\frac{\omega L}{\sqrt{R^2+\omega^2L^2}} & -\frac{R}{\sqrt{R^2+\omega^2L^2}} & 0 & 0 & 1 \\ 0 & -\frac{R}{\sqrt{R^2+\omega^2L^2}} & \frac{\omega L}{\sqrt{R^2+\omega^2L^2}} & 0 & 1 & 0 \\ -1 & 0 & 0 & 1 & 0 & 0 \end{bmatrix}\end{aligned} \tag{A.32}$$

Now the orthogonal matrix $\mathbf{Q}$ is obtained from (A.32) by applying the Gram-Schmidt orthogonalization. This results in

$$\begin{aligned}\mathbf{Q} &= \begin{bmatrix}\vec{q}_1 & \vec{q}_2 & \vec{q}_3 & \vec{q}_4 & \vec{q}_5 & \vec{q}_6\end{bmatrix} \\ &= \begin{bmatrix} 0 & \frac{1}{\sqrt{2}}\frac{\omega L}{\sqrt{R^2+\omega^2L^2}} & \frac{1}{\sqrt{2}}\frac{R}{\sqrt{R^2+\omega^2L^2}} & 0 & 0 & \frac{1}{\sqrt{2}} \\ 0 & \frac{1}{\sqrt{2}}\frac{R}{\sqrt{R^2+\omega^2L^2}} & -\frac{1}{\sqrt{2}}\frac{\omega L}{\sqrt{R^2+\omega^2L^2}} & 0 & \frac{1}{\sqrt{2}} & 0 \\ \frac{1}{\sqrt{2}} & 0 & 0 & \frac{1}{\sqrt{2}} & 0 & 0 \\ 0 & -\frac{1}{\sqrt{2}}\frac{\omega L}{\sqrt{R^2+\omega^2L^2}} & -\frac{1}{\sqrt{2}}\frac{R}{\sqrt{R^2+\omega^2L^2}} & 0 & 0 & \frac{1}{\sqrt{2}} \\ 0 & -\frac{1}{\sqrt{2}}\frac{R}{\sqrt{R^2+\omega^2L^2}} & \frac{1}{\sqrt{2}}\frac{\omega L}{\sqrt{R^2+\omega^2L^2}} & 0 & \frac{1}{\sqrt{2}} & 0 \\ -\frac{1}{\sqrt{2}} & 0 & 0 & \frac{1}{\sqrt{2}} & 0 & 0 \end{bmatrix}\end{aligned} \tag{A.33}$$

Now the SVD of (A.23) can be given by (A.33), (A.31), and (A.30).

Appendix B

Simulation model

The simulation model used to verify the validity of the time-domain circulating current model, presented in Chapter 3, is introduced in some detail in this Appendix.

In brief, the simulation model implemented in Matlab/Simulink consisted of three parallel inverter units with a common direct voltage source. The outputs of the inverters were connected in parallel through the current sharing inductors which were modeled as resistive-inductive branches. Furthermore, the inverters were feeding a resistive-inductive load. The applied circuit parameters are given in Table B.1 unless otherwise mentioned. As a control method, a constant Volts/Hertz control was used. Furthermore, as a modulation method, a space vector PWM was applied. The top level of the simulation model is presented in Fig. B.1.

Table B.1: Parameters for the circuit simulations.

Parameter	Value	Unit
dc link voltage u_{dc}	565	V
Output inductances L_1, L_2, L_3	100	µH
Output resistances R_1, R_2, R_3	0.1	Ω
Load inductance L_{L}	13.7	mH
Load resistance R_{L}	18.5	mΩ
Forward voltage drops $U_{\mathrm{F},1}, U_{\mathrm{F},2}, U_{\mathrm{F},3}$	2.0	V
Blanking times $t_{\mathrm{d},1}, t_{\mathrm{d},2}, t_{\mathrm{d},3}$	2.0	µs
Switching frequency f_{sw}	5	kHz

Figure B.2 shows the top level of the modulator block. The main function of the modulator block is to form the inverter gate drive signals from the given voltage reference vector. The gate drive signals of the inverters are formed from the (phase) switch commands. Although the same switch commands are basically sent to each parallel unit, the blanking times between the gate drive signals of the upper and lower switches can be set independently for each unit. This is performed in the safetime logic blocks. It is also possible to delay the rising and falling edges of the gate drive signals to simulate the finite turn-on and turn-off times of the switches. This, again, is performed in the delay generation blocks. A similar approach is used also in the experiments.

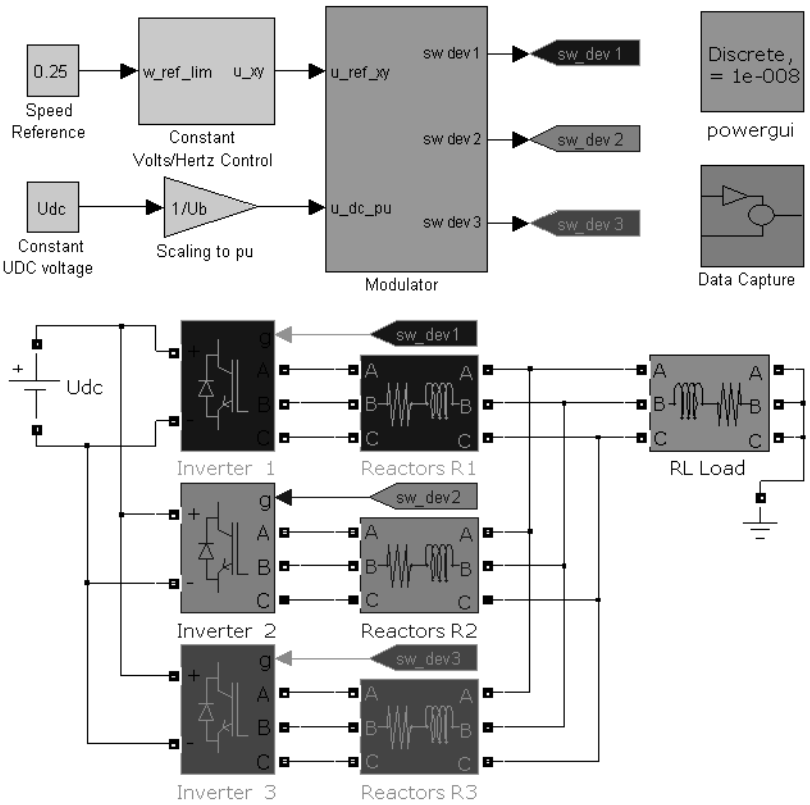

Fig. B.1: Top level of the simulation model. The main circuit consists of three parallel inverter units with a common direct voltage source. The outputs of the inverters are connected in parallel through the current sharing inductors modeled as resistive-inductive branches. The inverters are feeding a resistive-inductive load. As a control method, a constant Volt/Hertz control is used and as a modulation method, a space vector PWM is applied.

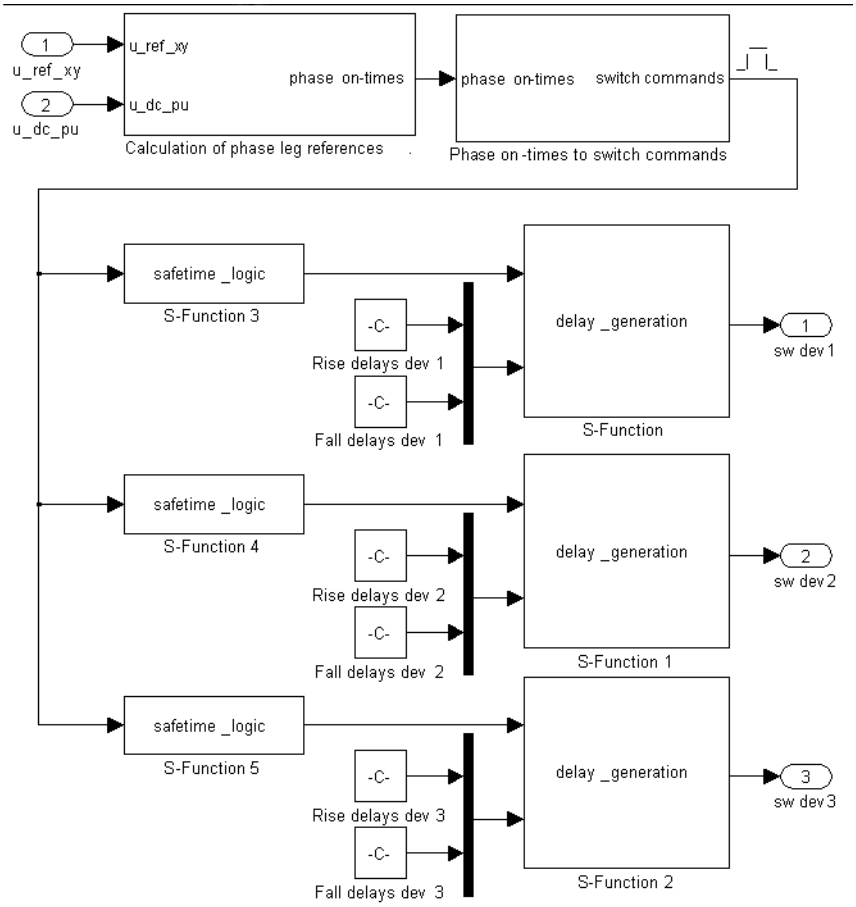

Fig. B.2: Top level of the modulator block. The main function of the modulator block is to form the inverter gate drive signals from the given voltage reference vector. The blanking times between the upper and lower gate drive signals are generated in the safetime logic blocks. The delaying of the rising and falling edges of the gate drive signals that are used to simulate the finite turn-on and turn-off times of the switches is performed in the delay generation blocks.

ACTA UNIVERSITATIS LAPPEENRANTAENSIS

347. KORKEALAAKSO, PASI. Real-time simulation of mobile and industrial machines using the multibody simulation approach. 2009. Diss.

348. UKKO, JUHANI. Managing through measurement: A framework for successful operative level performance measurement. 2009. Diss.

349. JUUTILAINEN, MATTI. Towards open access networks – prototyping with the Lappeenranta model. 2009. Diss.

350. LINTUKANGAS, KATRINA. Supplier relationship management capability in the firm´s global integration. 2009. Diss.

351. TAMPER, JUHA. Water circulations for effective bleaching of high-brightness mechanical pulps. 2009. Diss.

352. JAATINEN, AHTI. Performance improvement of centrifugal compressor stage with pinched geometry or vaned diffuser. 2009. Diss.

353. KOHONEN, JARNO. Advanced chemometric methods: applicability on industrial data. 2009. Diss.

354. DZHANKHOTOV, VALENTIN. Hybrid LC filter for power electronic drivers: theory and implementation. 2009. Diss.

355. ANI, ELISABETA-CRISTINA. Minimization of the experimental workload for the prediction of pollutants propagation in rivers. Mathematical modelling and knowledge re-use. 2009. Diss.

356. RÖYTTÄ, PEKKA. Study of a vapor-compression air-conditioning system for jetliners. 2009. Diss.

357. KÄRKI, TIMO. Factors affecting the usability of aspen (Populus tremula) wood dried at different temperature levels. 2009. Diss.

358. ALKKIOMÄKI, OLLI. Sensor fusion of proprioception, force and vision in estimation and robot control. 2009. Diss.

359. MATIKAINEN, MARKO. Development of beam and plate finite elements based on the absolute nodal coordinate formulation. 2009. Diss.

360. SIROLA, KATRI. Chelating adsorbents in purification of hydrometallurgical solutions. 2009. Diss.

361. HESAMPOUR, MEHRDAD. Treatment of oily wastewater by ultrafiltration: The effect of different operating and solution conditions. 2009. Diss.

362. SALKINOJA, HEIKKI. Optimizing of intelligence level in welding. 2009. Diss.

363. RÖNKKÖNEN, JANI. Continuous multimodal global optimization with differential evolution-based methods. 2009. Diss.

364. LINDQVIST, ANTTI. Engendering group support based foresight for capital intensive manufacturing industries – Case paper and steel industry scenarios by 2018. 2009. Diss.

365. POLESE, GIOVANNI. The detector control systems for the CMS resistive plate chamber at LHC. 2009. Diss.

366. KALENOVA, DIANA. Color and spectral image assessment using novel quality and fidelity techniques. 2009. Diss.

367. JALKALA, ANNE. Customer reference marketing in a business-to-business context. 2009. Diss.

368. HANNOLA, LEA. Challenges and means for the front end activities of software development. 2009. Diss.

369. PÄTÄRI, SATU. On value creation at an industrial intersection – Bioenergy in the forest and energy sectors. 2009. Diss.

370. HENTTONEN, KAISA. The effects of social networks on work-team effectiveness. 2009. Diss.

371. LASSILA, JUKKA. Strategic development of electricity distribution networks – Concept and methods. 2009. Diss.

372. PAAKKUNAINEN, MAARET. Sampling in chemical analysis. 2009. Diss.

373. LISUNOV, KONSTANTIN. Magnetic and transport properties of II-V diluted magnetic semiconductors doped with manganese and nickel. 2009. Diss.

374. JUSSILA, HANNE. Concentrated winding multiphase permanent magnet machine design and electromagnetic properties – Case axial flux machine. 2009. Diss.

375. AUVINEN, HARRI. Inversion and assimilation methods with applications in geophysical remote sensing. 2009. Diss.

376. KINDSIGO, MERIT. Wet oxidation of recalcitrant lignin waters: Experimental and kinetic studies. 2009. Diss.

377. PESSI, PEKKA. Novel robot solutions for carrying out field joint welding and machining in the assembly of the vacuum vessel of ITER. 2009. Diss.

378. STRÖM, JUHA-PEKKA. Actived*u*/d*t* filtering for variable-speed AC drives. 2009. Diss.

379. NURMI, SIMO A. Computational and experimental investigation of the grooved roll in paper machine environment. 2009. Diss.

380. HÄKKINEN, ANTTI. The influence of crystallization conditions on the filtration characteristics of sulphathiazole suspensions. 2009. Diss.

381. SYRJÄ, PASI. Pienten osakeyhtiöiden verosuunnittelu – empiirinen tutkimus. 2010. Diss.

382. KERKKÄNEN, ANNASTIINA. Improving demand forecasting practices in the industrial context. 2010. Diss.

383. TAHVANAINEN, KAISA. Managing regulatory risks when outsourcing network-related services in the electricity distribution sector. 2010. Diss.

384. RITALA, PAAVO. Coopetitive advantage – How firms create and appropriate value by collaborating with their competitors. 2010. Diss.

385. RAUVANTO, IRINA. The intrinsic mechanisms of softwood fiber damage in brown stock fiber line unit operations. 2010. Diss.

386. NAUMANEN, VILLE. Multilevel converter modulation: implementation and analysis. 2010. Diss.

387. IKÄVALKO, MARKKU. Contextuality in SME ownership – Studies on owner-managers´ ownership behavior. 2010. Diss.

388. SALOJÄRVI, HANNA. Customer knowledge processing in key account management. 2010. Diss.